U.PORTO

FEUP FACULDADE DE ENGENHARIA
UNIVERSIDADE DO PORTO

Kinematic evaluation of Parkinson's disease patients during Deep Brain Stimulation surgery and pre-operative procedures

Ana Sofia Miranda de Castro Resende Assis

Supervisor: Eng. João Paulo Cunha: INESC, PhD

Collaborator: Eng. Pedro Costa: MSc

Mestrado Integrado em Bioengenharia

June 2016

Faculdade de Engenharia da Universidade do Porto

Kinematic evaluation of Parkinson's disease patients during Deep Brain Stimulation surgery and pre-operative procedures

Ana Sofia Miranda de Castro Resende Assis

Dissertation submitted to Faculdade de Engenharia da Universidade do Porto to obtain the degree of Integrated Master in

Bioengineering

June 2016

Abstract

Deep Brain Stimulation (DBS) has proven to be valuable in the treatment of severe forms of Parkinson's Disease. Intraoperative evaluation of the efficacy of stimulation includes evaluation of the effect on rigidity. A subjective semi-quantitative scale is used, dependent on the examiner's perception and experience, through passive wrist flexion. So, the system proposed herein aims to tackle this subjectivity, using quantitative data and providing real-time feedback of the computed rigidity reduction, hence supporting the physician decision.

The system comprised of a gyroscope-based motion sensor embedded in a textile band is placed on the patient's hand, which communicates its measurements to a smartphone or a personal computer. The latter computes a signal descriptor from the angular velocity of the hand during wrist flexion in DBS surgery and applies a polynomial model to determine the rigidity reduction, which is communicated to the physician. This model was trained using previously acquired signals from patients during DBS surgery, for different stimulation settings.

To improve previous results (83.9% of accuracy), multiple models were designed according to the baseline rigidity and cogwheel rigidity was considered. However, these did not allow increased performance. Still, performance is consistently over 75% and mean error under 5% which supports the polynomial model-based approach. Furthermore, the usability of the system was further enriched: the feedback may be provided by a smartphone and by a smartwatch to be worn by the physician.

Additionally, this system in a small cohort proved to be reliable in distinguishing tremor and bradykinesia states before and after DBS surgery which proves its applicability to a wider range of motor symptoms (affecting other movement disorders other than Parkinson's Disease).

To introduce this rigidity evaluating system into the growing market of Deep Brain Stimulation for Parkinson's Disease, partnering with established companies is pivotal for their expertise in the procedures to be eligible for CE marking and also to reach a wider number of centers performing Deep Brain Stimulation surgery. For that purpose, attention should be paid in terms of intellectual property protection to secure the invention, which was already initiated with a patent application. Still, a utility model application could be of interest to secure protection in case the patent is not granted.

Keywords: Parkinson's Disease, wrist rigidity, deep brain stimulation, kinematics, gyroscope, medical device market

Resumo

A Estimulação Cerebral Profunda (ECP) tem a sua eficácia já provada no tratamento de formas severas da doença de Parkinson. A avaliação intra-operativa da eficácia da estimulação inclui a avaliação do seu efeito na rigidez. Uma escala semi-quantitativa é usada, dependente da percepção e da experiência do examinador, através da flexão passiva do pulso. O sistema proposto doravante tem por objectivo abordar esta subjectividade, usando dados quantitativos e dando feedback em tempo real da redução da rigidez calculada, apoiando deste modo a decisão do médico.

O sistema é composto por um sensor de movimento com giroscóscopio preso numa banda elástica, colocada na mão do paciente, que comunica as suas medidas para um *smartphone* ou computador. Este último calcula um descritor de sinal com base na velocidade angular da flexão do pulso durante a cirurgia de ECP e aplica um modelo polinomial para determinar a reduçao de rigidez, que é comunicada ao médico. Este modelo é treinado com base em sinais previamente adquiridos de pacientes na cirurgia de ECP para diferentes parâmetros de estimulação.

Para melhorar os resultados anteriores (83.9% de precisão), múltiplos modelos foram desenhados com base na rigidez de base do paciente e a rigidez de roda dentada foi considerada. No entanto, estes não permitiram melhoria da performance. Ainda assim, a precisão esteve consistemente acima de 75% e erro médio abaixo de 5%, o que suporta o uso de uma abordagem baseada em modelo polinomial. Ademais, a usabilidade do sistema foi ainda mais enriquecida: o feedback pode ser dado tanto pelo *smartphone* como pelo *smartwatch* a ser usado pelo médico.

Adicionalmente, numa pequena amostra de pacientes, o sistema provou ser fidedigno em distinguir os estados de tremor e bradicinésia antes e depois da cirurgia de ECP, o que comprova a aplicabilidade do sistema a uma maior variedade de sintomas motores (afectando outros doenças do movimento para além da doença de Parkinson).

Para introduzir o sistema de avaliação de rigidez no mercado de ECP para a doença de Parkinson, a formação de uma parceria com empresas já estabelecidas é uma etapa essencial pela experiência que têm nos procedimentos para receber a marca CE e também para alcançar um maior número de centros que realizam cirurgia de ECP. Com esse objectivo, deve prestar-se atenção à protecção de propriedade intelectual para assegurar a invenção, o que já foi iniciado com um pedido prévio de patente. Apesar disso, uma candidatura a modelo de utilidade pode ser de interesse caso a patente não seja atribuída.

Palavras-chave: Doença de Parkinson, rigidez do pulso, estimulação cerebral profunda, cinemática, giroscóspio, mercado de dispositivos médico

Agradecimentos

Cinco anos findados neste (multi-)curso terminam assim, num documento com mais de 100 páginas, que meramente conta a história incompleta de um só semestre. O restante tentarei compactar nesta secção (seguindo o antigo acordo ortográfico se me permitirem). Tentarei dar expressão ao muito sentimento relativo à meia década que passou.

Começarei por distribuir os agradecimentos relativos a esta mesma peça: doutores, enfermeiros, pacientes e o grupo BRAIN. Em particular aos meus orientadores: prof. João Paulo Cunha por dar sempre uma visão mais experiente e diferente sobre o trabalho e ao Pedro Costa por me ter apresentado este projecto e por ter dado apoio ainda que a centenas de quilómetros de distância.

De seguida, agradeço ao curso de Bioengenharia por estar a apoiar indecisos há 10 anos, pela inspiraçao que evoca e pela sua extrema, incomensurável e titânica exigência. Ainda deixo um agradecimento à saída da troika de Portugal em 2014, a que está associada um crescimento desde então no número de concursos para bolsas diversas (avançando para um futuro em que a vida na ciência não equivale a precariedade?). A seguir não pode faltar uma palavra de apreço aos fundadores do Núcleo de Estudantes de Bioengenharia (fundado a Novembro de 2013) pois deram-me uma oportunidade insubstituível de trabalhar e conhecer uma equipa fantástica e admirável. Agradeço também à União Europeia por me ter possibilitado aprender ou relembrar a dizer *merci*, 谢谢 , *ekele gi*, *dziękuję*, شكرا لك, *danke schön*, спасибо, *terima kasih*, *grazie*, *gracias*, *Tapadh leat* and *danke je*. Depois deste passeio internacional, volto a terras lusas, para agradecer às bravas e inconscientes almas que entraram no MIB e que foram além da obrigação para dar uma lição. E, não esquecendo quem já me acompanha há mais anos, obrigada por terem contribuido para aqui estar hoje.

Finalmente, e mais importante, agradeço às pessoas mais presentes na minha vida desde sempre: à minha mãe pelo acompanhamento e apoio constante e incansável, ao meu pai por me recordar quais são aquelas três coisas na vida realmente importantes e ao meu irmão pela vigilância e pela assistência na descompressão. Estou eternamente grata e espero que o futuro seja a retribuição de tal.

Sofia

If you think you are beaten, you are;
If you think you dare not, you don't.
If you'd like to win, but you think you can't,
It is almost a cinch that you won't.

If you think you'll lose, you're lost;
For out of the world we find
Success begins with a fellow's will
It's all in the state of mind.

If you think you're outclassed, you are;
You've got to think high to rise.
You've got to be sure of yourself before
You can ever win the prize.

Life's battles don't always go
To the stronger or faster man;
But sooner or later the man who wins
Is the one who thinks he can!

Walter D. Wintle

Contents

List of Figures

List of Tables

List of Abbreviations

A-DBS	After DBS surgery
B-DBS	Before DBS surgery
BRAIN	Biomedical Research and Innovation
CA	Cogwheel Artifacts
C-factor	Crest factor
DB	Difference of Bias
DBS	Deep Brain Stimulation
DT	Decision Tree
e	Threshold for application of cogwheel-related penalty
EMG	Electromyography
EPO	European Patent Office
FM	Fast Movement
GPi	*Globus Pallidus Internus*
IEC	International Electrotechnical Commision
IEETA	Institute of Electronics and Telematics Engineering of Aveiro
IMU	Inertial Measurement Unit
INESC	Instituto de Engenharia de Sistemas e Computadores - Tecnologia e Ciência
IP	Intellectual Property
ISO	International Organization for Standardization
K	Elasticity Coefficient
kNN	k-nearest neighbors
JS	Jensen-Shannon's
LD	Local Deviation
MoMo	Motion Mote
NT	Nose Tapping
PD	Parkinson's Disease
PF	Peak Frequency
PP	Peak-to-peak
RL	Rigidity Label
RT	Rotation Time
RMS	Root Mean Square
S	Skewness

SM	Slow movement
STN	Subthalamic Nucleus
SVM	Support Vector Machine
UPDRS	Unified Parkison Disease Rating Scale
UM	Utility Model
V	Viscosity
Z	Mechanical Impedance
W	Work

Chapter 1

Introduction

1.1 Context

This project is being developed at the Biomedical Research and Innovation (BRAIN) group in the Instituto de Engenharia de Sistemas e Computadores - Tecnologia e Ciência (INESC-TEC) under the supervision of Eng. Dr. João Paulo Cunha. This project was first initiated by Eng. Pedro Costa and has the collaboration of the Functional Surgery and Movement Disorders Unit of Hospital São João, coordinated by Dra. Maria José Rosas and Dr. Rui Vaz.

The proposition presented herein is to improve the current solution to accurately evaluate reduction in rigidity in intra-operative conditions. This could work as a support device during Deep Brain Stimulation (DBS) surgery to assess motor improvements in real-time. Moreover, we intend to extend the analysis to other cardinal parkinsonic symptoms, such as tremor.

1.2 Background: Parkinson's Disease

The Parkinson's Disease (PD) is a neurodegenerative disorder, first described in 1817 by James Parkinson in "An essay on the shaking palsy"[1]. It is characterized by the loss of dopaminergic cells in the *substantia nigra*. Usually, signals are propagated from the *substantia nigra* to the striatum and, from here, to the motor cortex. With a decrease of dopamine release, the ability to effectively control movement is lost and abnormal neurofiring patterns occur. This leads to the most known motor symptoms of PD: tremor at rest, rigidity and akinesia (or bradykinesia, which is the slowness of movement). The prevalence of this condition shows increase with age across all regions of the world and higher in males in the 50 to 59-years age group [2]. The costs associated to PD are direct (*e. g.* drugs, home visits by general practitioners, nursing homes) and indirect (loss of productivity, lost of leisure time, career replacement). In the UK, it is predicted that at least £449 Million are spent because of PD and costs ranges from about £4-9 thousand *per* year and *per* patient [3].

1.2.1 Pathophysiology

PD, as already mentioned, results from the degeneration of the *substantia nigra pars compacta*, whose dopaminergic nerve fibers connect to the caudate nucleus and putamen. The causes are unknown. The dopamine secreted by the *substantia nigra* to the *caudate nucleus* and putamen works as a inhibitory transmitter. By having a decreased release, the latter would become over active and continuous excitation of the motor cortex would occur and, consequently, continuous muscle contractions. This would explain the usual rigidity. Also, by not having inhibitory signals, the control mechanisms would cause an oscillation between "on" and "off" in the excitatory signals, leading to tremor. There is no formulated cause for the difficulty of performing movements in patients with PD and for their rigidity and discontinuity, *i. e.*, akinesia [4].

1.2.2 Diagnosis and Assessment

The diagnosis of PD is based on the presence of the aforementioned motor features (tremor, rigidity, bradykinesia, loss of balance, shuffling gait) which are also present in other neurogenerative disorders. The progression of the latter combined with the response to levodopa [5] are necessary to distinguish PD from others (Essential Tremor, Multiple System Atrophy, Progressive Supranuclear Palsy). Suboptimal methods are still used because there is lack of validated biomarkers specific for this disease with adequate sensitivity and specificity. Furthermore, common medical imaging is unable to easily and clearly identify disease symptoms[6].

1.2.2.1 PD motor symptoms

Tremor may be classified as:

- Rest tremor: occurs when body is fully supported and there is no voluntary activation
- Action tremor
  - Postural: occurs while voluntarily sustaining a position against gravity
  - Kinetic: occurs in any voluntary movement

Rest tremors occur at 3 and 6 Hz [7] and is prominent in the distal part of an extremity and has been shown to be present in over 70% of the PD patients [6]. Patients with PD often have postural tremors, which are stronger and, therefore, more disabling than rest tremors [8]. Kinetic tremor may be:

- simple, when volitional movement is not target-directed
- intentional, whose amplitude increases in visually-guided movements (*e.g.*, finger-to-nose test)
- task-specific, which only appear or becomes exaggerated in specific task, such as writing
- isometric, occurs during voluntary contraction against a rigid stationary object (*e.g.* squeezing examiner's hand)

Bradykinesia is defined as slowness in movement and is related to a higher difficulty in planning, initiating and executing movements and in performing sequential and simultaneous tasks. That results in micrographia, lessened finger manual dexterity and shuffling walk, for example [6]. This feature is the one which shows best correlation to the degree of dopamine deficiency [9].

Rigidity, present in almost all PD patients [6], is the resistance of a limb to passive movement (flexion, extension or rotation about a joint). One considers a joint rigid when more force than expected is needed to move it. During examination, cogwheel rigidity in the movement may be identified, which is similar to the ratchet pattern of a gear [6, 8], caused by episodic bursts of muscle potential which lead to increment of resistance [10].

Other than motor symptoms, PD is associated to behavioral changes, sensory symptoms as chronic pain and sleep disorders [8].

To classify the severity of these symptoms, the most used scale is the Unified Parkinson Disease Rating Scale (UPDRS), which was first introduced in 1987. The different parts of this evaluation tool are in Table 1.1. Parts I, II and III contain 44 questions and the fourth part 11 questions. However, the latter is included only when adjunct therapy is being used. To answer each question, a 5-point scale is used, ranging from 0 to 4 where 0 is "not affected" and 4 "most severely affected". This assessment is qualitative and subjective and depends on the doctor clinical experience and perception.

Table 1.1: Total UPDRS parts. Adapted from [11].

I	**Mentation, behavior and mood**	intellectual impairment, thought disorder, motivation/initiative, depression
II	**Activities of daily living**	speech, salivation, swallowing, handwriting, cutting food, dressing, hygiene, turning in bed, falling, freezing, walking, tremor, sensory complaints
III	**Motor examination**	speech, facial expression, tremor at rest, action tremor, rigidity, finger taps, hand movements, hand pronation and supination, leg agility, arising from chair, posture gait, postural stability, body bradykinesia
IV	**Complications of therapy**	dyskinesia-duration, dyskinesia-disability, dyskinesia-pain, early morning dystonia, "offs"-predictable, "offs"-unpredictable, "offs"-sudden, "offs"-duration, anorexia-nausea-vomiting, sleep disturbance, symptomatic orthostasis

1.2.3 Treatment of Parkinson's Disease

So far, there are no methods to cure the PD, only to control its symptoms. With that purpose, existent approaches tackle the dopamine deficit or the unbalance of dopamine and other neurotransmitters [6, 9]. The gold-standard is levodopa (L-dopa), which was introduced in 1961 in an injectable form and, a decade afterward, orally. It is believed that L-dopa is converted to dopamine

in the brain, therefore, restoring balance between inhibition and excitation in the caudate nucleus and putamen [4].

When the efficacy of L-dopa decreases and incidence and severity of side-effects increases, a different approach is needed [9]. Deep brain stimulation (DBS) is based on the electrical stimulation with a tetrapolar electrode at high frequencies (130 Hz) with pulse length at 60 μs in a given target of the brain. Firstly, relying on pre-operative imaging (representation in Figure 1.1), the surgery of electrode implantation is planned and orientation of the implantation device defined. After correctly aligning the device, the patient's skull is drilled and exploration electrodes are inserted at a given deepness (usually 30 mm superior to the target). Then electrophysiological exploration is performed to determine anatomical structures location and to determine where is the region of interest. This is a required step because after opening the skull and consequent depressurization, the brain shifts, invalidating the imaging previously acquired and the planning. At this newly defined location, the 4 electrodes are used to stimulate the brain structures, varying the intensity from 0 onwards and, simultaneously, the severity of the symptoms of PD may be evaluated (except for gait). Most often, the improvement in rigidity is evaluated in a semi-quantitative manner by a clinician [12], by imposing passive flexion of the wrist, which is easier to maneuver and most accessible. For his evaluation, he compares the difference in the assessed rigidity to the patient's baseline rigidity state. Moreover, the physician assesses whether there are side-effects of the stimulation such as dyskinesias (involuntary movements) and muscle contractions. Usually, side-effects start to appear at 3.5 V and improvements at 2.0 V. The scale used for rigidity change is based on the subjective assessment of the doctor involved in this process. Therefore, the classification given depends only on the experience of the medical doctor and his own perception. After surgery, the patient's drug doses are reduced and set at a compromise level: low enough to prevent side-effects and high enough to prevent apathy and hypophonia.

The working principle of DBS is still unclear, although this surgical procedure has shown up 21 years ago. With an electrical stimulation approach, rather than ablation of functional targets, as it has been done, DBS is able to promote their inhibition, as dopamine does. Most often, the anatomical target is the subthalamic nucleus (STN) or *globus pallidus internus* (GPi). It is theorized that their inhibition may be due to jamming of the neuronal pathways, inhibition of neuronal firing with stimulation or inhibition of production of neurotransmitters [13].

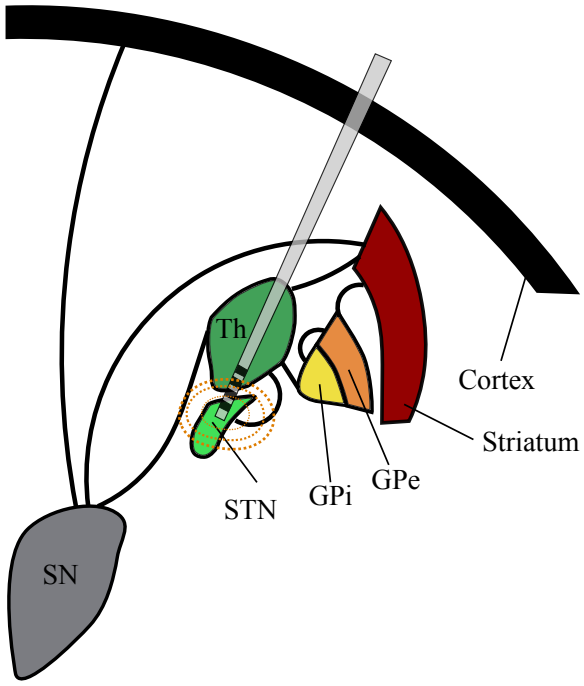

Figure 1.1: With the incidence of Parkinson's Disease, the balance between the several structures of brain is broken leading to the cardinal symptoms of the disease. A way to reduce them is through Deep Brain Stimulation. In this case, a tetrapolar electrode is targeting the subthalamic nucleus (STN). As the voltage of stimulation increases, a larger volume of the structure is stimulated. GPi stands for *globus pallidus internus*, GPe for *globus pallidus externus*, SN for *substantia nigra* and Th for thalamus.

1.3 Motivation and Goals

In the DBS surgery procedure, the evaluation of the rigidity reduction by passive joint flexion is performed by a physician, hence it is subjective and dependent on his experience and perception and relies in no quantitative information. In opposition to other DBS-specialized centers, where they implant the electrode in the pre-defined target (without any other test), the Functional Surgery and Movement Disorders Unit of Hospital S. João resorts to the blind agreement between two physicians, using passive wrist flexion to evaluate rigidity, for being accessible and easy to maneuver. Therefore, the goal of the project was to add to the subjectivity of the experts' agreement a quantitative procedure to determine the improvement in wrist rigidity by using a system adequate for intra-operatory conditions and providing precise real-time feedback. Such setup has been developed and tested in Hospital São João and showed an accuracy of 83.9% [14]. This will be further presented in Chapter 3. Even though it proved to be reliable, some shortcomings may be pointed out: the classification method used for evaluation of rigidity reduction with stimulation does not consider either the patient limb baseline rigidity and the occurrence and severity of cogwheel rigidity (which is an important parameter in the medical assessment of improvement).

Based on previous work, the goals for this thesis are to:

1. improve current model for rigidity evaluation namely by considering cogwheel rigidity
2. interface current mobile application with a smartwatch to improve usability in the operating room
3. assess the feasibility of using other relevant features in the current system such as tremor

It is an implicit goal to perform signal acquisition during DBS surgeries related to rigidity as well as before and after the surgical intervention. Patient monitoring was authorized by the Hospitals Ethic Committee (Appendix A) and all patients signed an Informed Consent form.

1.4 Contributions

Over the course of this thesis project, the reliable detection of cogwheel rigidity artifacts was achieved, even though its inclusion into the model did not improve the performance of the system. Still, this information was incorporated in the previous mobile application to enrich the feedback provided to the physician.

Furthermore, a multi-model approach where polynomial models designed specifically for different initial rigidity status (according to the assessment of the physician in the UPDRS scale) were tested in intra-operatory conditions (leading to no significant improvement in performance). These results were submitted as a 4-pages paper in the 38^{th} Annual International Conference of the IEEE Engineering in Medicine and Biology Society [15], which was accepted (Appendix B).

Another goal of this thesis' work was to further enhance the system's usability by having the display of the computed rigidity reduction in a smartwatch to be worn by the physician who is per-

forming the assessment. This communication was achieved and used in intra-operatory conditions, as in Appendix F.

Also preliminary results related to tremor and bradykinesia assessment showed the system ability to identify differences namely before and after DBS surgery.

Out of the scope of the initial goals, an analysis of the system in a commercial viewpoint was performed, covering the industry landscape, the procedures for CE marking and intellectual property protection.

1.5 Dissertation structure

This dissertation is organized as follows: Chapter 1 encompasses a contextualization of the thesis; Chapter 2 presents current approaches to assess cardinal symptoms of PD, Chapter 3 introduces the status of the system and its performance when the thesis work initiated; Chapter 4 presents developments and results of the rigidity reduction model; Chapter 5 is related to cogwheel rigidity, where its detection and inclusion into the system is explored; Chapter 6 introduces final features of the mobile application and other possible uses for the proposed system; Chapter 7 studies the system as a commercial product and Chapter 9 revisits all the work developed and conclusions taken from it.

Chapter 2

State of Art

Herein, the traditional methods for assessment of some motor symptoms will be presented, followed by an introduction and analysis to market and research solutions for their quantification, approaching not only the hardware, but the processing techniques as well.

2.1 Semiology for PD

As aforementioned in Chapter 1, the Unified Parkison Disease Rating Scale (UPDRS) is a standard scale which evaluates namely rigidity, tremor and bradykinesia.

2.1.1 Rigidity

For rigidity assessment, the clinician imposes passive joint flexion in the neck and in the left and right upper and lower extremities. The passive flexion of the wrist or elbow is represented in Figure 2.1. Based on the perceived resistance to flexion, he attributes a score, translating the severity of the muscle rigidity. In particular, during Deep Brain Surgery (DBS) surgery, there is preference to assess rigidity using the wrist joint because it is easier to maneuver and easily accessible. Additionally, contrary to the wrist, the elbow does not have cogwheel rigidity, which features only on the wrist.

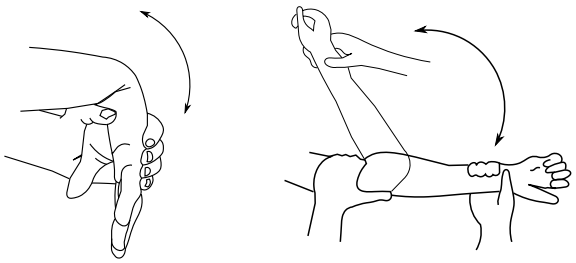

Figure 2.1: Clinician method to assess (left) wrist and (right) elbow rigidity.

Figure 2.2: Tasks for assessment of, from left to right, rest tremor, postural tremor and action tremor. From [17].

2.1.2 Tremor

Tremor, as described in Chapter 1, is a motor symptom transverse to several neurological diseases as dystonia, multiple sclerosis, PD and essential tremor (ET). It may be categorized as rest, postural or kinetic/dynamic tremor and may be assessed in the extremities, namely in the hand [11]. In Figure 2.2, tasks to assess each of these are represented: rest tremor while body is fully supported; postural tremor while arms are lifted and dynamic tremor when patient taps his nose with his finger, from extended arm position. Its amplitude (in centimeter) has been shown to be logarithmically related to the UPDRS rating given by a clinician [16].

2.1.3 Bradykinesia

Bradykinesia, defined as slowness in movement, is assessed by having the patient performing left- and right-hand finger-taps, opening and closing of hands, pronation/supination of hands (Figure 2.3), and heel taps. The speed, amplitude and halts may be analyzed by the clinician [8].

2.2 Commercial and research methods of assessment

2.2.1 Rigidity

At the moment, there are no devices in the market available for parkinsonian rigidity quantification in the wrist or elbow because there is no device which is cheap to produce nor to sell, and also

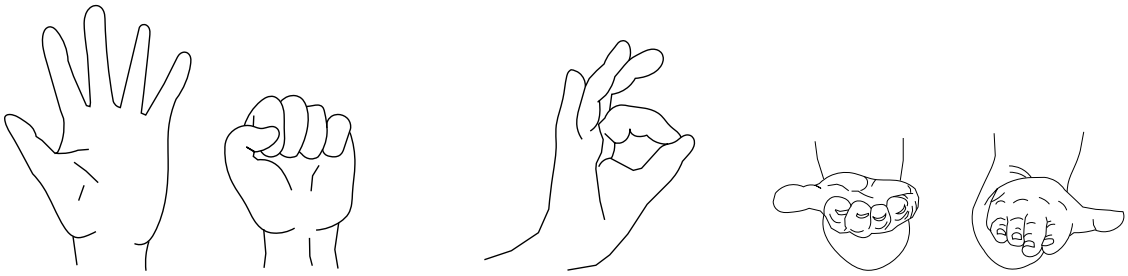

(a) Hand Grasp. (b) Finger Tapping. (c) Hand supination/pronation

Figure 2.3: Tasks for bradykinesia clinical assessment.

providing evaluation and classification presented in a meaningful away for the clinical centers. However, researchers have proposed several approaches with that purpose. These usually rely on the passive movement of the elbow [18, 19, 20, 21] or wrist [19, 22, 23, 24], but it has been also attempted to analyze trunk rigidity [25]. These systems require passive joint movement, imposed by a torque motor [18, 25, 26] or by an examiner [19, 20, 21, 22, 23, 24]. In Table 2.1, an assessment of the features related to the setup (size, wireless), processing and feedback provided is presented, which summarizes the analysis done over the different proposals.

Table 2.1: Summary of methods for rigidity assessment. *Z* stands for mechanical impedance, *DB* for difference of Bias, *V* for viscous damping, *K* for elastic stiffness and EMG for electromyography. The amount of '+' represents the level of performance.

Author and Year	Method	Focus Body Region	Parameters	Signal Process	Size	Motorized	Real-time feedback	Wireless
Patrick *et al.*, 2001	EMG, torque-angle	Elbow, Wrist	Z	+	++	No	No	No
Shapiro *et al.*, 2007	EMG, torque-angle	Elbow	EMG, Work	+	+	Yes	No	No
Mak *et al.*, 2007	Torque-angle	Trunk	Peak Torque	+++	+	Yes	No	No
Endo *et al.*, 2009	EMG, torque-angle	Elbow	V, K, DB	+	+++	No	No	No
Levin *et al.*, 2009	EMG and goniometer	Elbow	EMG	++	++	No	No	No
Park *et al.*, 2011	Torque-angle	Wrist	V, K, work, impulse	+	++	No	No	No
Kwon *et al.*, 2014	Torque-angle	Wrist	V, K, work	+	++	No	No	No
Costa *et al.*, 2015	Angular velocity	Wrist	Average and peak angular velocity	+++	+++	No	Yes	Yes

Patrick *et al.* (2001) [19] reported having developed a custom made device which comprises two pads placed where the physician will force the joint flexion, which measured the resultant force applied on them, and a gyroscope mounted in one of the pads (Figure 2.4), which measured the angular velocity and used to compute the angular displacement. The force pads would allow us to determine an angular velocity normalized by the applied force, which decreases the influence of the variability of how the physician imposes joint passive flexion.

They modeled the wrist joint as a viscoelastic system following the Equation 2.1:

$$T = Kx + Vv + C \tag{2.1}$$

where T stands for torque measured, x and v for angular displacement and angular velocity, respectively, K for elastic stiffness, V for viscosity and C for constant offset of the sensors. These parameters were obtained with the performed measurements and using a least-squares parametric

Figure 2.4: Patrick *et al.* setup for rigidity quantification consisting of two-force pads and a gyroscope. From [19].

method. As to quantify rigidity, they determine the mechanical impedance (Z) which is given by vector sum of K and $V\omega$ (where ω is $2\pi\times$ the mean frequency of the cyclical displacement by the clinician). Z was related to the elbow and wrist rigidity subscore in UPDRS scale assigned by the clinicians using an exponential relation. The sensors used in this work are relatively small; still these are connected to a data acquisition box which then communicates to a computer the data. Along with this, it requires calibration in each use.

Shapiro *et al.* (2007), contrary to the Patrick *et al.* (2001), imposed flexion to the elbow by having a torque motor (Figure 2.5), instead of having a physician. This allowed to measure the force applied by the motor to achieve a controlled angular velocity. In this case, over several cycles of oscillation, they obtained the average work done by the motor (W), which was obtained by integrating the resistive torque over the angular displacement and then dividing by the number of these cycles. Both angle and torque channels are low-pass filtered in order to remove the tremor associated to parkinsonic tremor (4-8 Hz). W proved to distinguish healthy and PD patients. Additionally, the EMG signal from the *biceps* and *triceps brachii* was acquired, which further supported that performing facilitation maneuvers increases muscle resistance to passive movement.

Regarding the setup, predictably, because it relies on a motor to impose movement, it is quite bulky. Also, each cycle lasted 60 seconds and twenty repetitions were done, thus being a lengthy procedure.

Another example of complex structure for quantitative assessment of rigidity is the component of Cybex®Norm Isokinetic dynamometer (Lumex, Inc., Ronkonkoma, NY) used by Mak *et al.* (2007) [25], shown in Figure 2.6. Yet it targeted trunk rigidity and their goal was to assess the influence of movement speed on rigidity, evaluated in relation to the work and peak torque. They concluded that higher movement speed increased these measures. This serves as example as an unpractical system to be used, even in medical appointments, requiring the positioning of the patient in this large device.

Another system that overall is similar to Patrick *et al.* setup, is from Endo *et al.* (2009), presented in Figure 2.7. It also presented two force sensors, in the wrist and a gyroscope in-between.

Figure 2.5: Shapiro *et al.* (2007) setup for rigidity quantification in the elbow joint, comprised of a motor imposing its flexion/extension. From [18].

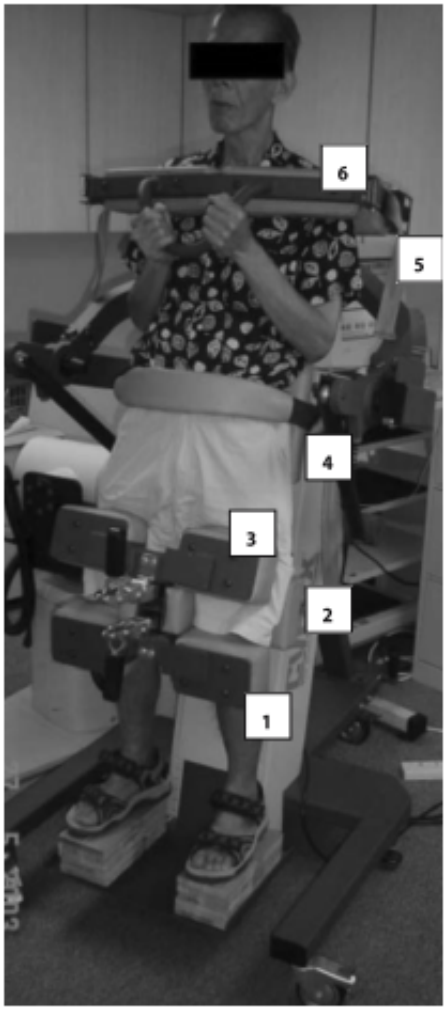

Figure 2.6: Mak *et al.* (2007) setup for rigidity quantification in the trunk. From [25].

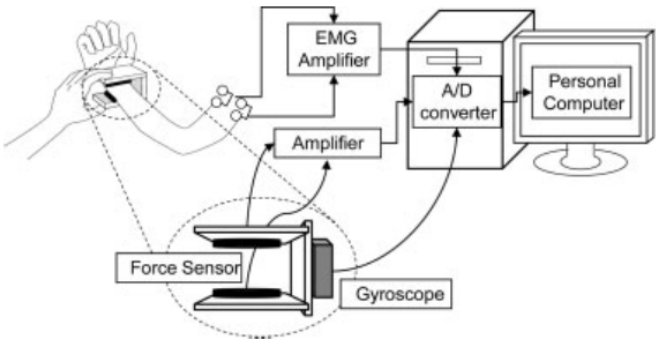

Figure 2.7: Endo *et al.* (2009) setup for rigidity quantification in the elbow. From [20].

In their case, they determined the elastic coefficient for flexion and extension separately by estimating the slope of the regression line for both movements, based on torque-angle data. They also defined a new feature: difference of bias (DB). To determine the DB, for flexion and extension the torque values at a given angle are averaged, subtracted and then there is the summation of the differences. Both features were shown to be correlated with the rigidity severity, such that higher perceived rigidity by the examiner translated into higher DB and elastic coefficients [20]. Still, in this case, no significant different between flexion and extension was found. Their work was further enriched with EMG signal (in *biceps* and *triceps brachii*), which they used to compute an index by first rectifying and smoothing the signal, then integrating the signal over a second during maximal extension and flexion stances and finally computing the ratio between them. This index was able to better distinguish all different levels of rigidity when considering the *biceps brachii* muscle, while the EMG-index from *triceps brachii* only indicated rigidity for medical assessments of high severity rigidity[20]. Such conclusion is also supported by the work by Levin *et al.* (2009) [21].

Apart from the EMG signal acquisition elements, this is a compact system but still wired to an analog-to-digital converter. Comparing their processing methodology of the torque-angle data to Patrick *et al.* (2011), it is equally complex because it requires the determination of a regression line for both flexion and extension to estimate its slope, even though there are overall less parameters to be determined.

Park *et al.* (2011) and Kwon *et al.* use the same device for rigidity evaluation, designed for the imposition of wrist flexion by a clinician. This consisted of a potentiometer to measure the joint angle, a load cell and an accelerometer to measure inertia (Figure 2.8). Kwon *et al.* (2014) in particular used the device during DBS surgery.

They modeled the wrist joint as a viscoelastic system in the following form:

$$I\alpha = \tau - V\omega - K\theta + C \tag{2.2}$$

where τ is the torque applied to move the joint, θ the joint angle, ω and α are the angular velocity and acceleration, I the total inertia of the moving part, K is the spring constant (elastic stiffness), V is the damping constant (viscosity) and C is an offset torque [22, 23]. These are obtained by

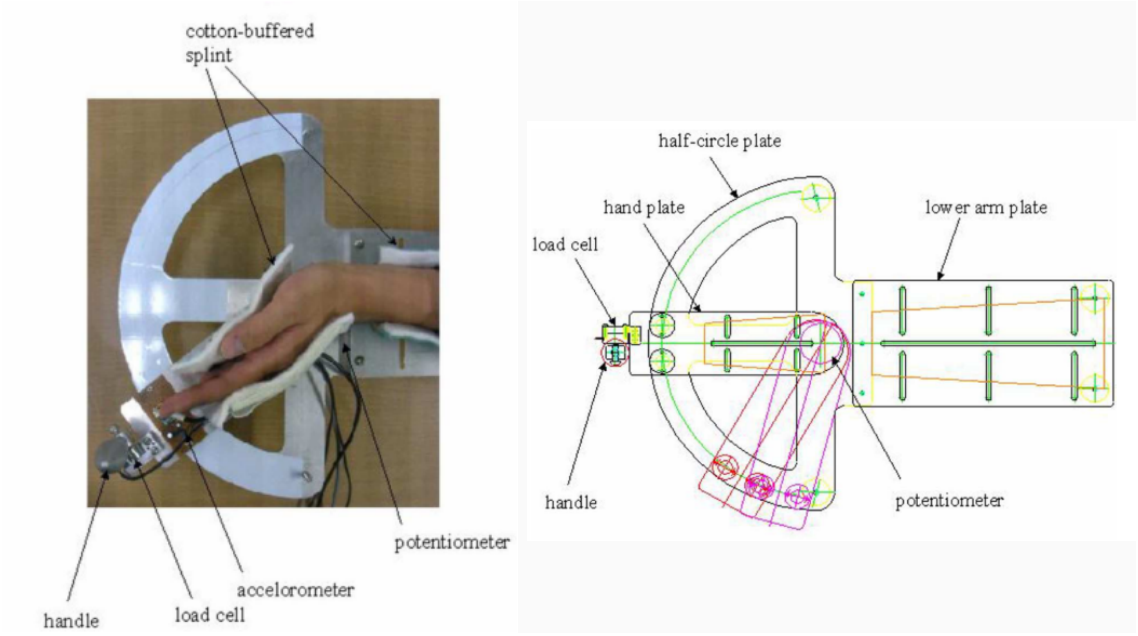

Figure 2.8: Park *et al.* (2011) and Kwon *et al.* (2014) setup for rigidity quantification in the wrist. From [22, 23].

fitting the experimental data to the spring-damper model.

Between V and K, viscosity has shown better capability in distinguishing different degrees of rigidity [22, 23]. They proposed that the wrist joint can be modeled as a two dampers and one spring system, by having a damping constant for flexion and another for extension [22]. This could be related to an asymmetric contribution to rigidity of the flexor and extensor muscles, more pronounced in imposed extension of the wrist [27].

Also, they computed work (W) and impulse (I, torque integration with respect to time) for flexion and for extension. It was assessed that work was phase-dependent and allowed distinguishing healthy from parkinsonian patients. Nevertheless, better discriminative power was identified when computing total W, *i. e.*, throughout flexion and extension [22]. In the case of I, it proved to be also phase-dependent and showed moderate performance when comparing between the baseline rigidity and with the optimal setting of DBS [23]. Because both work and impulse are resultant of resistive torque, and are susceptible to the movement range and speed, normalization by the range and excursion time, respectively, was done. This improved the correlation of both to the improvement in surgery. Still, their velocity-dependent nature prevails [23].

This device was used during DBS surgery which supports its usability. However, it required connection to a computer through wires. Also, as all other proposals, no real-time feedback was provided. To emphasize, the computation of the viscous damping and elastic coefficient would hinder the latter implementation in a smartphone, for example, for local processing.

The only proposal so far for rigidity evaluation during DBS surgery and providing real-time feedback to the clinician is the work done by Costa *et al.* (2015) [14]. This dissertation will describe this system in more detail in the Chapter 3.

Table 2.2: Summary of methods for bradykinesia and tremor assessment. A stands for accelerometer, G for gyroscope, IMU for Inertial Measurement Unit and NA for not applicable. The amount of '+' represents the level of performance.

Author and Year	Device	Type of Device	Focus Body Region	Signal Process	Size	Real-time feedback	Wireless
Motus Bioeng. Inc., 1993	Motus	G	Hand	+	+++	Yes	No
Spyers-Ahby *et al.*, 1999 O'Suilleabhain *et al.*, 2001	3Space Fastrack	Electromagnetic Tracking Device	Hand	++	+++	No	No
Salarian *et al.*, 2007	ASUR	G	Wrist	+	+++	No	No
Lorincz *et al.*, 2007 Patel *et al.*, 2009	SHIMMER	A	Body	+	+++	No	No
Heldman *et al.*, 2011 Mera *et al.*, 2011	Kinesia	A , G	Hand	+	+++	No	No
Joundi *et al.*, 2011	iPhone (iSeismo)	A	Hand	+++	+++	Yes	Yes
Synnot *et al.*, 2012	Nintendo Wii remote	A	Upper Limbs	++	+	No	Yes
Dai *et al.*, 2015	-	IMU	Finger	++	+++	Yes	No
GyroGear, 2015	GyroGlove	G	Hand	NA	+++	NA	Yes

2.2.2 Tremor and bradykinesia

For the quantification of both symptoms, the apparatuses mainly involve the use of accelerometers and gyroscopes placed in the hand, as evidenced in Table 2.2. As for parameters, in the time-domain, the root mean square (RMS) of their signals has been used to translate the magnitude of the tremor [17, 28, 29, 30]; also several parameters in the frequency domain have been used from center frequency, frequency dispersion (related to the consistency of the tremor) and crest factor [30, 31, 32].

MOTUS is an example of a commercial gyroscope-based system (Figure 2.9) that was proposed to be used for tremor assessment during DBS surgery and also for bradykinesia. The gyroscope is placed in the back of the hand, attached to a glove, and data processing is PC-based, which includes fast-fourrier transform, computation of sharpness of resonance, root mean square of angular velocity and position [33]. So, even though the sensor communication to the PC is wireless, relatively heavy computation is performed. Additionally, the parameters by themselves do not give any intuitive interpretation and with no meaning by themselves in the clinical context.

Using as well a gyroscope to assess tremor and bradykinesia, Arash Salarian *et al.* (2007) [28] have produced a custom-made sensor, ASUR (Figure 2.10). However, they aimed at having their sensor used during daily activities of a patient (such as lying in bed, sitting, eating and drinking). To achieve that, tremor was detected and a bandpass filter to the angular velocity signal applied, with cutoff frequencies of 3.5 and 7.5 Hz, then integrated; finally, the root mean square value was computed (translating the amplitude of the tremors). Regarding bradykinesia, a low-pass filter was

Figure 2.9: Motus system for quantification of movement [33].

applied to remove the tremor effect (3.5 Hz cutoff frequency) and a Hilbert transform was applied. Then, three features were evaluated: the root mean square of the resultant angular velocity signal (hand mobility), percentage of time where extremity was moving during the task (hand activity) and, by integration, the range of rotation of the hand. These measures were successfully related to the severity of symptoms. Still, significant processing was required.

Contrary to the previous approaches, SHIMMER [29, 34] used an accelerometer-based system, comprised of sensors placed over the whole body (see Figure 2.11), which allowed measuring the both tremor (amplitude and frequency) and bradykinesia and relate them to the corresponding severity score with reduced error, after optimizing the window size for features computation, parameters and kernels to be used in SVM classification. They used as features for tremor the root mean square of the sensors signal, the range of the covariance, the dominant frequency and periodicity (ratio between energy of the dominant frequency and the total spectral energy). For bradykinesia, they evaluated body coordination by examining the correlation of the signal magnitude over all body, the delay and similarity. The sensors are wireless and the output is related to an existent scale of severity of the symptom, which make this system attractive. However, it could pose a computational burden to devices with less processing capabilities.

By combining both gyroscope and accelerometer data in the Kinesia^{TM} (CleveMed) device, Heldman *et al.* (2011) were also able to detect, discriminate and quantify different types of tremor during the simulation of patient's daily activities, using the peak power of both gyroscope and

Figure 2.10: An ASUR unit developed by [28], which includes a gyroscope.

(a) One of the units of SHIMMER system (b) Placement of the sensors

Figure 2.11: SHIMMER System for quantification of bradykinesia and tremor. From [34].

accelerometer [35].

Moreover, the same device was used to develop a tuning map for DBS programming (Figure 2.13, system is patent pending [37]) which would represent visually the tremor and also the bradykinesia severity for different stimulation intensities to facilitate the decision about the optimal settings of DBS [38]. To represent the severity of each symptom, the peak power of the angular velocity (tremor and bradykinesia) and of its integration were determined (bradykinesia). The concept of a tuning map is quite intuitive, yet the tremor reduction assessment is an easy task to assess visually so it is not a pressing need.

Similarly, by combining different motion sensors, Dai *et al.* (2004) have built a device comprised of a wrist band connected to an IMU placed in the finger, shown in Figure 2.14 (patent pending [39]) to relate quantified tremor (rest and postural) to the clinician rating. The tasks performed are shown in Figure 2.2. As signal features, alike other authors previously, the peak power of the three-axis accelerometer and gyroscope was determined and used to build a linear regression model which related those measures with the UPDRS tremor subscore. The assessment of action tremor was not achieved [17]. The greatest disadvantage is the USB communication needed to the

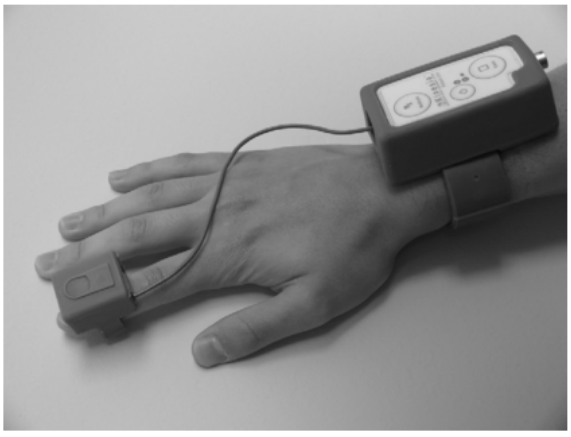

Figure 2.12: Kinesia^{TM} from CleveMed [36].

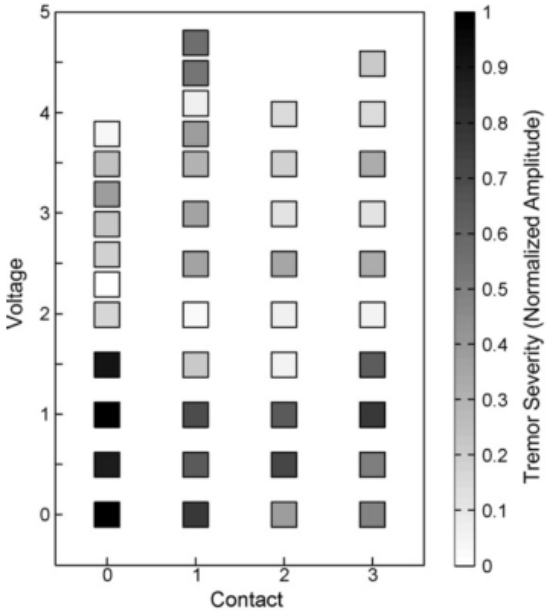

Figure 2.13: Example of a tuning map considering during DBS programming. From [38].

PC, where the computation of the features occurs.

Another recent effort was the GyroGlove (patent pending) which is a glove capable of countering the hand tremor in PD patients, comprising of a dynamically adjustable gyroscope. Yet, a similar concept has already been patented in 1991: a hand-held gyroscopic device [41] to eliminate the effect of naturally occurring tremors such as essential tremor or other tremor.

Other approaches relying on day-to-day devices have been proposed. One example used the iPhone application, iSeismo, to determine the dominant tremor frequency, whose validity was confirmed by comparing to the frequency calculated from an EMG-based system [43]. Another case was the use of Nintendo Wii to monitor motor performance of PD patients, depending on games and on the remote's accelerometer from which metrics related tremor and bradykinesia severity were computed [44].

Another system type is an electromagnetic tracking device (3Space Fastrak®) [45, 46], which showed potential to be used as a screening tool and even as a diagnostic aid. The root mean square of the hand displacement was computed, which proved to significantly distinguish healthy and patients and, additionally, people with different neurological diseases (PD, Essential Tremor and Multiple Sclerosis).

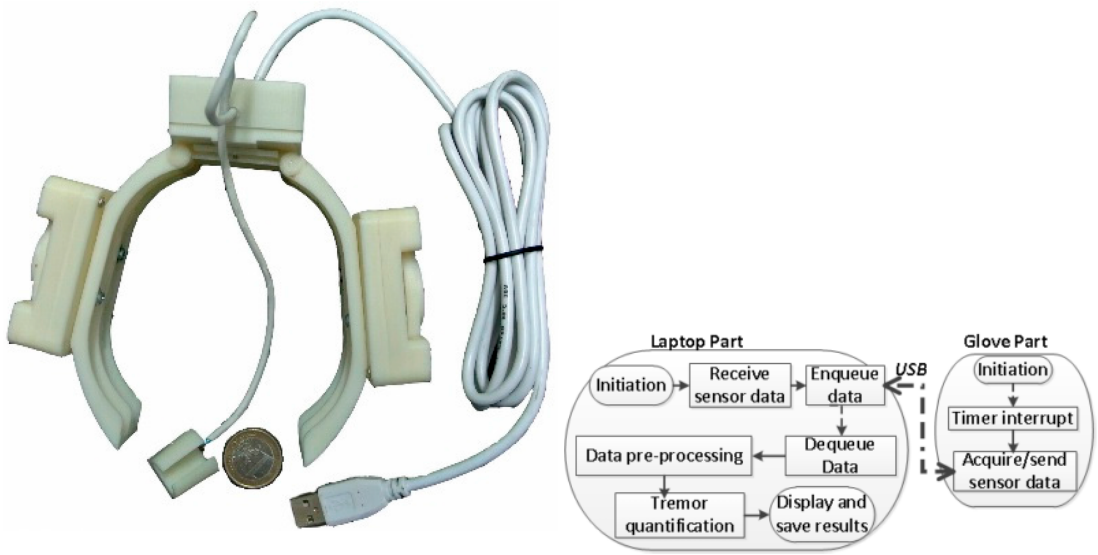

(a) Setup comprising of an IMU in the finger an a wristband.

(b) The flowchart of the signal processing for tremor quantification.

Figure 2.14: System proposed by Dai *et al.* (2013). From [40].

Figure 2.15: GyroGlove by GyroGear. From [42].

Chapter 3

Existing System

As seen in Chapter 2, some systems for PD symptoms evaluations were bulky or required connection to a PC for processing; others relied on relatively heavy processing which may lead to delays in the output and, therefore, increase patient exposure time; also some provided values of features could hamper the intuitive understanding of the physician about the rigidity severity. Additionally, it was clear the availability of commercial products tackling both tremor and bradykinesia but, as for rigidity, a system to evaluate it in a prompt manner is lacking, besides being suitable for intra-operative conditions. Therefore, Costa *et al.* (2015) have developed such a system, to evaluate decrease in muscle rigidity in the wrist joint during DBS surgery, to meet the needs in the Functional Surgery and Movement Disorders Unit of Hospital São João. This system will be further improved during the course of the thesis and respective range of application broaden. For now, in this section, their approach will be introduced in detail.

3.1 System architecture

The architecture of the system is summarized in Figure 3.1. This comprises of an Motion Mote (MoMo), a Bluetooth-enabled Inertial Measurement Units (IMU) developed at the Institute of Electronics and Informatics Engineering of Aveiro (IEETA), attached to a textile band, which communicates via Bluetooth with an external device. When this sensor was introduced for wrist rigidity evaluation [14], this was communicating with a personal computer which allowed data visualization and computation of the reduction in rigidity during DBS surgery, through LabView. In later work, an Android mobile application was developed to fulfill that role, in order to improve usability in intra-operatory conditions. This approach, contrary to all others presented in Chapter 2, uses only kinematic information. From the signal of angular velocity acquired, a signal descriptor was computed and related to a percentage of rigidity reduction through a second-degree polynomial function. Currently, the system is patent pending.

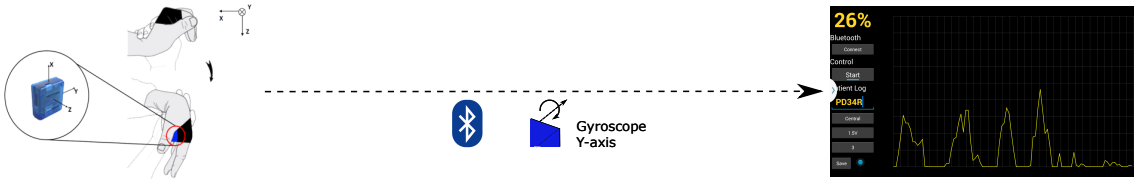

Figure 3.1: System architecture: IMU communicates with a personal computer or to a smartphone.

3.1.1 Measuring device

The MoMo is relatively small which allows its use in the hand for assessment of rigidity (see Figure 3.2). This comprises of:

- an Invensense's ITG-3200 gyroscope (range of $\pm 2000^{\circ}/s$)
- an accelerometer KXTF9-1026 by Kionix (ranges of $2g$, $4g$ and $8g$)
- a Honeywell's magnetometer, HMC5883L (minimum range of $\pm 1,0 \times 10^{-4}$ T and maximum of $\pm 8,0 \times 10^{-4}$ T)
- a battery, allowing the MoMo to stream data continuously up to a full day on single charge
- a microcontroller, transmits the data at about 42 Hz from these sensors to a synced device.

Each of the sensors has its own axis orientation, represented in Figure 3.3.

3.1.1.1 MoMo Workflow

Once the MoMo is turned on through a switch, it becomes visible to other bluetooth-enabled devices. Upon request for connection, if they have never connected previously, these have to be paired using the code '0000'. MoMo may work on three different operation mode and one should be selected at start-off by the paired device. Those are for streaming data, either in quaternion, sensor raw data plus quaternion and quaternion plus euler angles (send 'q', 'r' and 'e' respectively).

3.1.1.2 Data Packages and value conversion

Regarding the raw data from the MoMos, this is structured in such a way that the data correspondent to each sensoris preceded by a characteristic identifier and, then, the measurement for each axis is sent successively. This is shown in Table 3.1, where the second and third row represent the number of bits used to represent each value and the range of each sensor, respectively.

The data for each sensor needs to be set in physical units, based on the following equations, where x is the raw data value and g is the gravity acceleration:

$$a = \frac{(x-127)}{64} g(m \cdot s^{-2}) \tag{3.1}$$

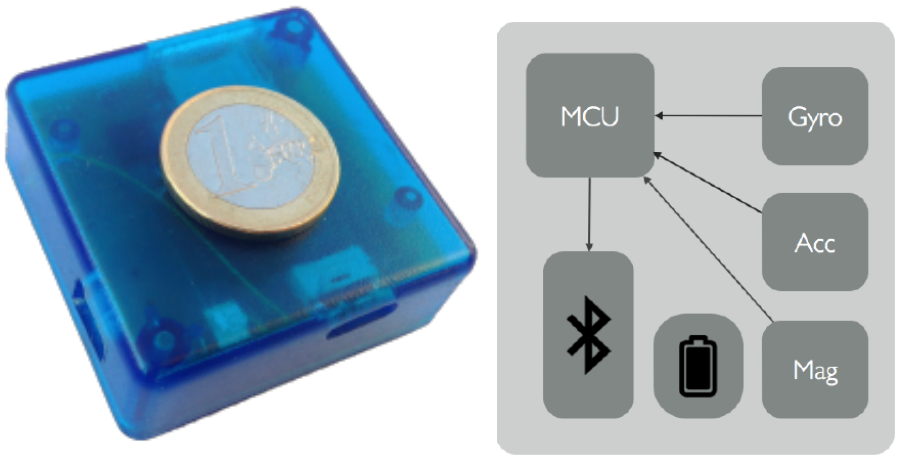

Figure 3.2: Representation of MoMo's architecture

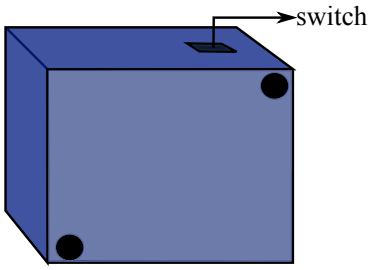

(a) MoMo orientation.

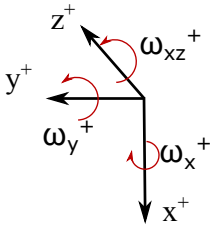

(b) Accelerometer and Gyroscope axes.

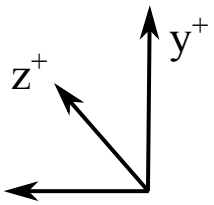

(c) Magnetometer axes.

Figure 3.3: Orientation of MoMo axes.

Table 3.1: Structure of raw data package (identifier in hexadecimal) and sensors' bit resolution and range.

240300	x y z	**240301**	x y z	**240302**	x y z
Accelerometer	8 bit $\pm 2000\ ^\circ/s$	**Gyroscope**	16 bit $-2.000\ g$ to $+1.984\ g$	**Magnetometer**	12 bit $\pm 1,0 \times 10^{-4}\ T$

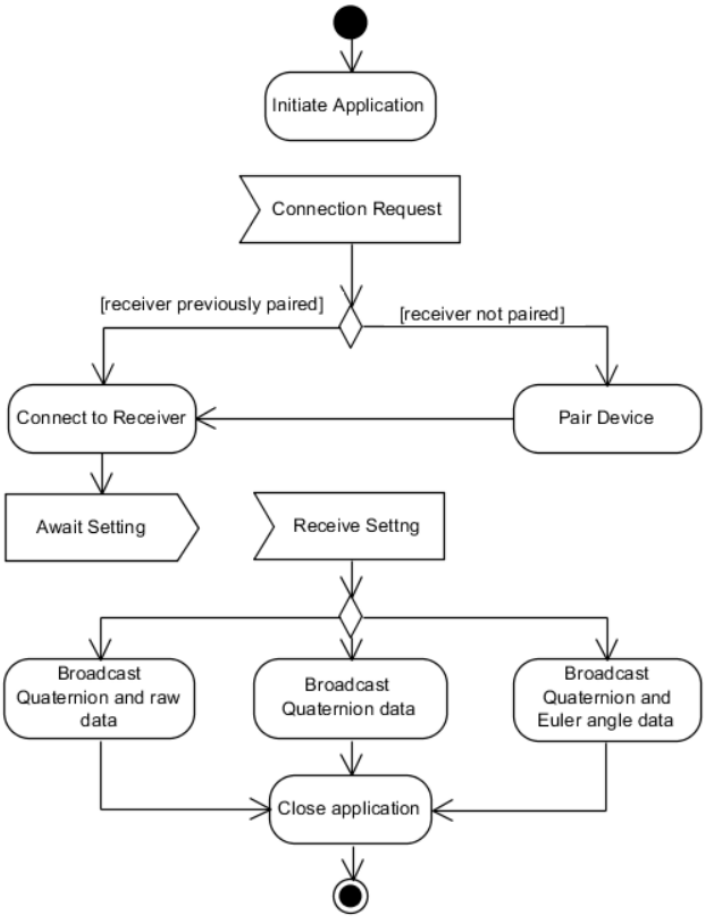

Figure 3.4: MoMo Activity Diagram

$$\omega = \frac{x}{32767} 2000(^{\circ}s^{-1}) \tag{3.2}$$

$$B = \frac{x}{2047} 10^{-4}(T) \tag{3.3}$$

The firmware of the MoMo normalizes the gyroscope values using the other sensors, to ensure that the measurements are given considering the reference axis as the MoMo rather than "world coordinates". This allows great flexibility in its use by a physician when handling the patient's hand. Furthermore, no calibration is required.

In present work, only gyroscope data from the y-axis (correspondent to the direction of hand flexion/extension) is being used. Additionally, the MoMo is attached to a textile band to be worn by the patient.

3.1.1.3 Frequency assessment

To determine the rate at which the MoMo was broadcasting data to the computer, acquisition of data was performed for a minute with Realterm. 20 trials were made and the frequency found was

of 50.07±0.14 Hz. Thus, higher than indicated in other sources [14, 47].

3.1.2 Receiving device

Both LabView and Android requested, at kick-off, similar information: a patient identifier, stimulation electrode (anterior, medial, lateral and central) and voltage of stimulation (0 to 4 V). In particular the activity diagram of the mobile application when initiating is in Figure 3.5. A screenshot is presented in Figure 3.6)

After device pairing, raw data broadcasting by the MoMo and its reception from an external device, only the part of interest is extracted (later detailed). When a significant amount of samples has been collected, they are used to compute and provide the user with the calculated percentage of rigidity improvement. While the device is acquiring and classifying, it is also saving the data into a text file that can be parsed by a custom-made script.

3.2 Acquisition, processing and classification

3.2.1 Acquisition Protocol

The system was used during the bilateral DBS surgery (both to the STN and GPi) of parkinsonian patients, while an examiner was assessing the improvement in rigidity for different stimulation settings. The subjects had their medication withdrawn 12h prior to the procedure and were under local anaesthesia during the surgical intervention. A stereotactic target for stimulation and a trajectory for the electrode were defined beforehand based on medical imagery. Electrophysiological exploration was done during surgery in order to define the best electrode placement. The stimulation frequency was set at 130 Hz; voltage and placement were varied while rigidity was assessed, by imposition of passive wrist flexion. Definite conditions of stimulation were agreed by two experienced physicians. The textile band (with the attached sensor) was worn in the hand by the patient while optimal settings were being searched. The MoMo was synced with an external device (initially a computer, later, a smartphone), which received the raw data and decoded it. From then on, the physician expressed the improvements in rigidity as percentage of rigidity reduction, in a decimal scale between 0% and 80%. For each signal acquired (length of 300 samples), this medical label was registered.

There were two evaluation phases prior to this thesis work. In the first, where a computer was used as a receiver, a total of 48 (from 12 limbs) signals were used to train a model, whereas 156 (from 8 limbs) to test it; while later, for the mobile application validation, 97 were used to train (from 16 limbs) and 83 (from 10 limbs) for testing.

Initially, the medical label assigned to each signal (correspondent to the decrease of rigidity with DBS) ranged from 0% to 80%, where 80% was considered the optimal reduction with DBS. For a later rigidity reduction model, only labels from 40% onwards were considered to build it because (1) slight improvements are harder to be assessed by an examiner, and (2) such reductions

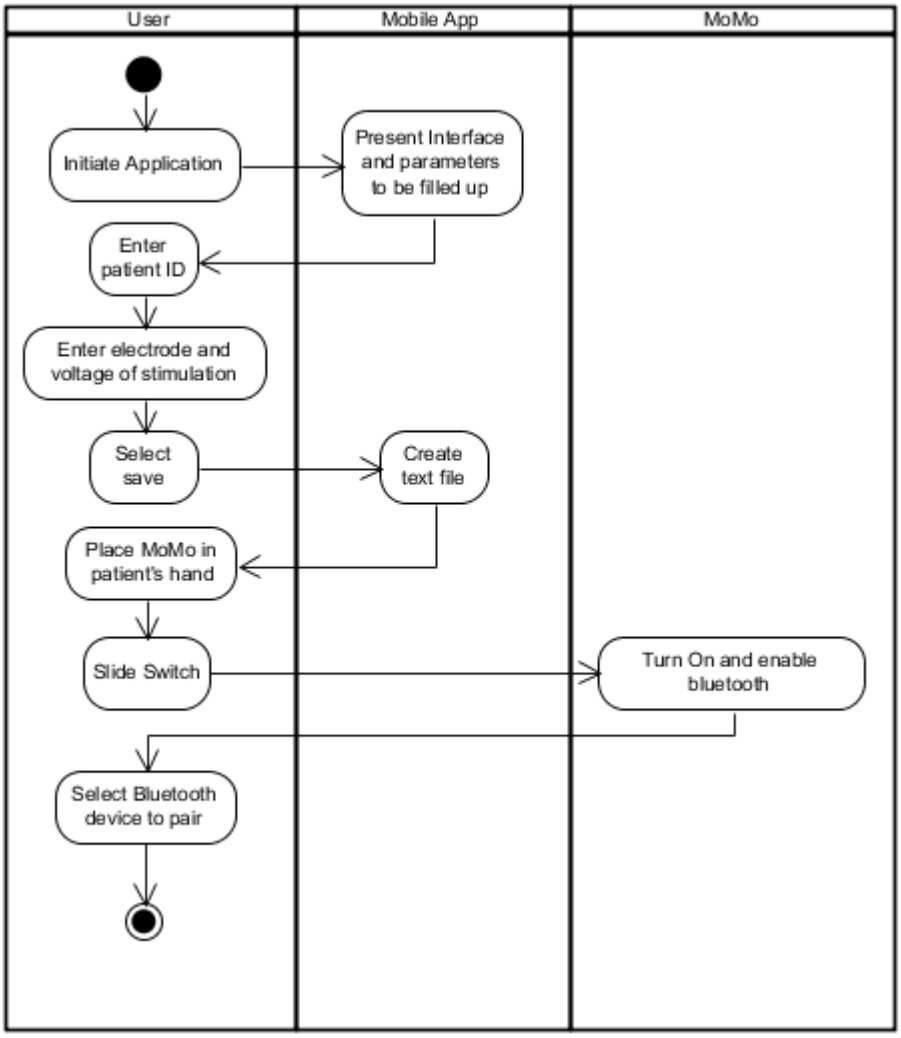

Figure 3.5: Activity Diagram for the initialization of the acquisition.

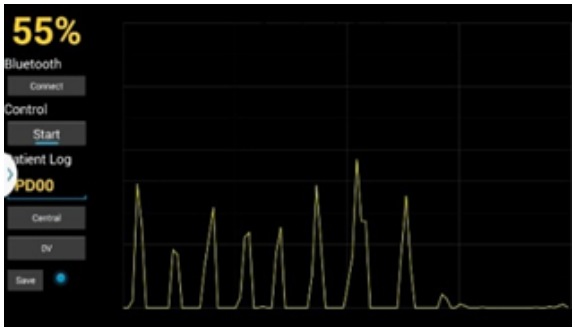

Figure 3.6: Interface of mobile application while acquiring and classifying data.

have no clinical relevance, therefore, the correct classification of more significant improvement is pivotal.

This procedure of acquisition was kept constant from previous work and over the course of this thesis work.

3.2.2 Signal processing

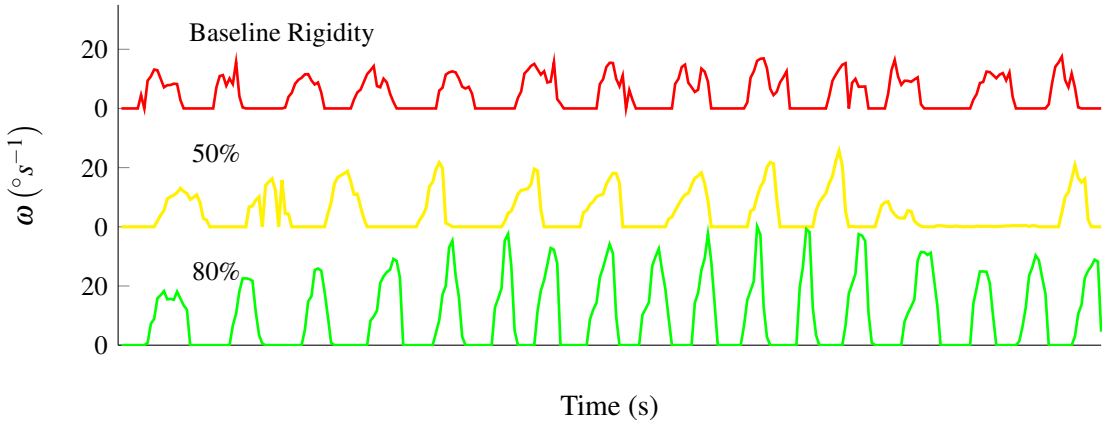

Figure 3.7: Example of angular velocity signals correspondent to when baseline rigidity was being assessed (UPDRS score of 3), to 50% and 80% improvement in rigidity. Each arcade corresponds to a wrist flexion. With reduction of rigidity, it is clear that the signal becomes smoother and higher peak values are achieved.

The signal acquired (rotation over the y-axis of the gyroscope) is invariant to the hand supination/pronation and position and is converted to angular velocity using Equation 3.2. Only the part of the signal relative to wrist flexion was considered (*i. e.* only the negative arcades of the signal). The remainder was set to zero.

As stated before, rigidity is the resistive force to imposed movement, which affects the amplitude, range and smoothness of the angular velocity signal of the wrist flexion, as shown in Figure 3.7. The less rigid is the wrist joint, higher is the velocity achieved by the hand. Moreover, the cogwheel rigidity is easily identified in the baseline conditions as the sudden breaks in the flexion movements.

So, two features may be computed: average angular velocity, μ_ω, and average peak angular velocity, μ_p(Figure 3.8). The peaks considered are the highest values separated by a valley, over a margin of 0.2°/s. These features are expected to have higher value when the joint is less rigid.

In [14], because these features are highly susceptible to the signal's shape (few peaks, flat signal, elongated arches), the signal descriptor ϕ was proposed, combining both features which was expected to lead to a higher discriminative power. This is defined in Equation 3.4.

$$\phi = \sqrt{\mu_\omega \cdot \mu_p} \tag{3.4}$$

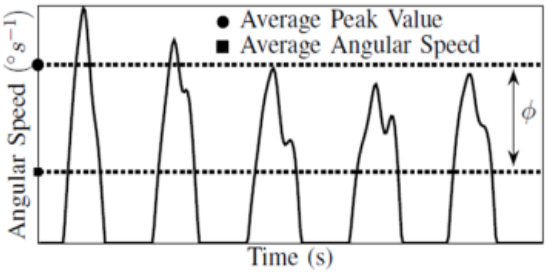

Figure 3.8: Representation of the average velocity and average peak velocity. From [14].

The descriptive power of the aforementioned features were evaluated through statistical analysis using the two-tailed t-test (the normal distribution was checked beforehand by performing Jarque-Bera hypothesis test [48]). Two data clusters were considered: low rigidity reduction, with those signals labeled with 40% and 50% and high rigidity reduction, considering reductions of 70% and 80%. The t-test was performed by assessing whether both followed the same normal distribution.

3.2.3 Model for rigidity improvement

Each signal has its own category, correspondent to the examiner assessment of rigidity decrease with DBS (from 0-80% in steps of 10%). Thus, we can perceive its quantitative assessment as a machine learning problem, where we use a classification approach (the output of the model is a numerical category as those assigned to training data) or a regression one (the model considers the numerical value of the labeling and considers a continuous function to represent the improvement). The choice for this system was the latter, since it allows to indicate sub-scale rigidity states and a continuous evaluation scale. This can be particularly advantageous to distinguish between similar rigidity profiles which are, in reality, correspondent to different physiological conditions.

The training set was used to obtain a second degree polynomial mathematical model that would better relate the perceived improvement in rigidity with the mean value of signal descriptor. The polynomial fitting considered the average value of ϕ for each of the assigned labels by the physician. A higher-degree polynomium could lead to over-fitting to the training data. Other methodologies, such as Support Vector Machine (SVM), k-Nearest Neighbor (kNN), Decision Trees (DT) and k-Means, to model the relationship between the signal descriptor were discarded because they aimed to implement it in a mobile application for *in situ* classification, so light-computing methodologies were privileged.

To test the obtained model, during rigidity assessment in DBS surgery, the percentage of rigidity reduction was compared to the clinical assessment of the physicians: the classification was accepted if it was within a range of $\pm$ 5% away from their evaluation (because doctors use a scale with steps of 10% and we are using a continuous scale). The overall procedure for training and testing is represented in Figure 3.9.

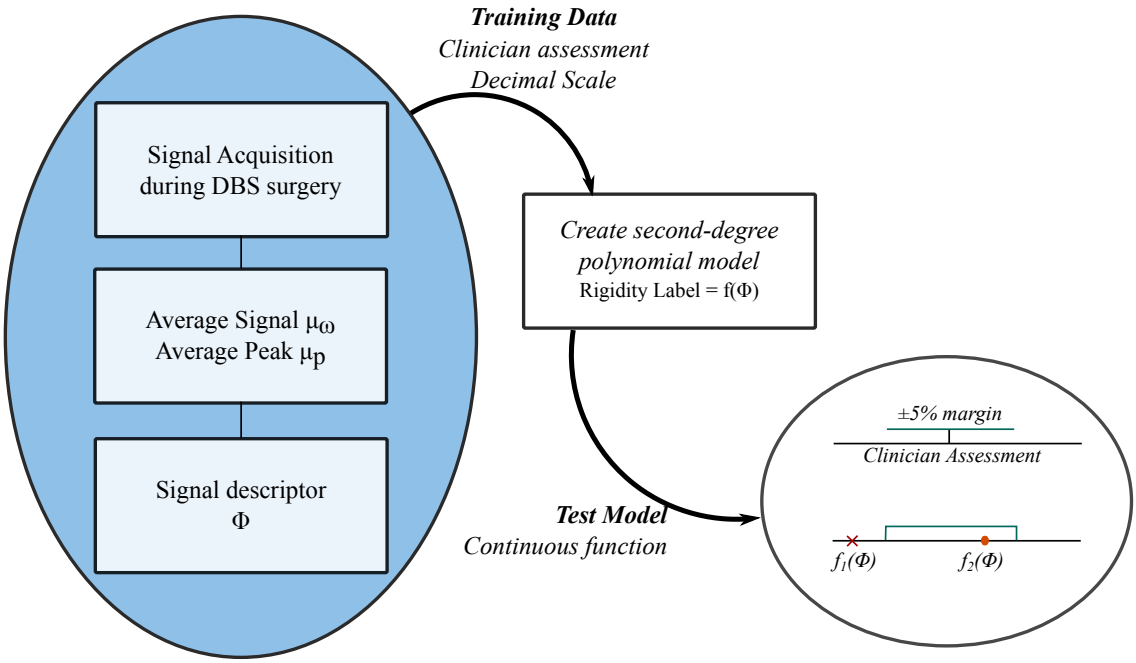

Figure 3.9: Methodology to create and test the model for rigidity reduction based on the signal descriptor ϕ. $f_1(\phi)$ is considered a wrong classification by the model, contrary to $f_2(\phi)$ since it is within the $\pm$ 5% margin.

3.3 Results

The first results were presented at the 37^{th} Annual International Conference of the IEEE Engineering in Medicine and Biology Society [14]. Here, the system presented relied on a personal computer running LabView to apply the model obtained. After this proposal, the same authors developed a mobile application to classify *in situ*, during the surgery, the input signal and to provide real-time feedback, by having an assistant holding the smartphone in the operating room.

In both cases, the discriminative power of ϕ, μ_ω and μ_p was assessed, whose results are presented in Table 3.2. This shows that, indeed, the use of the signal descriptor was slightly more able to distinguish low and high severity rigidity by revealing a smaller p-value; however, with a larger dataset, all of the aforementioned features show a statistically significant difference, with $p < 0.001$. So, a good prognosis can be made that a good correlation will be found between the signal descriptor and the rigidity label, which indeed happens in the presented model. As expected, greater values of the descriptor are associated to a more significant reduction in rigidity: such decrease would allow higher velocities to be achieved during the wrist flexion and consequently both μ_ω and μ_p are higher.

In Figure 3.10, the polynomial function achieved for both situations are presented. In the later approach, only improvements of $\geq 40\%$ were considered to build the model: low reductions in rigidity are harder to be assessed by the examiner, and, in common practice, lower values do not satisfy the the least improvement expected, so have no clinical relevance and, thus, it is more important to assess correctly more significant improvements. By removing the lower rigidity

Table 3.2: Summary of results for features descriptive power, considering 48 and 97 signals for the implementation in Labview (Evaluation Phase 1) and in the mobile application (Evaluation Phase 2), respectively. HR and LR stand for high and low rigidity, respectively.

Evaluation Phase		**1**		**2**	
Rigidity Severity		**HR**	**LR**	**HR**	**LR**
μ_ω	*Mean*	3.33	12.9	4.59	7.76
	Std	0.58	3.13	0.89	1.42
	p	0.034		<0.001	
μ_p	*Mean*	12.9	29.9	12.91	22.87
	Std	3.13	6.60	3.89	5.14
	p	0.029		<0.001	
ϕ	*Mean*	6.55	11.3	7.76	13.03
	Std	1.22	3.07	1.19	2.55
	p	0.027		<0.001	

values, we allow the fitting function to adapt better to the data that is more clinically relevant. A good fitting in this higher range is actually achieved as seen in the functions representation.

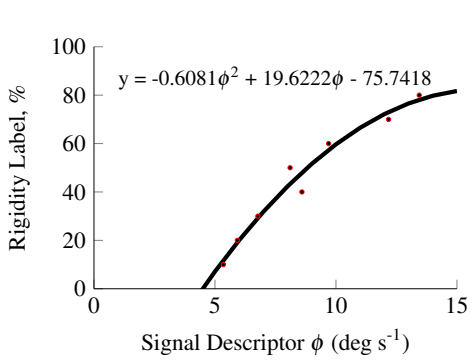

(a) Adapted from [14].

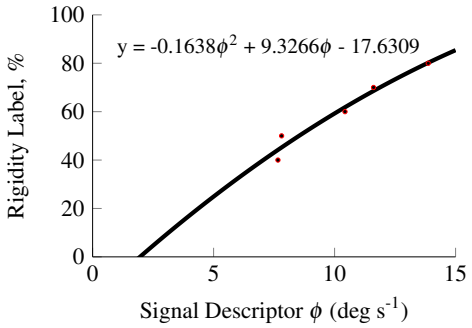

(b) Used in Evaluation Phase 2 (with a smartphone).

Figure 3.10: The polynomial functions that best correlate the wrist rigidity and the average value of the signal descriptor ϕ for a given percentage of rigidity reduction (*i. e.*, rigidity label).

In published work (using LabView and a smaller dataset), an accuracy of 83.9% was obtained, while the latter revealed 77.1% of accuracy and a mean error of classification of 3.2% (Table 3.3). Also, in Table 3.4, the percentage of wrong classification *per* range of rigidity reduction is presented, which shows a higher misclassification in the lower range of rigidity reduction. This translates into a better performance of the system when it needs to: on the detection of higher reduction of rigidity, which correspond to possible electrode implantation profiles.

Table 3.3: Results from the different phases of model evaluation. The number of signals (limbs) used for training and for testing are presented. Phase 1 corresponds to when the receiving device was a computer and Phase 2 when a smartphone was used.

Evaluation Phases	**1** (EMBC'15)[14]	**2** (NeuroIberia'16)[49]
Train	48 (12)	97 (16)
Test	156 (8)	83 (10)
Accuracy	83.9 %	77.1 %
Test Error	-	3.3±3.4 %

Table 3.4: Distribution of wrong classification by the system according to the medical label for rigidity reduction.

Improvement range (%)	**Percentage**
(40-50)	42%
60	32%
(70-80)	26%

3.4 Discussion

In both cases, a good accuracy was achieved (around 80% in both cases), which support the reliability of the proposed solution. Also, the error of classification of 3.2% (mean absolute deviation of the system classification from the medical label) supports that this model represents them quite well, even when we are comparing a continuous scale with a decimal one, which by itself is an inherent source of error.

Both models have shown a higher capacity to classify significant recoveries (70%-80% reductions in rigidity). This improved performance backs up the use of this system to support the physician decision when comparing possible final settings for stimulation (those which lead to more significant rigidity reduction), thus where we find clinical relevance. The main difficulties were found when distinguishing high and intermediate rigidities, which could be already predicted based on the corresponding fitting found in Figure 3.10: here, the mean values of the signal descriptor in the lower range of reduction do not fit the function as well as the remaining values. This could be associated with a higher difficulty by the examiner to distinguish smaller improvements. Also, cogwheel rigidity may play a role for small improvements, where it may still be present: it causes a higher variability in the average angular velocity and average peak angular velocity, causing the model fitting to worsen.

In the introduction to this work [50], conditions of use for the device were identified. Because only the angular velocity around the y-axis of MoMo, the imposed flexion should be such that largest amplitude occurs on the y direction and avoid rotational movements which do not comply with that. Moreover, it is expected that the force applied by the physician does not vary greatly over the course of DBS surgery and between surgeries as well. This system requires some training of the examiner in terms of imposed force intensity, so the system provides a valid result.

Furthermore, it is important to emphasize that reduction in rigidity is not linearly related with the range and amplitude of angular velocity. The presence of the cogwheel rigidity artifacts are of utmost importance and affect greatly the perceived rigidity. In this sense, the described approach does not encompass the presence and disappearance of this feature of parkinsonian rigidity: μ_ω, μ_p and, consequently, ϕ do not translate the smoothness of the signal, overlooking this cardinal characteristic. A first approach for the detection of these artifacts in presented in Section 3.5.

Besides, the provided improvement is computed in relation to an average rigidity state, determined by the training dataset used for modeling rigidity reduction.

3.5 Detection of cogwheel artifacts

As evident in Figure 3.7, the shape of the angular velocity signal for baseline rigidity is not smooth: some jerks done by the muscles occur, which characterize cogwheel rigidity. To the author knowledge, there is no proposal for identification of these events other than by Costa *et al.* [14]. These jerks lead to the occurrence of a local-minima in the angular velocity signal during a wrist flexion. Thus, for their detection, all peaks and valleys in the signal were identified and every triangle pos-

sible enclosing the valley and the two immediate neighboring peaks was drawn, as represented in Figure 3.11a. Smoother signals will have larger triangles whereas cogwheel-parts lead to smaller and tilted triangles. The detection criterion is as follows:

$$h \cdot (\Delta t \cdot A)^{-1} < \lambda \tag{3.5}$$

where h stands for the distance between the valley and the midpoint between the flanking peaks, Δt is the time span of the triangle, A is the area and λ is the threshold value for the detection of a cogwheel artifact. For optimization of the threshold and assessment of the accuracy, a ROC curve was built [51], using some training signals, whose ground-truth had been previously agreed between observers.

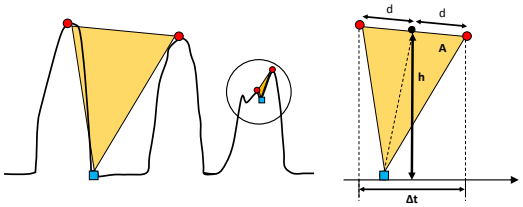

(a) Cogwheel effect is detected defining triangles from fiducial points. From [14].

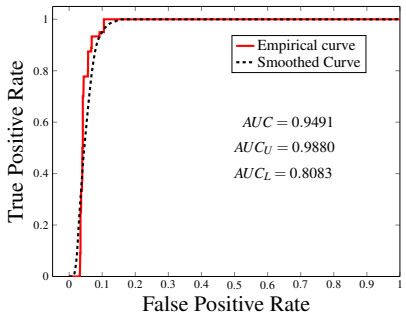

(b) The ROC curve for the detection of cogwheel artifacts on the angular speed signal. Optimal operating for $\lambda \bar{1}00$.

Figure 3.11: Detection of cogwheel rigidity artifacts.

The analysis of the ROC curve (Figure 3.11b) tell us that the optimal threshold λ is 100, yielding a sensitivity of 0.93. The low computational requirements and simplicity of this method are extremely appealing for *in situ* processing. Still, few signals were considered (30) at the time and is only applicable after acquiring the whole signal, so further work is needed, especially because, as mentioned already, this is a cardinal feature of parkinsonian rigidity and important for its assessment.

3.6 Preliminary studies

In the monograph report [50], the methodology of building a polynomial model was compared to other regression and classification approaches (support vector machine, regression and classification decision-trees, k-means and k-nearest neighbors) and the first was confirmed as the most adequate for the problem at hand (as in Appendix C). Besides, some other potential features were extracted from the angular velocity signal and their ability to discriminate different levels of rigidity was confirmed. However, as it is the case of the already in-use, average angular velocity and average peak angular velocity, they do not properly depict the shape of the signal, hence the occur-

rence of cogwheel artifacts is overlooked. This was set as one of the pivotal goals of this thesis' project.

An interesting finding was how early this polynomial modeling approach performance stabilized, in terms of data size required for training: with 85 signals, the error stabilize at around 8.4%. This fact leads to the conclusion that no further improvement in performance should be expected by only increasing the data-set. Also, if it were to be applied in a new hospital, quickly the model could be trained and used. New approaches may be explored, but there should be significant focus on exploring other applications of this system.

Also, a proposal for a different manner for the context of rigidity was initiated, by exploring the possibility of a multi-model approach, relying on the design of a specific model for different baseline rigidities. This will be further presented in Chapter 4 and respective results.

3.7 Final Remarks: limitations and future work

The use of the MoMo as a sensor and of the overall system, using a smartphone for *in situ* processing has been validated and with good performance. To the best of our knowledge, this is the only proposal for real time evaluation and feedback of reduction in rigidity, appropriate to be used in intra-operatory conditions, during DBS.

However, the improvement in rigidity obtained from the polynomial model originates from a wide variety of patients, whose baseline rigidity differ, *i. e.*, their UPDRS scores before starting stimulation were unregarded. Because the medical scale used is a percentage of reduction in rigidity, this will be a function of the patient baseline state. Thus, the possibility of having a multi-model approach should be explored, *i. e.*, considering the baseline signal acquired at the beginning of the medical procedure or the UPDRS scale assigned by the clinician, select the most appropriate model for such rigidity, obtained from previous training.

The premise of this analysis is that the assessment is being performed correctly, *i. e.*, in any way the patient is actively trying to counter or help in bending the wrist. Such behavior could lead to undesired rigidity profiles and it is the doctor's task to discard these cases. In our application it is easy to do that because, after indication of the surgeon, we can label these signals as "invalid".

Moreover, this kinematic-based approach is highly dependent on the consistency of how the clinician imposes wrist flexion due to its velocity dependency. A decrease in wrist rigidity signifies less resistive force to imposed movement and, if a clinician applies about the same force for each

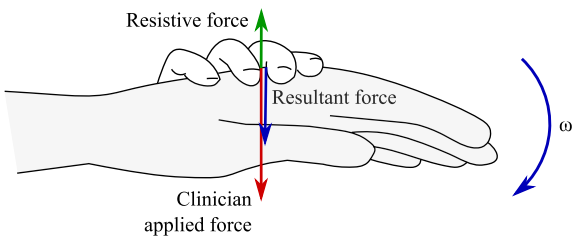

Figure 3.12: Forces involved in passive wrist flexion.

assessment, then higher values of angular velocity will be achieved. Nonetheless, if the clinician, when feeling less resistance, imposes as well less force, then no significant change in velocity will occurs, thus no improvement or less than expected is computed. This is a fragility of the system because it perceives only the effect of the resultant force (see Figure 3.12). Other approaches introduced in Chapter 2 had a gyroscope for measurement of angular velocity combined with a force transducer to measure the applied force by the clinician. Also, when assessing the reduction in rigidity, the presence and disappearance of cogwheel rigidity plays a role as well. So, just considering the amplitude of the signal is not enough. Hence, a reliable method for detection of this event and its inclusion into the model is needed.

The system classifies every train of 200 samples, so at least one full signal of 4 second should be captured with significant information, meaning that if the patient is not cooperating (by actively flexing the wrist) or the signal has few flexion events these hinder an adequate classification by the model. The latter case will influence the classification because it might lead to a low average angular velocity, whereas the few existent peaks reveal a high amplitude of the signal pointing to a significant improvement.

Other than the potential of this system for decision support, it could help conceiving a system for teaching, to help new examiners in the assessment of rigidity. However, this could be hampered by the fact that no measurements of the resistive work were made and at least some reference would be needed in order to properly recreate the situation. An approximation could be used to normalize the measurements and by profiling the different rigidity status, and using a robotic arm to reproduce them so interns can perceive different reductions in rigidity. Withal, this could work as a method to have a closed-loop DBS (detailed in Chapter 6), by having stimulation only when it is required (*e. g.*, detection of a large number of cogwheel artifacts on daily life, or the user can perform a specified number of flexions to activate the system and, thus, the stimulator if the rigidity level without stimulation remains high). This increased efficiency (contrary to having constant stimulation) would prolong the longevity of the stimulator battery.

Chapter 4

Rigidity Model

As already ascertained previously during the monograph, using the polynomial model for classification of rigidity was found to be the most suitable approach for the problem at hands. Still, this did not consider the baseline rigidity of the patient, nor did it assess cogwheel rigidity significantly. This motivated the development of a multi-model approach, *i. e.*, design an unique and individual polynomial classification model based on the initial rigidity status of the patient, as perceived by the assessment of the physician's score on the UPDRS scale. In this chapter, a survey over this approach will be introduced, as well as the final rigidity model, after testing all possible configurations and strategies to include baseline information.

4.1 Multi-Model Approach

As mentioned in the Final Remarks of Chapter 3, the existent system computes a general polynomial model for every patient with Parkinson's Disease (PD), regardless of his baseline rigidity. If we go back to Section 1.2.2, the UPDRS scale was introduced and it defines that rigidity may be assessed in a scale from 0 (non-existent) to 4 (severe). Because we are determining a percentage of rigidity reduction, this should be a function of an initial rigidity assessment before any stimulation, either by the physician or by considering the sensor measurements. Therefore, a preliminary study was performed on the ability of the signal descriptor:

$$\phi = \sqrt{\mu_\omega \cdot \mu_p} \tag{4.1}$$

(where μ_ω is the angular average velocity of wrist flexion and μ_p the average peak angular velocity) to discriminate (1) low and high levels of improvement in rigidity within two different groups, where patients were separated accordingly to the initial severity of this symptom and (2) the initial level rigidity severity for equivalent improvements assessed by the physician.

Later, using different approaches to define the signal descriptor (the basis for building the polynomial model), an optimal definition was identified and its validity investigated.

4.1.1 Preliminary study on the signal descriptor

Firstly, the full potential of the aforementioned descriptor, ϕ, to distinguish different levels of rigidity's severity was explored. For that purpose, to every signal acquired, a label was assigned correspondent to the rigidity sub-score in the UPDRS scale assessed by the physician before any stimulation was applied. A total of 237 signals (34 limbs) were then separated between low and high rigidity severity: signal with sub-scores of 1 and 2 were grouped separately from the remainder. The number of signal *per* UPDRS label is presented in Table 4.1. Furthermore, within each cluster , data was separated into low improvement (signals with classification of 40% and 50%) and high improvement (signals with classification of 70% and 80%).

Table 4.1: Number of signals *per* initial UPDRS score.

	Baseline Rigidity (UPDRS)	**# Signals**
Low baseline rigidity patients	1	24
	2	74
High baseline rigidity patients	3	139

Within each group, to test whether their data followed a normal distribution, the Jarque-Bera hypothesis test [48] was performed: if *p-value* of a dataset was over 0.05, then it was considered a normal distribution. The descriptive power of the signal descriptor ϕ was assessed by performing a two-tailed t-test, when both sets (low and high improvement) followed a normal distribution; otherwise, a Wilcoxon rank sum test was used. The mean values of ϕ and its standard deviation were calculated in order to understand the influence of the baseline rigidity on it. The results are presented in Figure 4.1.

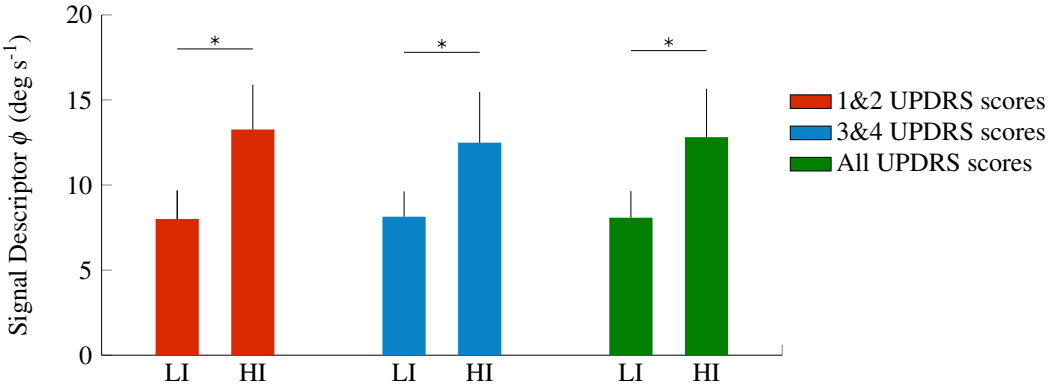

Figure 4.1: The mean + standard deviation of the signal descriptor ϕ are represented. High statistical significance (indicated by *) was found between low (LI) and high (HI) rigidity improvement for both separating the analysis according to initial rigidity UPDRS sub-score and considering the data altogether ($p < 0.001$). ϕ does not distinguish patients with different baseline rigidity.

The descriptor ϕ considering the full dataset and its sub-clusters (according to baseline rigidity), allowed distinction between low and high rigidity-related improvement. However, its mean values for low and high reduction in rigidity across initial rigidity scores are similar, contrary to the expected. For someone with more severe rigidity, his starting velocity range and amplitude is expected to be smaller and, consequently, smaller ϕ. By the same reasoning, for an equivalent improvement, this person would also have a smaller ϕ than someone with lower baseline rigidity (lower initial UPDRS score). However, Figure 4.1 shows such a difference does not exist: both cases have similar mean values and even standard deviations. Consequently, we may conjecture that the polynomial functions of the personalized models would be alike the model obtained using a general approach and no improvement in accuracy would occur relying only in ϕ. This could be related to the cogwheel rigidity, which is unregarded. This feature highly distinguishes rigidity scores of 2 and 3. We hypothesize that by including into the signal descriptor this effect, models that effectively consider the baseline rigidity could be obtained and, thus, improve the performance of the overall system.[1]

4.1.2 Proposal of multi-model

Using only ϕ, as analyzed previously, may lead to no improvements. Therefore, it was hypothesized that a different signal descriptor could be used for each cluster of rigidity severity. For that purpose, other different kernels functions were considered. These are common practice in machine learning to project features, from a domain N, being N the number of features, to a higher dimension $N+1$, by recurring to kernel functions. These rely on the combination of features to achieve better data separability in the dimension $N+1$, leading to more distinct averages or centroids. Such fact enables better recognition of patterns in the data.

Hence, the performance of using the kernel functions in Table 4.2 as signal descriptor was assessed, by comparing the training error of the polynomial model, computed as the Leave-One-Out error, whose procedure is as follows:

1. split entire dataset into training and test dataset, where the latter is composed by a single sample, i ($\phi_{ttest} = \phi_i$), randomly selected

2. training dataset is used to determined the best fitting polynomial model, $P(\phi)$ (in a least-squares sense), relating ϕ and the rigidity label (reduction perceived by the physicians)

3. compute the rigidity label for the test sample, $RL_{\text{test}} = P(\phi_{\text{test}})$

4. determine absolute difference between real rigidity label (assigned by a physician) and the one given by the polynomial model ($error = |RL_{\text{physician}} - RL_{\text{test}}|$)

5. repeat from 1. onwards if number of iterations intended was not reached

[1] These results were presented in the international neurosurgery congress NeuroIberia 2016 [49]. The respective abstract may be found in Appendix D.

The leave-one-out error of each model was the average and standard deviation across all 2000 iterations performed. Each of these iterations simulates a classification that would be given by the system in the operating room. An optimal descriptor was found for each rigidity UPDRS sub-score. 237 signals from 34 limbs were considered.

Table 4.2: List of kernels for regression.

Kernel	$k(\mu_\omega, \mu_p)$
Hellinger's	$\sqrt{\mu_\omega \mu_p}$
Intersection	$\min(\mu_\omega, \mu_p))$
χ^2	$2\frac{\mu_\omega \mu_p}{\mu_\omega + \mu_p}$
JS	$\frac{\mu_\omega}{2} log_2\left(\frac{\mu_\omega+\mu_p}{\mu_\omega}\right) + \frac{\mu_p}{2} log_2\left(\frac{\mu_\omega+\mu_p}{\mu_p}\right)$
Gaussian Homogeneous	$\sqrt{\mu_\omega \mu_p} \cdot exp\left(-\frac{log\left(\frac{\mu_p}{\mu_\omega}\right)^2}{2\sigma^2}\right)$

4.1.3 Results and Discussion

For the different definitions of the signal descriptor, the results are presented in Figure 4.2.

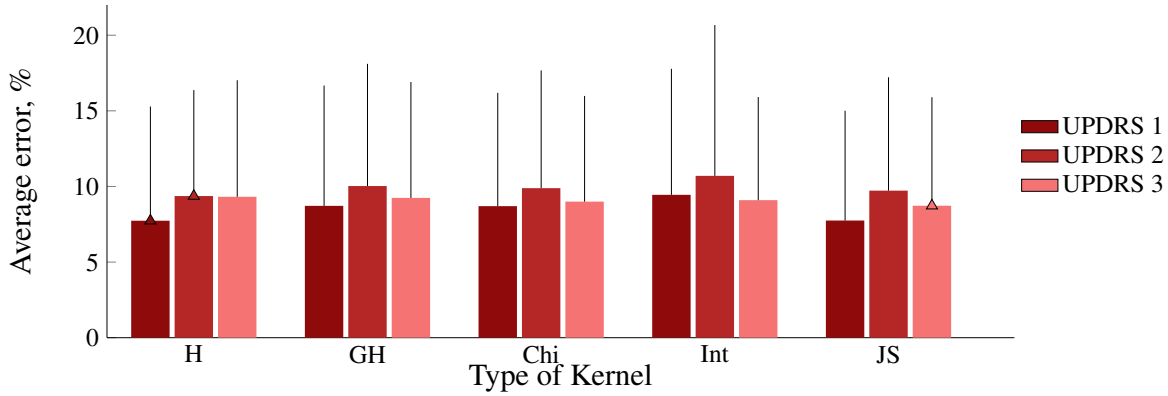

Figure 4.2: Finding an optimal descriptor to be used in the polynomial model, for each baseline rigidity severity level. The mean values + standard deviation are represented and minimum error for each UPDRS sub-score is represented with a triangle. H stands for Hellinger's, GH for Gaussian homogeneous, Chi for Chi-square, Int for intersection and JS for Jensen-Shannon divergence.

On one hand, for both 1 and 2 sub-scores of rigidity, the Hellingers kernel, *i. e.*, the same as the described in Chapter 3, presents less training error ($7.7 \pm 7.6\%$ and $9.4 \pm 7.0\%$, respectively). On the other hand, the remainder achieves a minimum training of $8.7 \pm 7.1\%$ when considering the JS kernel. The correspondent polynomial models are represented in Figure 4.3. To emphasize the fitting of the mean values of ϕ_{34} for each step of improvement with the correspondent model, over the whole range of improvement. For signals acquired from patients initially less rigid and

experiencing a low reduction of rigidity under stimulation, we can identify a worse fitting. This translated directly the difficulty for the examiner to identify small differences for stimulation stages when the baseline is itself low rigid and with a signal shape closer to that under stimulation.

The polynomial models which lead to the lowest training error for each baseline rigidity cluster (Hellinger's and Jensen-Shannon kernel functions) were used to test a multi-model system during DBS surgery (38 signals from 4 limbs). With these, approximately, the same accuracy was achieved as before (82.0% against 83.9% [14] and 77.2%, considered as in Chapter 3), by using a larger training set and by defining a model for two levels of baseline rigidity. The error of classification of 3.4% supports that this model representative, even when we are comparing a continuous scale with a decimal one. Also, cogwheel rigidity may play a role for small improvements, where it may still be present: it causes a higher variability in the average angular velocity and average peak angular velocity, causing the model fitting to worsen.[2]

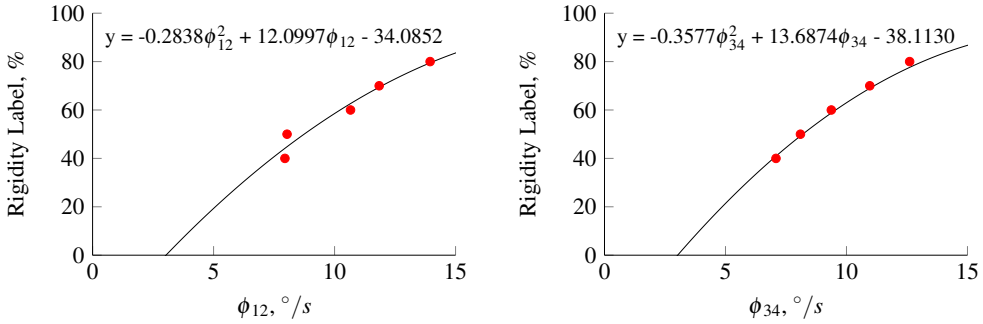

(a) For patients with low rigidity severity in the multi-model approach.

(b) For patients with high rigidity severity in the multi-model approach.

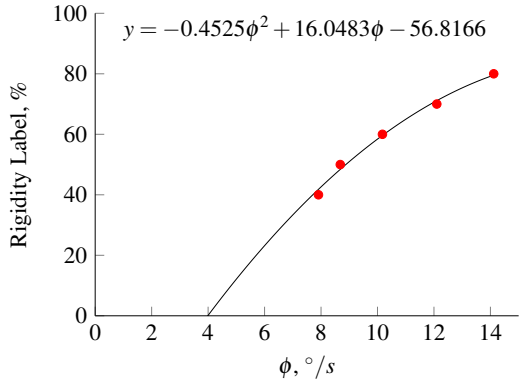

(c) Final Polynomial model tested.

Figure 4.3: Polynomial models obtained with different signal descriptor ϕ_{12} and ϕ_{34} for the multi model approach and final model obtained.

[2]These results were submitted as a 4-pages conference paper in the 38^{th} Annual International Conference of the IEEE Engineering in Medicine and Biology Society (EMBC'16), accepted and appointed for lecture [15]. This paper may be found in Appendix B.

4.2 Final Rigidity Model

As the multi-model approach lead to no significant improvement (at least, with the available dataset), the initial approach was pursued (*i. e.*, one single model for the whole dataset, iteratively improved after each surgery with new signals). This has the advantage of reducing steps in the mobile application usage (which can be considered as an additional error source), specially when no increase in performance is expected.

Using a dataset of 301 signals, which lead to the model in Figure 4.3c, a model similar to the previous was obtained, with a $R = 0.9926$ and a training error of 8.7 ± 7.7 %. For evaluation of the model, the same procedure as previously was undertook.

A total of 56 signals were evaluated, where 41 were correctly classified (accuracy of 77.1%), with an error of 4.2 ± 5.1 %. These results had a correlation of 0.85 with the assessment of the two physicians and during DBS surgery.

4.3 Overview of results

In order to have an understanding of the evolution of the validation results over the different phases, Table 4.3 presents the respective number of signals (and number of limbs) used from training the model and to test it, as well as the achieved training and classification error.

Table 4.3: Results from the different phases of model evaluation. The number of signals (limbs) used for training and for testing are presented.

Evaluation Phases	**1** (EMBC'15)[14]	**2** (NeuroIberia'16)[49]	**3** (EMBC'16)[15]	**4**
Train	48 (12)	97 (16)	237 (34)	301 (31)
Test	156 (8)	83 (10)	38 (4)	56 (8)
Accuracy	83.9 %	77.1 %	82.0 %	77.1 %
Test Error	-	3.3 ± 3.4 %	3.4 ± 3.6 %	4.2 ± 5.1

The consistency of these results (always over 75% of accuracy) lead to the conclusion of the suitability of the polynomial approach to model the reduction in rigidity and its ability to actually support in real-time the physician in his rigidity assessment. The training error similarity support previous results (Appendix C) about the influence of the training dataset size. All these phases encompassed the use of a polynomial model, with the particularity of the 3^{rd} using multiple model design, adaptive to the baseline rigidity UPDRS score. This proves the limitation of kinematic measures in further distinguishing different rigidity levels since both approaches lead to similar results, even though differences were expected. It was envisioned that the detection and inclusion of the cogwheel effect on the wrist flexion would be a pivotal step, which is introduced and explored in Chapter 5. It was hypothesized that the integration of velocity-related information and occurrence of cogwheel artifacts could compensate the variability on the physician's force to impose movement.

As already mentioned, the validation in a single center performing DBS surgery has been achieved. Still, this it an isolated case, requiring further proof of concept in other settings/practices, to prevent over-fitting to the two physicians. In that sense, the purview of this project must encompass broadening the clinical partners, to build a diversified dataset.

Chapter 5

Cogwheel Rigidity

Under the assumption that the applied force by the physician is approximately the same over several trials, a procedure to evaluate the reduction in rigidity was developed relying on a signal descriptor extrapolated from the amplitude of the signal. In Chapter 4, the baseline rigidity, given by the doctor's UPDRS rigidity sub-score, was considered in the development of models of rigidity reduction specific for different initial rigidity severity. However, this multi-model approach, relying on the amplitude of the flexion velocity signal, did not enable a more accurate feedback on the rigidity reduction occurred. Hence, it was hypothesized that the shape of this signal would be a pivotal step to upgrade the system, because it translates the smoothness of the wrist flexion and to a cardinal signal of parkinsonian rigidity, cogwheel rigidity.

5.1 Cogwheel Phenomenon

As previously described, parkinsonian rigidity is characterized by the occurrence of the cogwheel phenomenon, which is more noticeable in the wrist than in the elbow. The "cogwheeling" is caused by episodic bursts of muscle potential which lead to increment of resistance [10]. In terms of angular velocity, this leads to sudden decreases over the wrist flexion movement, as depicted in Figure 5.1.

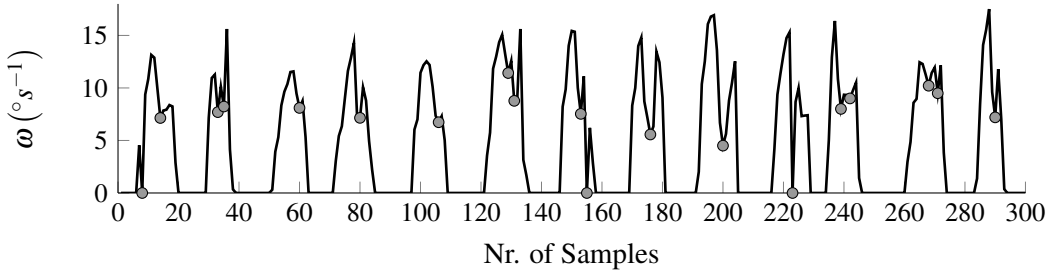

Figure 5.1: Example of angular velocity signal of consecutive hand flexion movements where the circles indicate cogwheel artifacts.

5.1.1 Dataset description

In this section, 186 signals were used from 9 patients (17 limbs) and their distribution according to their baseline rigidity UPDRS is in Table 5.1.

Table 5.1: Number of signals *per* initial UPDRS score.

Baseline Rigidity (UPDRS)	# Signals
1	24
2	74
3	89
4	0

5.1.2 Detection of cogwheel rigidity

5.1.2.1 Approach

When conceiving the detection technique of these events, simplicity was a goal in order to lessen the processing burden and, hence, not hamper the real-time feedback.

The valleys were identified and for them to be classified as cogwheel events, three criteria were considered:

- the local average within a 5-samples window is over a given threshold λ_1;8
- the smaller neighboring peak of the valley has an amplitude equal or over λ_2 (%) of the average peak angular velocity of the same signal;
- the neighboring peaks that shape a valley are within 15-samples window.

To optimize the parameters λ_1 and λ_2 and to evaluate the performance of this approach, the agreement of 4 observers was considered in 30 signals (as indicated in [52]) of angular velocity correspondent to the passive wrist flexion imposed by a physician during DBS surgeries. To define this ground truth, the observers were explained about the context of the problem and, in particular, about cogwheel rigidity and they were asked to indicate in a previously defined set of 30 signals where this phenomenon had occurred.

At first, the thresholds λ_1 and λ_2 were considered alone and, only latter, combined. These methodologies were compared using Operating Characteristic (ROC) curves.

5.1.2.2 ROC curves

These ROC graphs allows comparison between classification methodologies, representing the trade-off that exists between true positives and false positives. They are depicted in two-dimensional

graphs where the true positive rate (TPR) is plotted against the false positive rate (FPR) [53]. TPR and FPR are defined as follows:

The optimal classification methodology is one that correctly identifies every positive and never gives off a false alarm (false positive). However, that is never the case so the goal is always to reach an optimal proportion of FPR and TPR, appropriate to the problem at hands.

The overall information given by ROC curves may be represented by the area under the curve (AUC). This is a proportion ranging from 0.0 to 1.0 In particular, if the ROC curve were a diagonal between (0,0) and (1,1), which translates a random performance of the correspondent classifier, we would have an AUC of 0.5. This may be perceived as a boundary which defines whether a classifier is realistic (AUC over 0.5) or otherwise (AUC lower than 0.5) [53]. AUC translates the probability of a classifier of ranking a randomly chosen positive instance higher than a randomly chosen negative chosen negative instance. To be noted that a classifier, even though having higher AUC, may not have better performance in the whole ROC space. Still, AUC is considered a good tool to predict classifiers performance [53]. For parameter optimization, the thresholds were the values correspondent to the point of the ROC curve closest to the (0,1) coordinate of the ROC space.

5.1.2.3 Results on the cogwheel detection

When defining the ground truth, which relied on the cross-observer agreement, an accuracy of almost 61% was found. This relatively low agreement is related to the fact that no margin relative to the events detected by the observer was considered, hence some selections by different observers, which were in consecutive samples, were not considered. This zero-tolerance was applied because there are single-sample cogwheel artifacts.

Then, the use of a single or two thresholds into the detection method was compared, by using ROC curves analysis. λ_1 ranged from 0.001, 0.010 and 0.050 to 10.000, in steps of 0.05, while λ_2 ranged from 0.01 and 0.05 to 1.00, in steps of 0.05. The obtained ROC curves are in Figure 5.2 and some of the consequent results are in Table 5.2.

Using a single threshold, either regarding the average amplitude of the neighborhood of a given data point or the amplitude of the neighboring peaks of a valley, the ROC curves obtained had an AUC of 0.9951 and 0.9933, respectively. When combining both thresholds in a single detection method, this increased to 0.9954.

For λ_1, the optimal value was 3.75 $^\circ/s$, which allowed a TPR of 100% and a FPR of 1.31%. When considering a detection method relying only the peak average amplitude, the optimal λ_2 was 33.50%, with an equal TPR but a higher FPR (1.50%). When combining both thresholds (related to average amplitude of the data point neighborhood and to the peaks average amplitude), λ_2 was optimal at 33.50% still identifying every cogwheel event, with a lower FPR (1.13%). Hence, the final threshold values to be used in the mobile application were $\lambda_1 = 3.75\ ^\circ/s$ and $\lambda_2 = 33.50\%$.

The next step was to incorporate into the rigidity reduction model the effect of cogwheel rigidity.

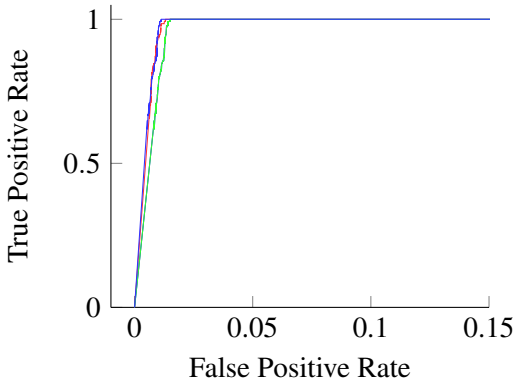

Figure 5.2: In red, green and blue the roc curves for using λ_1, λ_2 (separately) and λ_1 combined with λ_2, respectively.

Table 5.2: Results of ROC curve analysis. AUC stands for area under curve, TPR for true positive rate and FPR for false positive rate. TPR and FPR are those at the closest point of the curve to (1,0) of the ROC domain.

Methodology	**AUC**	**TPR**	**FPR**
λ_1	0.9951	100%	1.31%
λ_2	0.9933	100%	1.50%
λ_1 & λ_2	0.9954	100%	1.13%

5.1.3 Model with cogwheel effect

Up to this point, the model relied on amplitude features and barely and indirectly on the shape of the signal which depicts the smoothness of the flexion movement. As the smoothness is inversely related to the occurrence of cogwheel rigidity, it was thought that introducing it as a penalty to the output of the amplitude-based model would be effective to improve performance of the system. Furthermore, it was experimented having the rigidity label (RL) weighted according to a relationship between the number of events in baseline rigidity and the currently achieved.

5.1.3.1 Penalty Approach

The model initially validated by Costa *et al.* [14] was used at this stage, where the rigidity label of the system (RL_{system}) was given by:

$$RL_{system} = -0.1638\phi^2 + 9.3266\phi - 17.6309 \tag{5.1}$$

where this is a percentage of rigidity reduction. It was attempted to identify whether there was a penalty (P) that should subtracted to RL_{system}, to achieved less error, related to the occurrence of cogwheel artifacts (CA), as follows:

$$RL_{final} = RL_{system} - P(CA) \tag{5.2}$$

It was predicted that the penalty would increase linearly with CA.

Hence, we subtracted the RL_{system} of each of the 186 signals on the database to its current medical label and unregarded differences above 20%. The remainder of the signals was clustered according to the number of identified artifacts. Then for each of these clusters, the mean value (the respective cogwheel penalty) and standard deviation of this difference were computed. Furthermore, it was hypothesized that this penalty would be different according to the baseline rigidity. Therefore, the signals from limbs initially rated with 2 and 3 in the UPDRS scale for rigidity were also considered separately.

In Figure 5.3, the results are shown where the incidence of cogwheel artifacts is plotted against the mean difference between the classifications, considered as the penalty associated to cogwheel.

Contrary to the expectation, no growth tendency of penalty was found as the cogwheel artifacts increased, either regarding or not the initial rigidity score: the mean difference was rather constant, still distinct of the mean training error when fitting the polynomium to the data (8.2%). Thus, the penalty value considered was 6.7% which was the mean difference found between system's rigidity label and assigned label by physician (with a standard deviation of 4.7%).

This penalty would only be applied when the signal's number of CA was higher than a threshold for the number of cogwheel events, e: not always the occurrence of CA is significant, hence this threshold should be considered.

Then, the error of classification was re-computed, now considering the penalty (6.7%) when applicable. The mean training error and standard deviation are shown in Figure 5.4, as a function

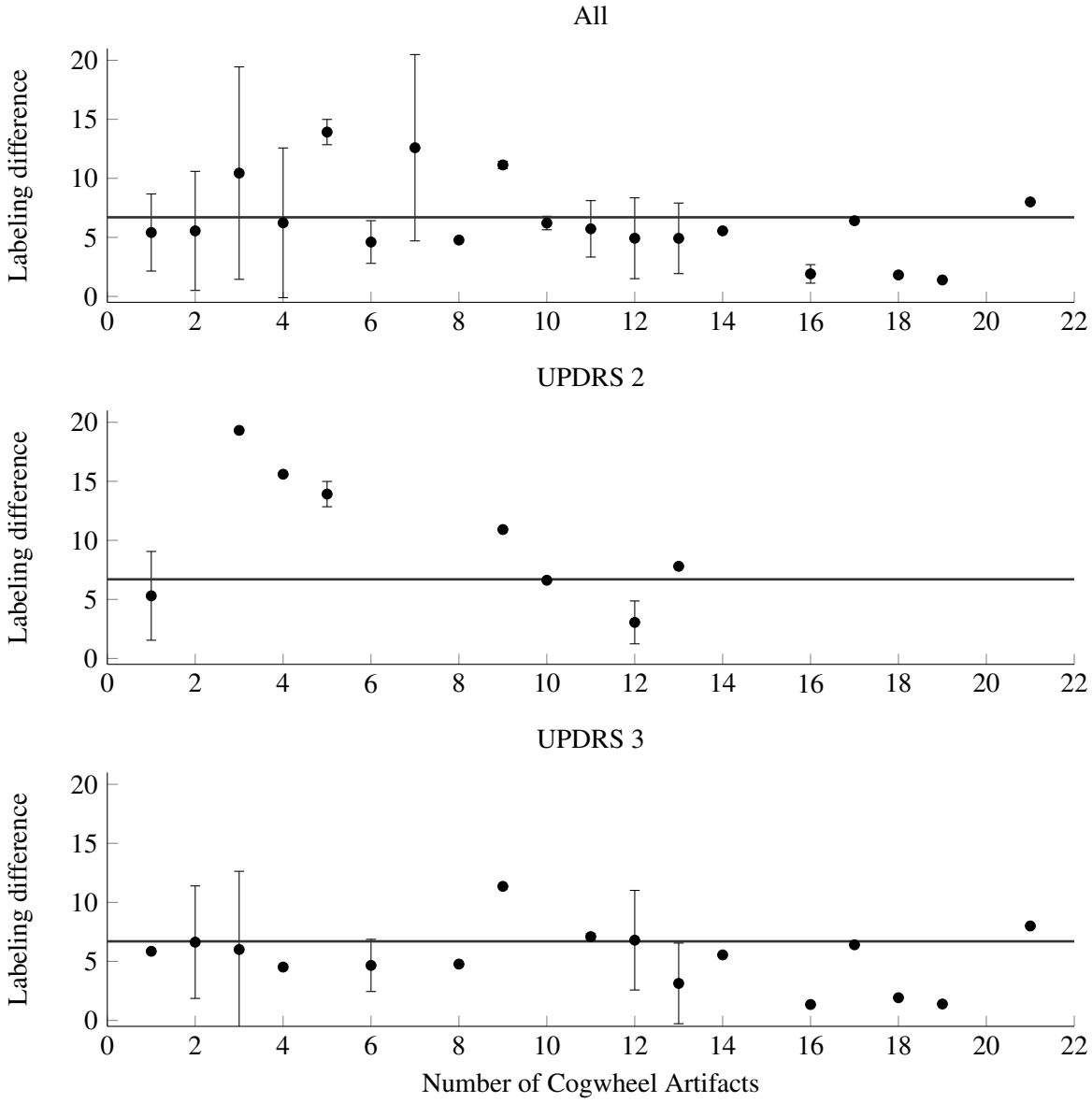

Figure 5.3: Mean ± standard deviation of difference between the system's classification and the medical label, given than the first was up to 20% higher than the latter. These penalties were computed considering every 186 signals together and by clustering them according to the UPDRS rigidity score. The black line indicates the global average deviation found (6.7%).

of the threshold for the number of cogwheel events, e. Also, the training error achieved when no penalty whatsoever is applied is presented.

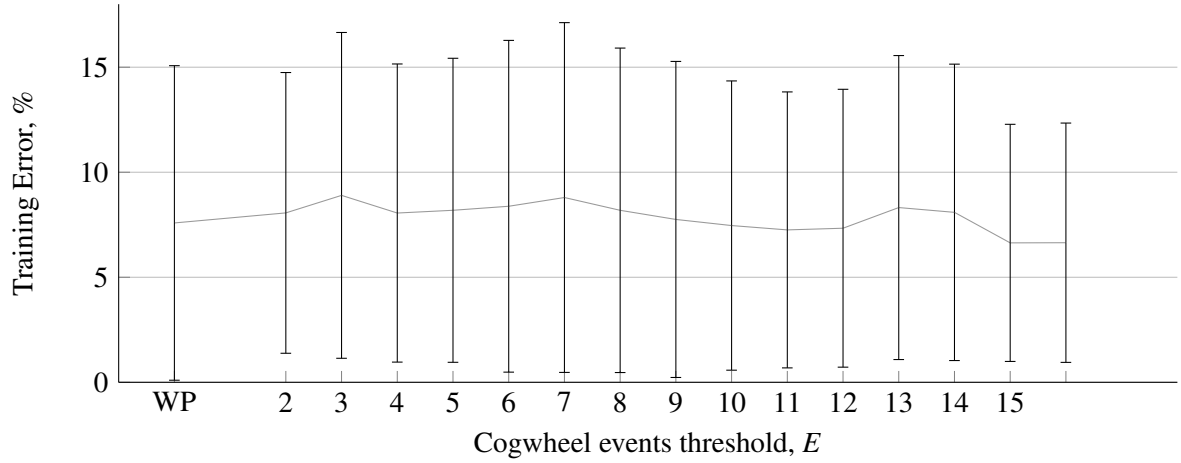

Figure 5.4: Mean ± standard deviation of training error achieved through the penalty approach considering the cogwheel artifacts detected. WP stands for "Without penalty" ($P = 0$).

These results lead us to the conclusion that this penalty-based approach to include the influence of cogwheel rigidity will bring no significant improvement to the performance of the system, since no significant difference is found for every e experimented.

5.1.3.2 Multiplicative-Factor Approach

The following approach relied on considering a multiplicative factor, F, which would affect the RL_{system} as follows:

$$RL_{final} = RL_{system} \cdot F \tag{5.3}$$

where F ranges from 0 to 1 and would be related to the occurrence of cogwheel artifacts. This was defined in various manners in order to reflect the severity and reduction of these events with electrical stimulation:

- as a ratio translating the loss of amplitude due to cogwheel, *i. e.*, the disparity from a smooth arcade and the actual signal. For each cogwheel artifact detected, the neighboring peaks were considered to create a temporary version of the signal. This would translate a smooth hand movement and was created by performing linear interpolation of the samples in-between the peaks, as exemplified in Figure 5.5. In this case, F would be equal to:

$$F = AL = \frac{\sum_i^N \omega(i)}{\sum_i^N \omega_n(i)} \tag{5.4}$$

where AL is a ratio for amplitude loss, ranging from 0 to 1 (no loss), ω is the angular velocity signal and ω_n is a version of the previous where, at every detected artifact, an interpolation was performed between the respective neighboring peaks.

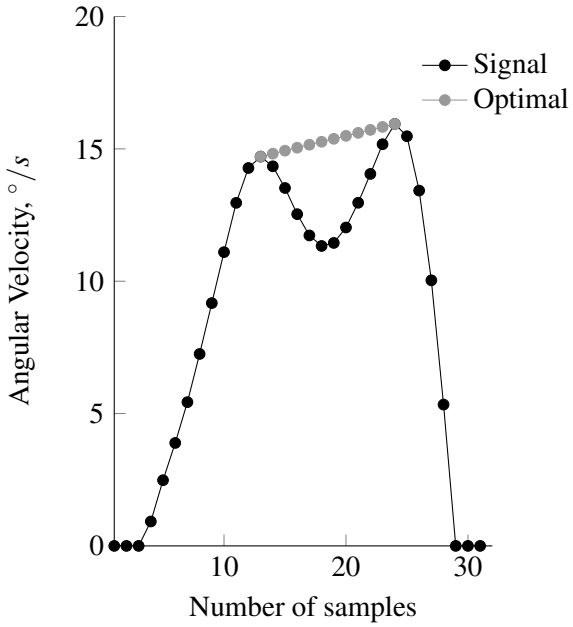

Figure 5.5: Representation of an arcade correspondent to a hand flexion movement with a cogwheel artifact and the interpolation of a perfect arcade using the neighboring peaks of the artifact.

- as given by a second degree polynomial scaling function of C:

$$F = f(C) = aC^2 + bC + c \tag{5.5}$$

where a, b and c are parameters such that $a = \frac{(O-1)}{\left(1-2AL_b^{-1}+AL_b^{-2}\right)}$ and $b = -2aAL_b^{-1}$ and $c = 1 + aAL_b^{-2}$ and $C = \frac{AL}{AL_b}$ and AL_b is AL of the respective baseline signal. An example of this function is in Figure 5.6, where O, the proportion factor applied when $AL = AL_b$, is equal to 0.80 and $AL_b = 0.92$. Because O translates the weight of having no improvement in terms of movement smoothness, this was varied from 0.84 to 0.98 to check whether tweaking this parameter would benefit the overall model performance.

For both definitions of F, the training error was compared to having no multiplicative factor. Furthermore, it was attempted to include baseline comparison, *i. e.*, when building the polynomial model, consider as well the $RL = 0\%$, correspondent to the respective baseline signal. Possibly by enriching the input data for building the model with the baseline signal's descriptor could enhance performance. The results may be found in Figure 5.7.

Neither including the effect of cogwheel as in Equation 5.3 or/and having baseline comparison when building the polynomial model bring any increased performance; in fact, it worsen the performance. Figure 5.7 shows that the error is worst for any value of O different from 1, both considering the baseline signal or not. Table 5.3 presents the error achieved with the first definition of F, which also proves to be unable to reduce the system's error. The struggle in finding an appropriate manner in which to include this cardinal feature in parkinsonic rigidity may be associated as well to some inconsistency of the specialist assessment regarding it.

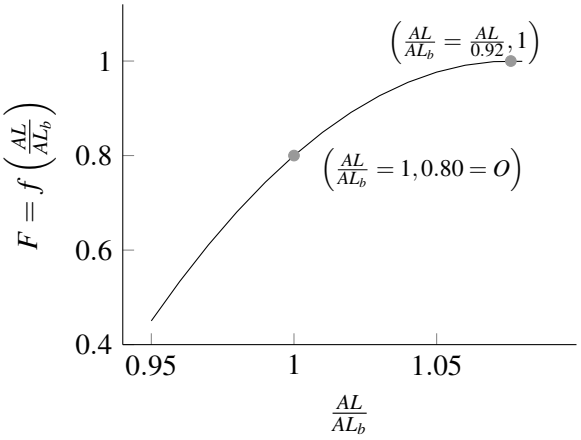

Figure 5.6: Example of $f(C)$ function to model weight of cogwheel artifacts impact on the rigidity label. In this case, $AL_b = 0.92$ and $O = 0.80$.

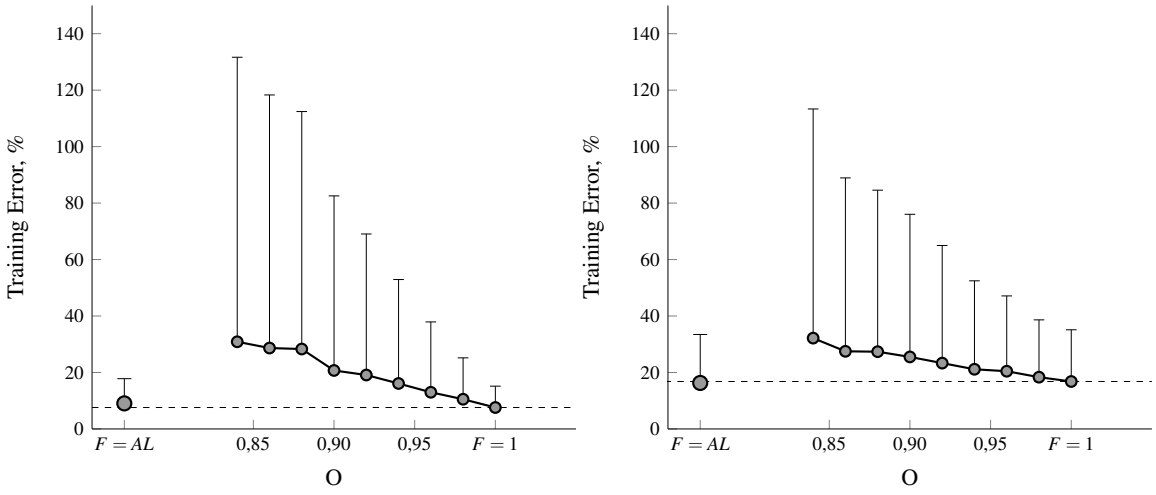

(a) No baseline comparison.

(b) Baseline Comparison.

Figure 5.7: Impact of having the F factor in the rigidity label on the training error (mean + standard deviation is represented). $F = AL$ is the first definition introduced, where AL translates a measure of amplitude loss by cogwheel (where 1 corresponds to no loss), $F = 1$ is the case where the multiplicative fator does not influence the final classification and O is the proportion factor F applied when the ratio $AL/AL_b = 1$ (*i. e.*, when the loss of signal amplitude in the current signal and in the baseline signal due to cogwheel is equal). The dashed line represents the mean training error achieved when $F = 1$.

Table 5.3: Comparison of mean $\pm$ standard deviation of training error when there is no influence of the multiplicative factor ($F = 1$) and when it is equal to the loss of amplitude due to cogwheel ($F = AL$).

	Baseline Comparison	**No Baseline Comparison**
$F = 1$	16.8±18.3 %	7.6±7.6 %
$F = AL$	16.3±17.2%	9.1±8.7 %

5.1.3.3 Random Forest

In introductory work (in Appendix C), a regressive decision tree-based approach, random forest (RF), using only the signal descriptor ϕ for classification of rigidity proved to have similar results as the polynomial model. With that in mind, it was hypothesized that such method, now considering as well cogwheel-related features, would be beneficial. The number of trees considered in the forest were 1, 2, 5, 10, 15, 25, 50, 80, 100, 150 and 200. The leave-one-out error was computed, performing 1000 iterations. The following combinations were used to build the trees:

1. ϕ_{signal}, CA_{signal} and $CA_{baseline}$ of every signal (377 signals)
2. ϕ_{signal}, CA_{signal} and $CA_{baseline}$ of every signal excluding baseline signals (341 signals)
3. ϕ_{signal} and CA_{signal} of every signal excluding baseline signals (341 signals)

where CA_{signal} and $CA_{baseline}$ are the number of cogwheel artifacts detected in the signal and its respective baseline, respectively. At this point, a larger dataset was considered than in previous sections (total of 377 signals from 40 limbs).

Figure 5.8 presents the results for these different combinations. As in Section 5.1.3.2, including the signals of baseline rigidity into building the model worsen the results, achieving a minimum training error of 10.1 ± 9.7 % for 50 trees (Figure 5.8a). As for the two others, they achieve, respectively, 7.1 ± 5.6 % for 80 trees (Figure 5.8b) and 7.4 ± 6.0 % for 50 trees (Figure 5.8c). The error for all RF converge with the increase of the number of trees. Still, such convergence does not translate into improved performance.

The performance of generated models relying on the angular velocity signal of bending seems to have reached a plateau, neither increasing the dataset size (based only on 2 physicians at least) nor by considering cogwheel occurrence seems to improve. Additionally, such methodology comprising of so many trees would affect significantly the response-time of the mobile application when classifying, which would not be worthwhile.

5.1.4 Incidence of Cogwheel Artifacts

Cogwheel rigidity causes further impairment to a patient and is more prominent as the disease status is as well more severe. That is shown in Figure 5.9a and 5.9b, respectively, by showing that, with a lessened rigidity perceived by the specialist, both number of jerk occurrences and their amplitude are smaller. This is further confirmed if we consider only the signals from baseline rigidity grouped according to the patient's UPDRS subscore, where, from 1 to 3, the mean value decreases (even though no statistical difference is found), as shown in Figure 5.10.

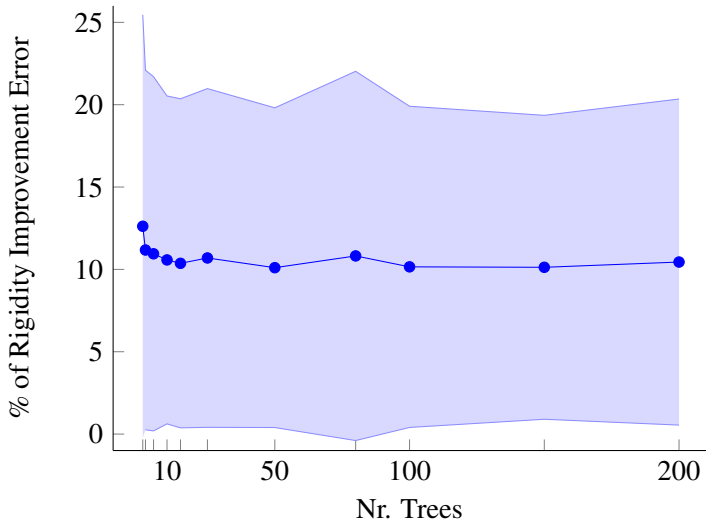

(a) Considering ϕ, CA_{signal} and $CA_{baseline}$. Including Baseline signals.

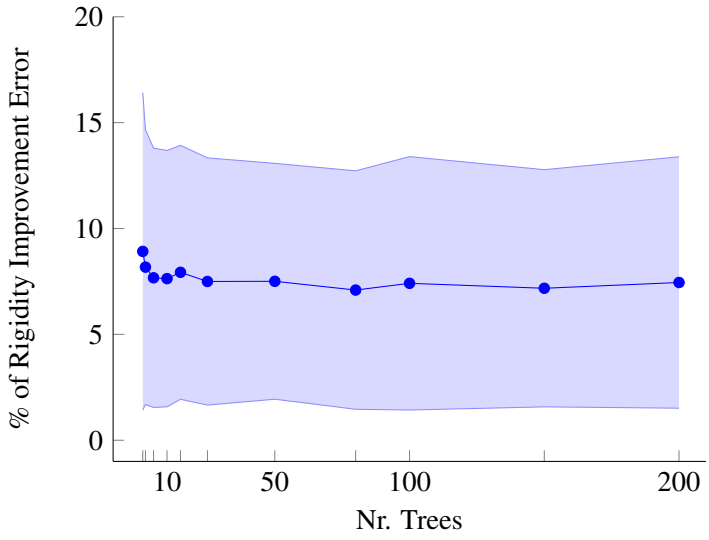

(b) Considering ϕ, CA_{signal} and $CA_{baseline}$. Excluding Baseline signals.

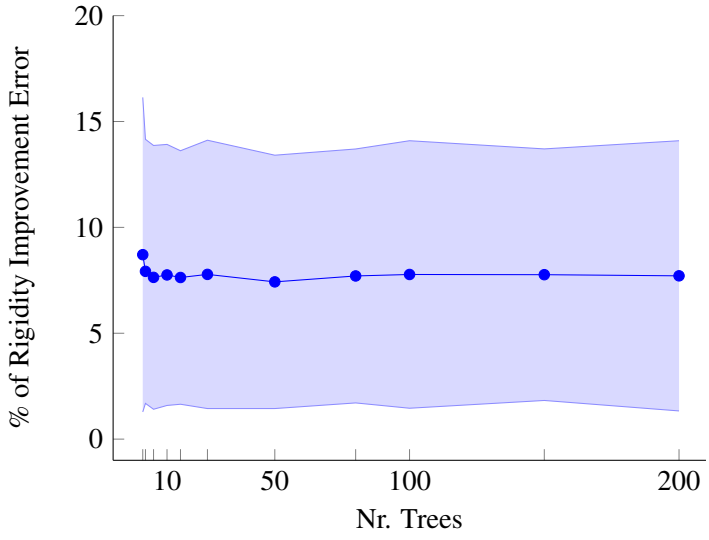

(c) Considering ϕ and CA_{signal}. Excluding Baseline signals.

Figure 5.8: Performance of random forest approach for classification of rigidity. ϕ is the signal descriptor, CA_{signal} the number of cogwheel artifacts detected in the signal and $CA_{baseline}$ the number of those same artifacts in the respective baseline state.

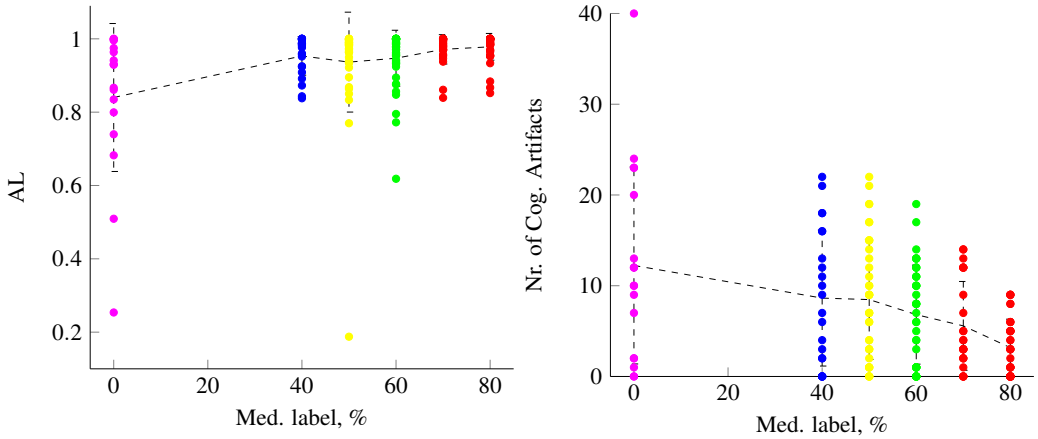

(a) Amplitude loss.

(b) Number of cogwheel jerks.

Figure 5.9: Tendency for a lessened rigidity perceived with less amplitude loss in hand flexion and less occurrence of cogwheel.

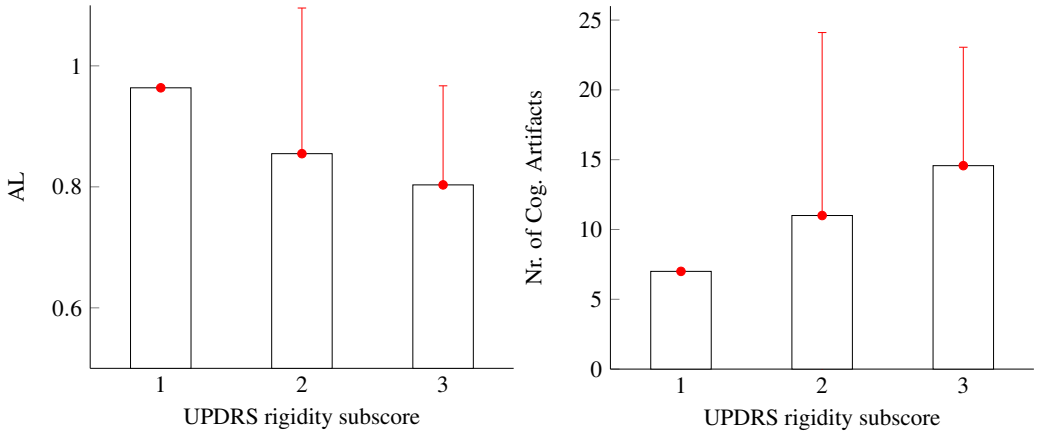

(a) Amplitude loss.

(b) Number of cogwheel jerks.

Figure 5.10: Tendency for a smaller rigidity score with less amplitude loss in hand flexion and less occurrence of cogwheel. Only the baseline signals were considered.

5.2 Categorization of cogwheel rigidity severity

The inclusion of a parameter related to the cogwheel occurrence did not lead to any improvement in the training error in comparison to the initial approach, still we considered as an important feedback to provide to the physician, hence the detection of cogwheel artifacts was included in the system (*i. e.*, mobile application). The concept followed was to give additional information to the user, by providing the number of jerks identified *per* signal (having a single indicator related to the hand movement smoothness), which would be associated to a visual scale:

- green - cogwheel of a low rigidity (LR) state
- yellow - cogwheel of a medium rigidity (MR) state
- red - cogwheel of a high rigidity (HR) state

From a total of 302 signals, every signal whose respective baseline signal had less than 4 cogwheel artifacts (CA) (3.07 is the average of CA in the signals with medical labels of 70% and 80%) was discarded, to keep only meaningful data and because, if baseline does not have cogwheel, neither will the others. 52 signals were discarded. Then, three clusters (HR, MR and LR) were defined as in Table 5.4 containing the number of cogwheel artifacts detected and the respective mean value *per* cluster was computed.

The mean values of each group were used as the seed points for a 3-means clustering to partition all the data distribution into three clusters. This was performed using the cogwheel events within a period of 300 samples and 200 samples (sample-interval set for the mobile application to provide each RL). These new cluster centers found allowed defining boundaries of each cogwheel rigidity realm as the mid-points between LR|MR and MR|HR. The results are presented in Figure 5.11, where the seed points, final cluster centers and boundaries are represented, considering both 200 samples and 300 samples signals.

To keep the feedback-rate of the mobile application at every 200 samples, the boundaries considered were:

- HR | MR: 7.807 ~8 CA
- MR | LR: 2.798 ~3 CA

Table 5.4: Association of the categories of low, medium and high rigidity cogwheel states (LR, MR and HR, respectively) to the medical label assigned by the specialist to a given signal and their respective mean number of cogwheel artifacts (CA) detected. 0% corresponds to the baseline signal of the limb.

Cog. Severity	**Range**	**Mean CA** (300 samples)
HR	(0/40/50)%	6.3
MR	60%	3.9
LR	(70/80)%	2.3

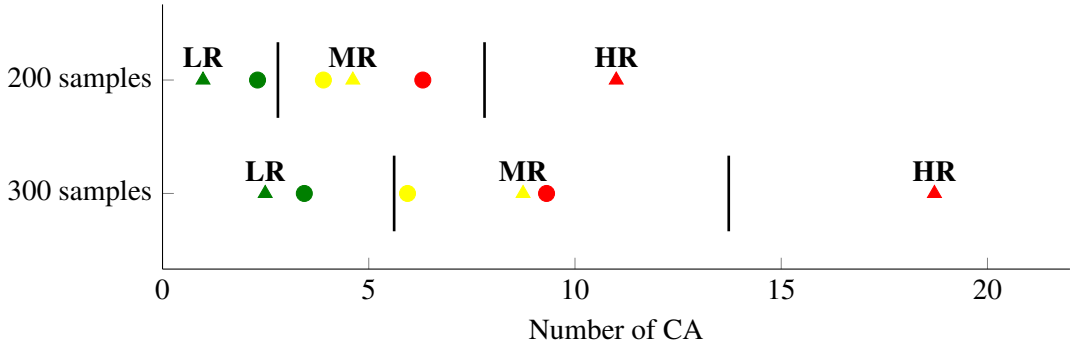

Figure 5.11: Result of 3-means clustering. The cluster centers for high, medium and low rigidity cogwheel (HR, MR and LR, respectively) are shown as triangles and the mean values of cogwheel artifacts (CA) as circles (*i. e.*, seeds for 3-means clustering). The frontiers HR-MR and MR-LR are represented as lines.

If we applied straight forward these hard-coded boundaries to classify a signal regarding cogwheel rigidity using the same set of signals as before, we would have an accuracy of 68.5% and sensitivity of 52.8%, whereas, using the 300-samples boundaries, 68.8 % and 44.3%, would be achieved.

It was further envisioned to have adaptive-boundaries for classification of the cogwheel rigidity severity. Hence, for any new limb under analysis, the baseline signal was acquired and processed, having obtained CA_b, the number of CA of the baseline signal. According to this value, the frontiers ($B_{HR|MR}$ and $B_{MR|LR}$) would adapt according to the distance to the HR cluster center, CC_{HR} (in the case of 200-samples analysis, 11 CA) as follows:

$$B'_{HR|MR} = B_{HR|MR}\frac{CA_b}{CC_{HR}} \tag{5.6}$$

$$B'_{MR|LR} = B_{MR|LR}\frac{CA_b}{CC_{HR}} \tag{5.7}$$

For every signal, its CA is positioned within one of these 3 realms having in mind the new values of the boundaries, $B'_{HR|MR}$ and $B'_{MR|LR}$, and categorized as high, medium or low cogwheel rigidity severity. These adaptive-boundaries lead to lower accuracy and sensitivity (63.5% and 45.2%, respectively) than before but still such approach was carried on for being more versatile and adaptable. Moreover, the goal is to categorize cogwheel rigidity in one of three distinct status to give a sense of changes in movement smoothness (base on quantitative data) rather than effectively to correctly classify. A summary of these results is presented in Table 5.5.

Table 5.5: Accuracy and sensitivity of the approaches to categorize the cogwheel rigidity severity.

	Accuracy (%)	**Sensitivity (%)**
300 samples, fixed boundaries	68,8	44,3
300 samples, adaptive boundaries	62,7	44,0
200 samples, fixed boundaries	68,5	52,8
200 samples, adaptive boundaries	63,5	45,2

5.3 Final Remarks

In this chapter, a cogwheel detection method was introduced which proved to be reliable (TPR = 100% and FPR = 1.13%) using light-processing. Then its combination with the current model, as a penalty or as a multiplicative-factor were attempted but no significant differences were found. Still, as cardinal feature of the symptom under scope, its occurrence could not be ignored, then a categorization system as searched for and developed sub-dividing into three realms (high, medium and low cogwheel rigidity severity) and as a function of the baseline rigidity of the patient. This allows having a perspective of both the improvement related to overall amplitude increase and also a rating system of movement smoothness. Its implementation and presentation will be introduced in Chapter 6.

Chapter 6

System Overview

Initially, the system had two components: a MoMo for hand-sensing and a smartphone for processing and visual feedback. The mobile application provided the last evaluation of rigidity, a real-time plot of hand flexion velocity and interface widgets for data-logging. Still, to incorporate the work present in Chapter 5 related to cogwheel detection and categorization, new features needed to be added. Additionally, improvement to usability of the application were introduced by adding an extra-interface to provide feedback at the hand of the physician performing the assessment, in a smartwatch. Furthermore, this system may provide capabilities other than rigidity assessment: both by assessing other motor symptoms and by complementing other under-study system (closed-loop DBS). Those will be introduced later in this chapter.

6.1 Intended System Capabilities

In Chapter 5, cogwheel rigidity was categorized considering the available dataset, as well as the cogwheel artifacts (CA) detected in the baseline signal acquired before any application of stimulation. Also, other usability improvements were planned (to enrich the interface). A summary of the new envisioned features may be found in Figure 6.1 (represented as white "Use Cases"):

- provide cogwheel-related information
- allow defining a signal as baseline signal (which requires a plot of baseline signal to check its quality/significance)
- represent a reference of average angular velocity peaks, μ_p (considered as the mean of those signal labeled with 70% or 80% improvement)
- provide a history of the most recent rigidity label provided by the system
- provide rigidity evaluation feedback through smartwatch.

A block diagram representing the system is in Figure 6.2, where the display unit may be a smartphone or a smartwatch.

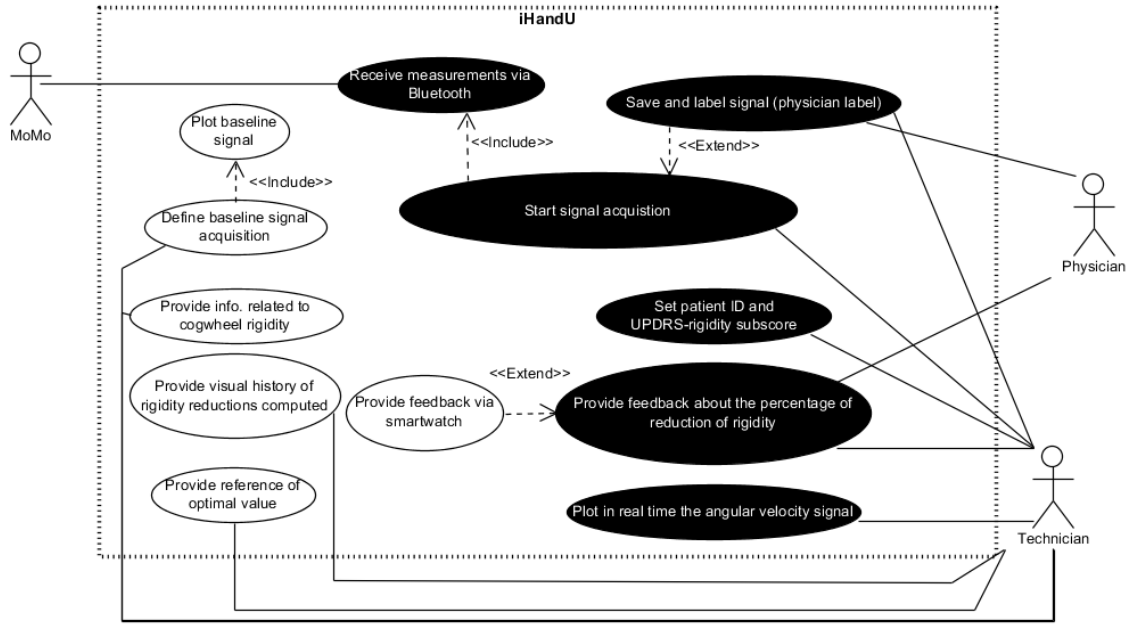

Figure 6.1: Use Case diagram of *iHandU* android application. White use cases depict new features to be added and black use cases the existing ones. The MoMo is the sensor being worn in the hand of the patient, whose rigidity is being assessed by the physician; the technician is the individual holding the handheld smartphone, where the application *iHandU* is running.

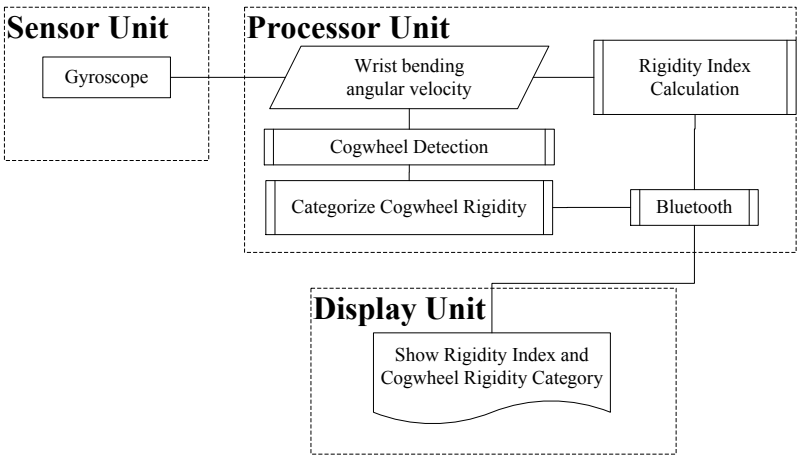

Figure 6.2: Block Diagram of proposed device. The sensor unit and processor unit could be a single module, communicating the resultant parameters to an external device with simply display function.

6.2 Implementation of cogwheel detection

Rather than having an "offline" processing for the artifact detection, *i. e.* waiting for the acquisition of all 200-samples and then analyze the signal, the implementation performed such that this detection was "on-the-fly". The flux diagram is in Figure 6.3.

After the computation of the number of CA this was categorized as high-, medium- and low-severity, applying the adaptive boundaries according to the CA identified in the saved baseline signal. In case the baseline signal had less than 4 CA, then this information was considered meaningless.

6.3 Visual Updates

The previous categorization of cogwheel is provided to the user as:

- green, low cogwheel rigidity severity
- yellow, medium cogwheel rigidity severity
- red, high cogwheel rigidity severity
- grey, baseline rigidity did not reveal significant number of CA (<4)

Furthermore, the feedback provided by the system, when the rigidity label was lower than 35% or the signal had a mean velocity value than that found in the baseline signal, changed to *NR* instead of the output given by the model, standing for "No Reduction". Also, a reference was placed in the graph (as the green plot) which depicts the average of μ_p of 70% and 80% reductions in rigidity so the operator has a sense of scale when observing the variation of angular velocity, as well as a visual threshold which defines an improvement. Withal, a history with the 3 previous classifications by the systems are presented.

With the cogwheel-related updates, features of baseline rigidity are required. For that reason, the visual-assessment of the quality of the baseline signal under use (check the signal significance, if it is representative by having an adequate number of flexion-arcades in the signal and meaningful information) was of interest which was added to the interface, accompanied by a control button for this signal acquisition.

The final user interface is as in Figure 6.4.

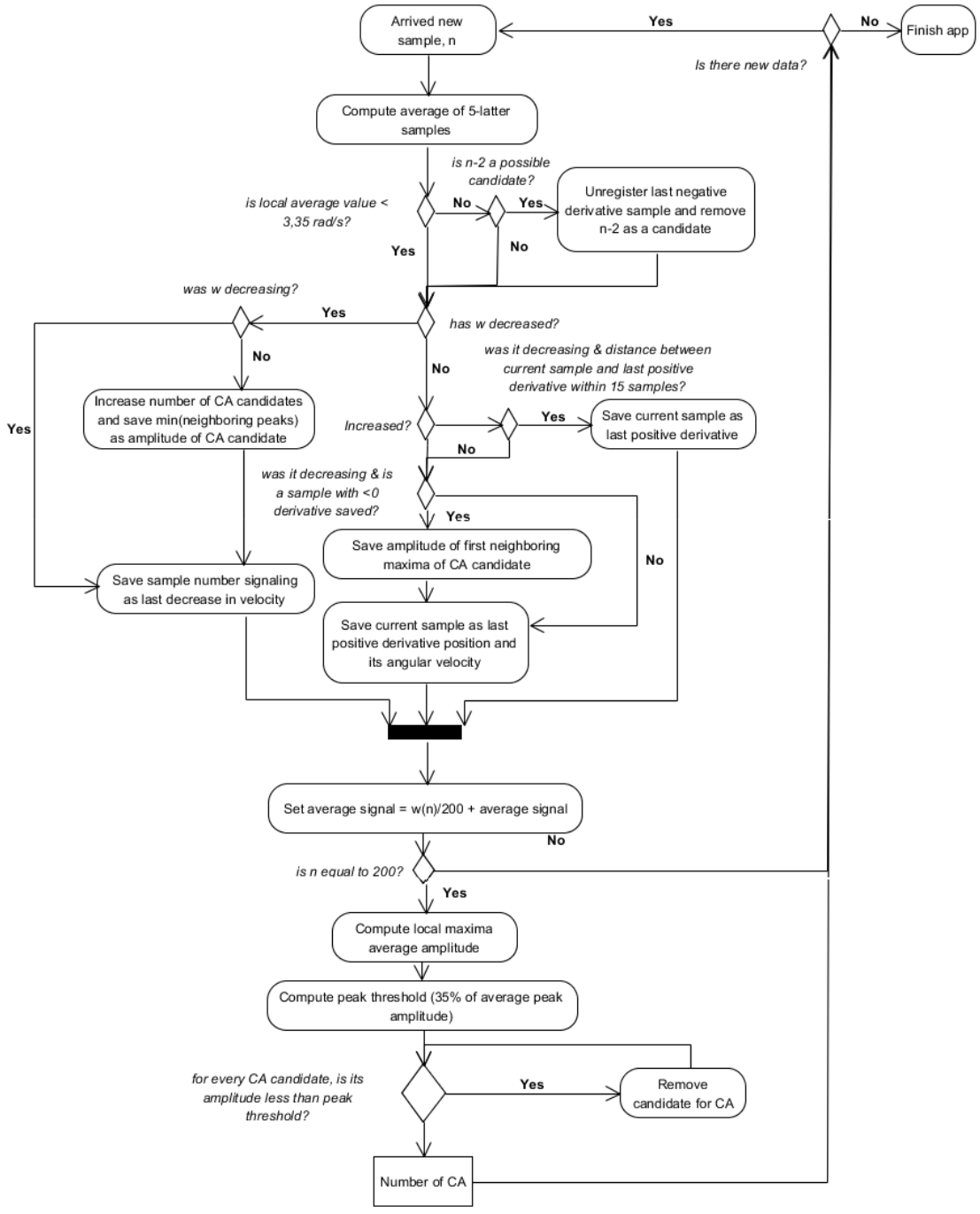

Figure 6.3: Flux diagram of "on-the-fly" cogwheel detection. CA stands for cogwheel artifacts. 200 is the number of samples *per* signal.

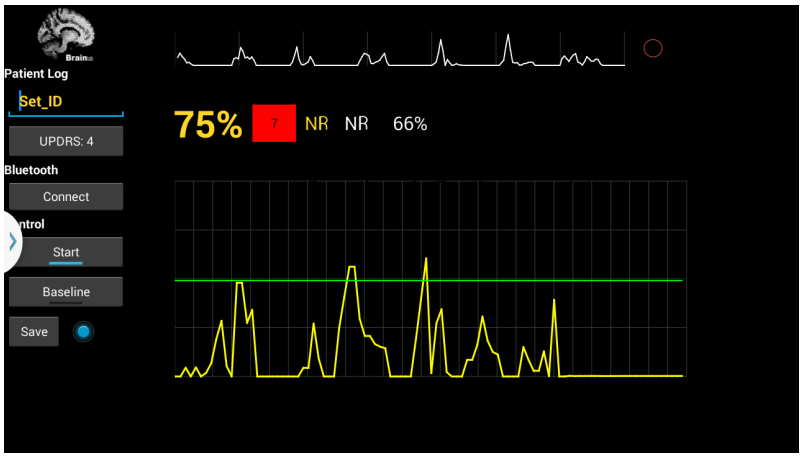

Figure 6.4: Screenshot of mobile application.

6.4 Usability Survey

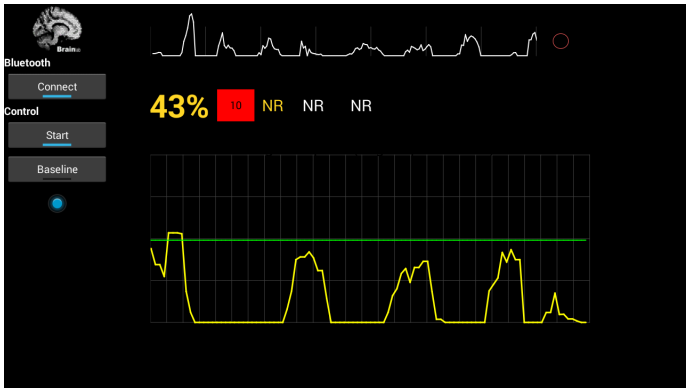

Figure 6.5: Interface of Mobile Application simplified (“end-user mode”).

To evaluate the easiness of use of the proposed system, 5 first-time users were invited to use it and do the following:

1. place the sensor correctly in a person
2. initialize the mobile application in the handheld
3. record a baseline signal
4. observe the provided feedback by the mobile application
5. finalize the acquisition

as it would occur in a DBS surgery context.

For this purpose, the mobile application was changed to a simpler interface (all widgets related to data acquisition were removed), as in Figure 6.5. The simplicity of the design may even be adapted, depending on the style and background of the physician (*e. g.* discarding the real-time signal plot), or reducing to the minimally required and relevant as in Figure 6.8 . Each of the steps and sub-tasks (e. g., visualization of the baseline signal shape, check rigidity label history) were evaluated as in Appendix G.

In a scale from 1 (highly difficult) to 5 (highly simple), the procedure has an average rating of 4.84 and an overall appreciation of 4.9.

6.5 Phone-Watch Communication

As the system was designed, the physician did not have direct visual access to the improvement computed by the system while making his assessment because it is only provided in the smartphone screen. This required for the physician to ask for the system's classification to the person holding the device. With that in mind, one of the goals of this project was to extend the feedback functionality, by allowing the examiner to check the computed feedback right away (impacting the overall time of consultation). For that purpose, the Google Play Services library of wearable devices was used.

When the mobile application starts, a *GoogleApiClient* is initialized to allow communication with the wearable data layer. This wearable should be connected through Android Wear to the smartphone. If this is available, every time a classification is computed in the smartphone, it sends the last 4 classifications, the number of detected CA and color associated to the cogwheel rigidity categorization (green, yellow, red and gray), decided by the processing in the handheld phone. This operation of connecting to the wearable data layer is initialized and performed in as an asynchronous task, which is terminated if there is no wearable available or after the message is sent. The information is sent as in Table 6.1.

Table 6.1: Message sent from handheld phone to wearable. R_i is the i^{th}rigidity reduction computed by the system, where $i = 1$ is the most recent.

Index	**1-2**	**3-4**	**5-6**	**7-8**	**9-10**	**11**
Item	R_1	R_2	R_3	R_4	CA	$Cog.Category$

The use case related to the smartwatch usage intra-operatively has been tested and validated (Appendix F).

After decrypting the message received by the wearable, this is displayed by the interface, as in Figure 6.6. Every update is accompanied by a vibration of the watch to warn the physician about the arrival of new data. The full system is represented in Figure 6.7 and the class diagram related to the MoMo communication may be found in Appendix E and a picture of the system under use in DBS surgery in Appendix F.

In a prototype stage, a factor to consider is the color code used in the display interface. The red color must be reserved to signal alarm and emergencies [54] (ISO 3864: Graphical symbols - Safety colours and safety signs). Furthermore, an even more simplified interface could be aimed for as exemplified in Figure 6.8, where the background color of the display changes according to the movement's smoothness categorization, provides only the most recent classification and shows $'+'$ or $'-'$ indicating increase or decrease of the classification in comparison to the previous classification.

Figure 6.6: Wearable application interface in smartwatch Moto360. From top to bottom, there is the most recent rigidity label, followed by the corresponding count of cogwheel artifacts which is associated to a color code related to severity of their occurrence and, finally, the history of rigidity labels.

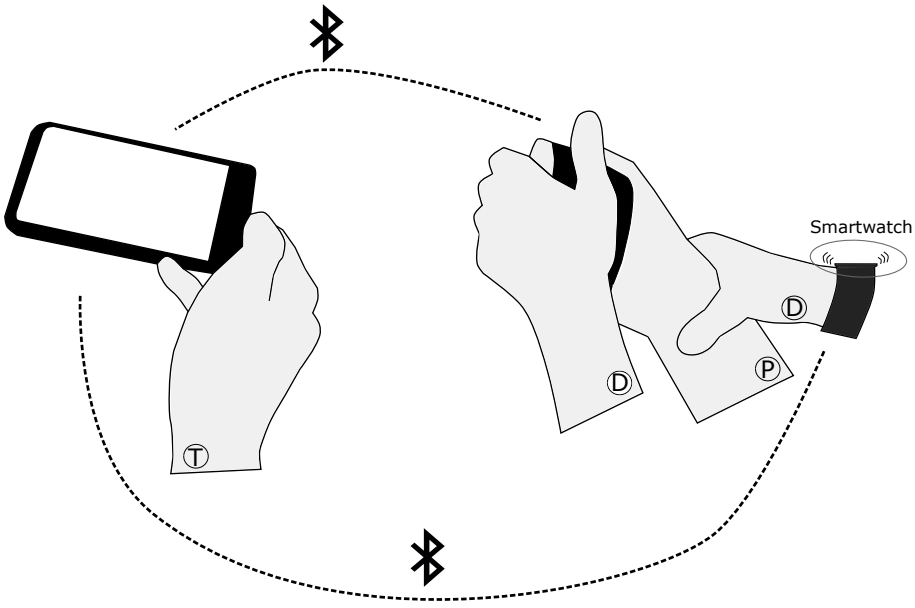

Figure 6.7: Overall System. "T" stands for technician, "D" for doctor performing the rigidity assessment and "P" for patient.The elastic band, within which lies the sensor, is placed in P's hand. The sensor communicates with the handheld smartphone via-Bluetooth. At its end, data processing, cogwheel artifacts detection and computation of the rigidity label take places and then forwarded to the smartwatch worn by the physician.

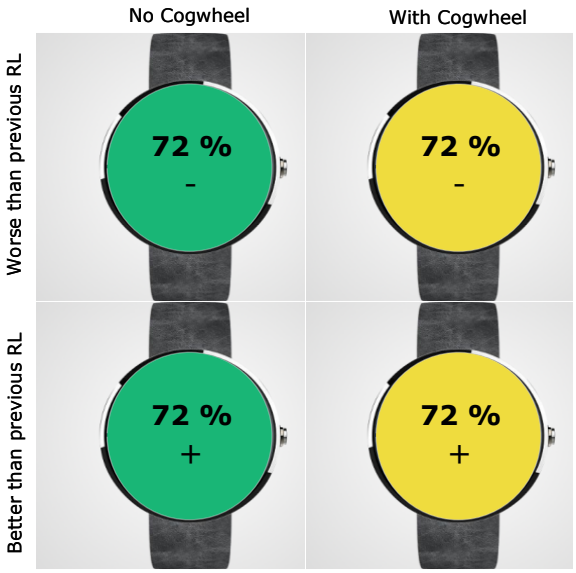

Figure 6.8: Simplified smartwatch interface.

6.6 Final Remarks

Additional functions were added to the system for rigidity assessment by (1) enriching the handheld mobile application with support features (*e. g.*, history of classifications) and cogwheel rigidity information and (2) adding a smartwatch to be worn by the physician who is making the assessment to provide him feedback on the computed rigidity reduction, instead of being shown the smartphone or being told.

However, as a proper medical device, can it be successful? Which requirements should be met? What is lacking? Who might be the partners and competition? This issues will be tackled in Chapter 7.

Chapter 7

System as a Business Opportunity

Up to this stage, we have presented a system which aims at quantitatively evaluate rigidity in intra-operatory conditions. But one who prospects to have it become a medical device to be added to the Deep Brain Stimulation surgery context should be aware of the industry environment, validation and legal procedures to be followed and how to protect the technology. This chapter will give an overview from this perspective.

7.1 Need and Stakeholders

In Deep Brain Stimulation (DBS) surgeries of patients with Parkinson's Disease (PD), the improvement caused by stimulation is assessed relying on the evaluation of wrist rigidity, performed by a physician. This is done relying on the physician assessment capabilities, experience and perception, with no supportive quantitative data, bestowing subjectivity over it. Hereby, a need of supporting the physician decision with quantitative data was identified, of mixed nature (no current solution still an increment to the context of deep brain stimulation surgery).

To meet this need, we are faced with the following stakeholders, who have their own interests/questions:

- Administration/Board: is the device cost-effective? how does it influence the time of occupation of an operating room? Does it reduce future revisits by the patient?
- Neurosurgical operating team: is the device easy-to-use? Is the device reliable? Is it time-consuming? Does it reduce future revisits by the patient?
- Patient: does it prolong the surgical procedure (notice that he is awake during the electrodes' implantation)? Does the device influence his comfort? Does it reduce the number of future revisits to the hospital?
- Buyer (private, government): cost of device? is the device cost-effective? how does it influence the time of occupation of an operating room? Does it reduce future revisits by the patient?

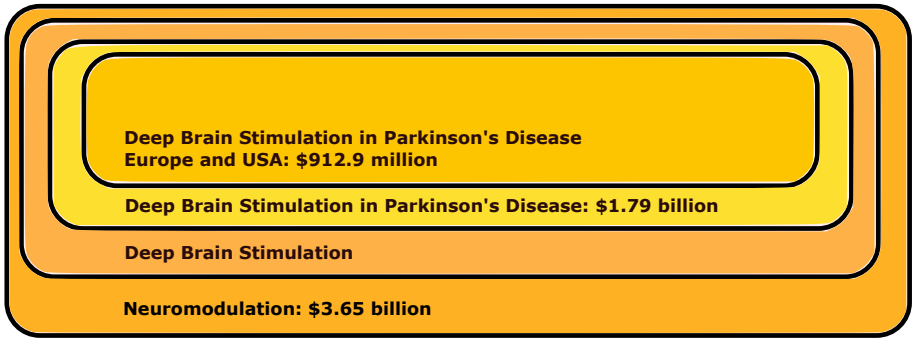

Figure 7.1: Top-down market segmentation. From Neuromodulation to Deep Brain Stimulation Surgery devices for Parkinson's Disease in Europe and USA.

7.2 Market of Deep Brain Stimulation

The neuromodulation [1] market is expected to reach a value of $6.20 Billion in 2020 (evaluated in $3.65 billion in 2015). One of its drivers is DBS due to its large growth potential (settled in the treatment of movement disorders but currently expanding in targeting diseases) [55].

The global sub-market of DBS Devices for PD also reveals growth tendency: in 2013 it was valued in $1.79 billion (or €1.60 thousand million) and the expectation is to reach a value of $3.21 billion (or €2.88 thousand million) in 2020 [56]. A CAGR [2] of 8.9% justified by (1) demand of minimally invasive surgical procedures and (2) increasing rates of incidence of target disorder [57].

A global incidence of 4.9-19 *per* 100,000 people was reported by the World Health Organization (WHO), as well as higher prevalence rates in Caucasians in Europe (108-257 *per* 100,000 [58]) and North America [59]. The European and USA DBS devices market for PD may be estimated as 51% [3] of the global market, *i. e.* , $912.9 million (€808.1 million). The growing market is a signal of attractability of this industry, thus attractive to introduce a product into it.

7.3 Industry Landscape

If one envisions to place a medical device on the market, knowledge of the players in the market of interest is required. These may play an important role on the future success (or not), either as competition or as partners. So, in the DBS devices market there are five main players to be emphasized [57]:

[1] Direct stimulation of nervous system with electrical signals

[2] Compound Annual Growth Rate (CAGR) is the mean annual growth rate of an investment over a specified period of time longer than one year.

[3] Considered $\frac{(N_{EU}+N_{USA})DBS_{EU\&USA}}{(N_{global}DBS_{global})}$ where N stands for number of patients worldwide ($global$), Europe (EU) and USA (6,954.2, 1,342.0 and 1,082.4, thousands, respectively [57]). DBS_{global} and $DBS_{EU\&USA}$ is the DBS treatment availability which was estimated as being equal to drug treatment availability provided by the WHO (60.6% and 88.1%, respectively [59]), where availability in USA was considered equal to the European's.

- Medtronic Inc. (USA): the initiator of this medical device segment with the first European approval in 1993 for tremor, dystonia and PD [60], FDA approval for PD in 2002 [61] and in 2010 was holder of an over 25% share of Europe Neurology Devices Market
- St. Jude Medical Inc. (USA): launched its therapy for PD in Europe in 2009 [60] and got FDA approval in 2015 [62]
- Boston Scientific Corp. (USA): got CE marking DBS system in 2012 [63]
- Deep Brain Innovations, LLC (USA): focus on increasing efficiency of deep brain stimulation systems
- Aleva Neurotherapeutics SA (Switzerland): focus on electrode fabrication for increased stimulation target specificity, start-up founded in 2008, received its third round of financing in 2016

There is also Precisis AG (Germany) which provides solutions for high precision intervention in neurosurgery, radiotherapy and stereotaxy, from software to hardware (*e. g.* drilling system and stereotatic frame). Furthermore, a start-ups rise in this field can be identified as demonstrated by [57]:

- Functional Neuromodulation Inc., focused on the application of DBS to the fornix area (with Medtronic and Genesys Capital - a Canadian-based venture capital firm - as Investors [64])
- Intelect Medical Inc., who developed a software to visualize and steer stimulation (acquired by Boston Scientific in 2011 for $78 million (about €68 million)
- Sapiens Steering Brain Stimulation GMBH (from the Netherlands, acquired by Medtronic in 2014 for €150 million)
- NeuroSigma, developing DBS systems for pos-traumatic stress disorder, obesity and cachexia
- Brainsway Ltd., tackling DBS through transcranial magnetic stimulation instead of an invasive approach

The role of these companies may be perceived as supporting existing products of possible acquirers, with larger market share ("for a possible tuck-in acquisition"), *i. e.*, complementing the current framework by exploring new target diseases for DBS, new ways to intra-operatively confirm that clinicians have reached the target of stimulation, diagnostics to help selecting eligible patients for DBS and also by providing supporting technologies to help clinicians advance therapies for diseases that are more complex and difficult [60]. Herewith, our proposed system may fit into the context of DBS as well, in particular, in the surgical stage in PD patients, as a guide to indirectly identify whether the stimulation electrode is placed in the optimal position. In this sense, by partnering with an already-established company could provide an opportunity, not only for their expertise on product regulation and manufacturing capability, but also easy access to a large number of centers providing DBS surgery to the population.

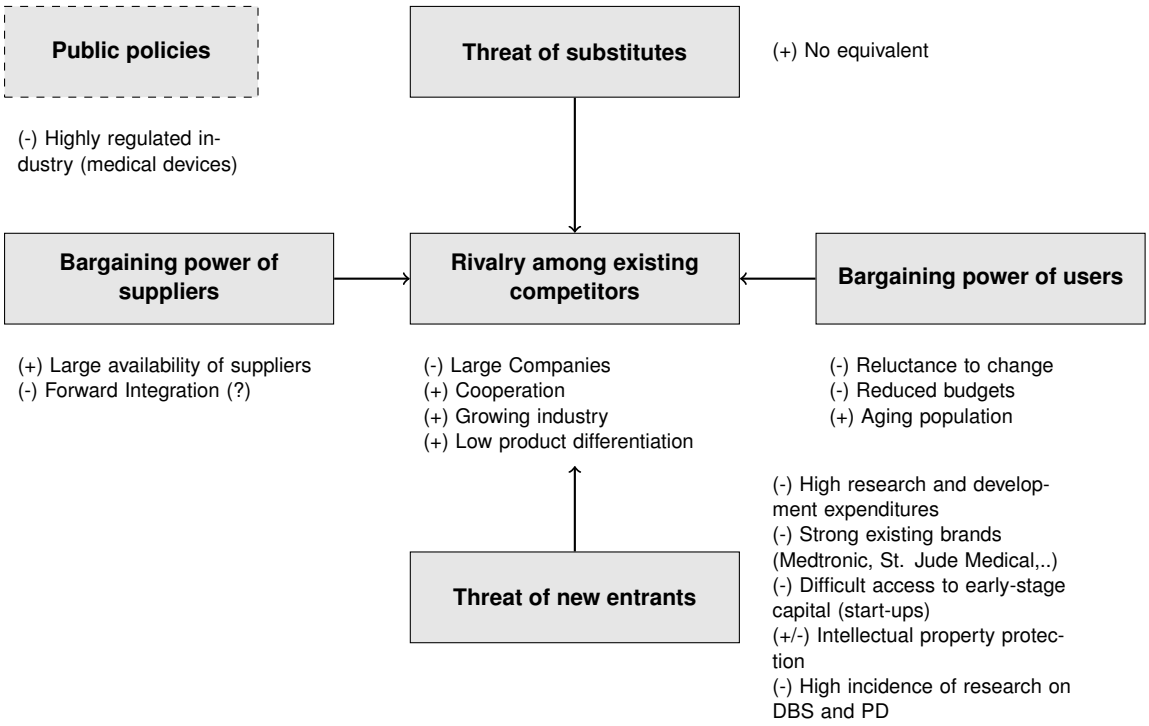

Figure 7.2: 6 Porter Forces related to the DBS-related devices industry.

To summarize the mentioned ideas and add some viewpoints, Figure 7.2 introduces the 6 Porter's Forces related to the DBS devices market. To meet the need of having a support tool for rigidity evaluation, the surgical operating teams may show reluctance to change which may hamper the acceptance of a new device into the procedure. Furthermore, there are well-established companies on this segment, with a strong brand. However, the product for DBS have relatively low differentiation which opens the possibility to endeavors to complement these already-marketed devices used intra-operatively by cooperating with these companies, specially considering the market's growth. The possibility of cooperation becomes even more important in the sense that there has been higher difficulty to access to early-stage capital for start-ups in recent years [65]. Still, this cooperation will only be possible if there is appropriate intellectual property protection to impede forward integration on the suppliers side (due to high simplicity of the system) and also among the competition, specially considering there is no substitute product available for the identified need, other than the end-users (physicians) themselves. The cooperation would be beneficial for both sides, namely regarding these companies' expertise in regulatory matters, inherent to the medical devices' market. Yet, one should consider that other research groups worldwide with affiliation to big player on the market can create a research project for a similar device.

7.4 Proposed Solution

As so far told, the system developed has three components:

1. Elastic band with a gyroscope placed in the patient's palm

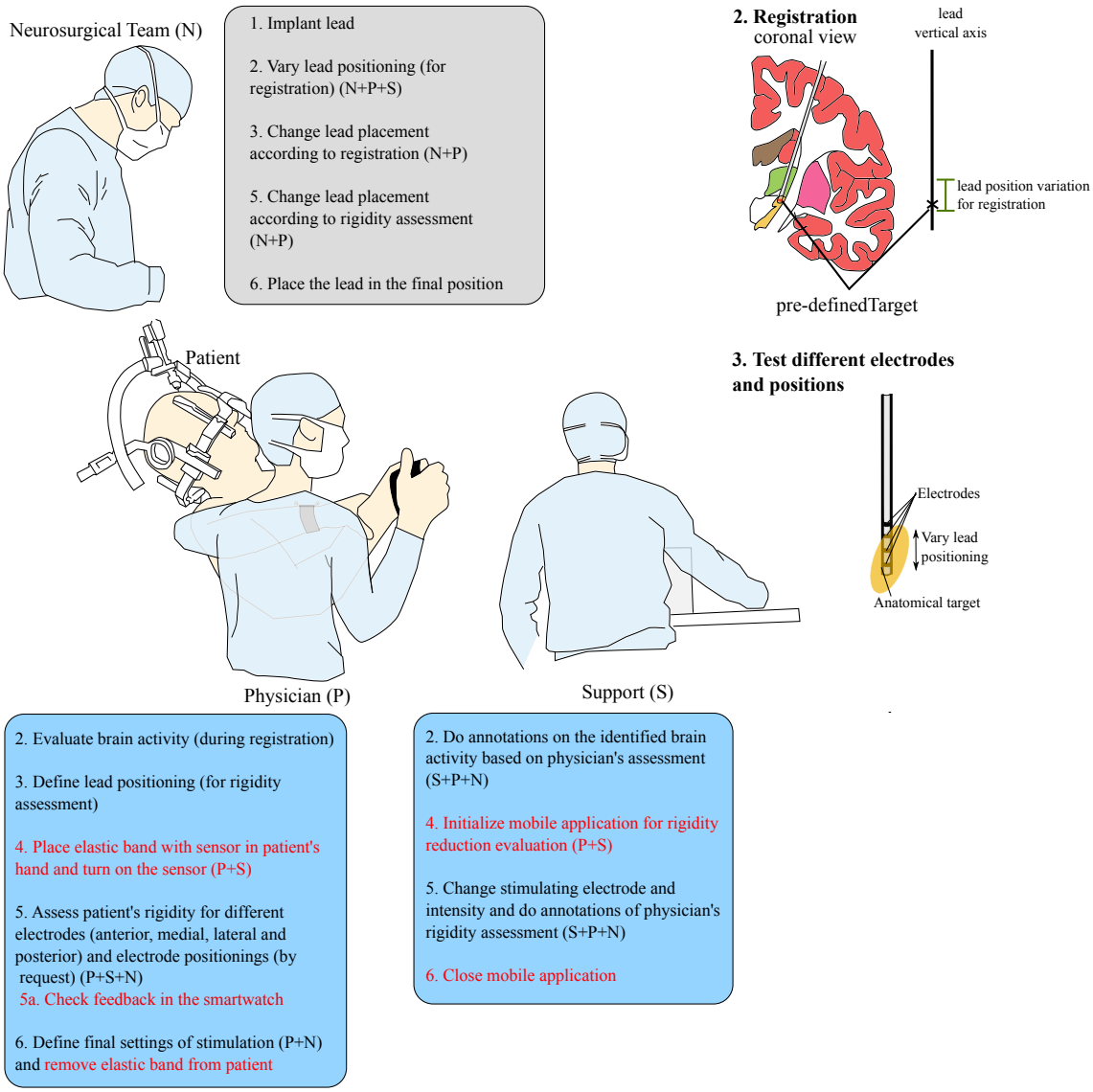

Figure 7.3: DBS surgery workflow: influence of the system for rigidity evaluation. In red are emphasized the additional tasks demanded by the use of the proposed system.

2. Smartphone as an acquisition, processing and feedback unit
3. Wearable (smartwatch) worn by the physician to receive feedback

which communicate between them via Bluetooth.

The impact on the DBS surgery workflow is depicted in Figure 7.3. As it is evidenced, this solution requires additional tasks that would slightly increase the duration of the overall rigidity assessment procedure. Thus, for an administrator, the benefit of this proposal does not rely on increasing the pace of the surgery but the possibility of reducing the number of reoperations due to suboptimal positioning of the stimulating electrodes, as it has been reported by Ellis *et al.* [66], which would benefit all involved stakeholders. To notice that a single surgery of DBS costs about €25 000 [67]. The miniaturized system is extremely easy to place and to be worn, and revealed accuracy. Finally, it is a device which can provide important information over the course of the

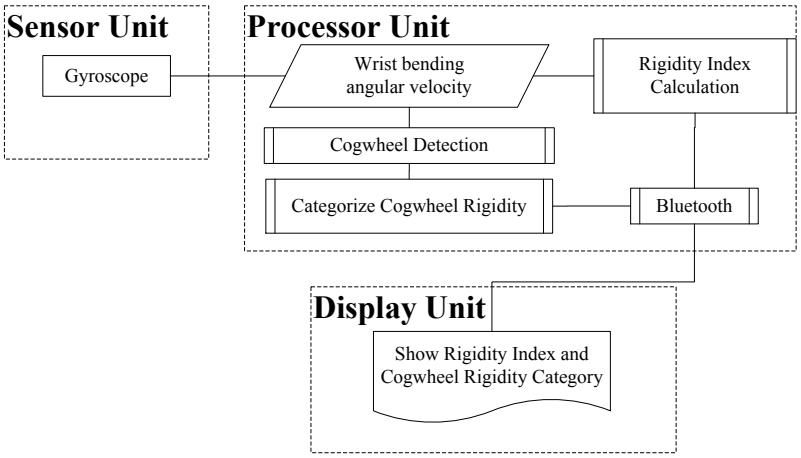

Figure 7.4: Block Diagram of proposed device. The sensor unit and processor unit could be a single module, communicating the resultant parameters to an external device with simply display function.

surgery, namely by reducing the subjectivity of the physicians' decision-making.

We could further miniaturize this system by having the sensor and processing unit in a single module which computes the needed parameters which are transmitted via Bluetooth to an external device working as a display unit (Figure 7.4). Such system would have the advantage of not being limited to the processing capabilities of an external device (smartphone or wearable). Hence, we could have it only as a glove/elastic band with a module for signal acquisition, processing and an accessory software to receive and display computed parameters from the later in an external device (*e. g.* android application).

As this system has two components, each should be considered separately as a medical device, as referred in Annex IX of the European Medical Devices Directive [68]. The hardware module would be classified as non-invasive (only in contact with intact skin) and as an active device for diagnosis because of his measuring and diagnosing capabilities of a state of health, which is to identify improvements in a motor symptom. Thus, it would be Class IIa medical device, compliant with rule 1 applicable to non-invasive devices (contact with intact skin) and rule 10 for active device for diagnosis (diagnosing feature) [69]. The accessory software would fall to the same category as it also provides diagnosing.

For such system to be placed in the European Union market, the CE mark (compliance label) is a must. However, several steps must be taken to apply for marking as in Figure 7.5.

Procedure Sequence for a Medical Device

1. Research Work
2. Clinical Testing under ethics committee ✗
3. Definition of final product
   (a) Voice of the customer: feedback from clinical staff and possible partners (*e. g.* Medtronic)
   (b) List of essential requirement and applicable standards for safety
   (c) From (a), define clear user scenarios, user needs and application environments
   (d) Risk analysis of the current solution based on the user scenarios defined in (c)
   (e) Definition of requirements from user scenarios
   (f) Planning development, deciding hierarchy of activities and initiate designing
   (g) Verification (of requirements through tests) and validation (of user needs through inquiries and observation)
   (h) Prototype production and validation
4. Application for CE mark

✗ *stands for current stage*

Figure 7.5: From research to marketing: the procedures [70].

7.4.1 Final Product Definition

Clinical Testing is under way, but what may follow other than continue the testing? Firstly, one should get feedback from the surgeon, nurses, patients and even other companies that have activity in this context. This would require to gather more centers, thus more DBS operational teams to evaluate the performance and usability of this system.

7.4.1.1 Requirements and standards

Secondly, one must identify requirements and standards that must be met. A medical device must not ever be considered absolutely safe because some shortcomings may only be experienced after extensive market experience. With this in mind, other than the essential requirements of Medical Devices (Annex I of Directive 93/42/EEC), there is a set of harmonized standards, related to the quality, safety and effectiveness of medical devices issued by International Organization for Standardization (ISO) and International Electrotechnical Commission (IEC). For the system under analysis in the European Union, the following are applicable [71]:

- Biological Evaluation of Medical Devices: Evaluation and testing within a risk management process (ISO 10993-1:2009)
- Quality management systems - Requirements for regulatory purposes (ISO 13485: 2012/AC :2012)
- Sterilization of medical devices - Information to be provided by the manufacturer for the processing of resterilizable medical devices (ISO 17664:2004)
- Medical electrical equipment - Part 1: General requirements for basic safety and essential performance (IEC 60601-1:2005/A1:2012)
- Medical electrical equipment - Part 1-6: General requirements for basic safety and essential performance - Collateral standard: Usability (IEC 60601-1-6:2010+A1:2013)
- Medical device software - Software life-cycle processes (IEC 62304:2006)
- Medical devices - Part 1: Application of usability engineering to medical devices (IEC 62366-1:2015, respective tutorial 62366-2:2015)

7.4.1.2 Risk Analysis

Also, when proposing a medical device, a risk assessment should be performed to identify where and when it could become hazardous and result in safety problems and harm. According to the category of the medical device, the degree of regulation imposed varies. For manufactures to develop an appropriate risk management approach, the ISO provides a framework which includes risk analysis, risk evaluation and risk control in medical device design (ISO 14971:2007).

Even though the device is non-invasive, there are some risks that must be considered. Just to name a few:

- occurrence of surgical complications (venous infarction or air embolism, leading hypoxia, incidence rate ranging from 1 to 10% [72]) which requires deciding: (1) proceed with identifying optimal stimulation settings and (2) use (or not) the system for quantitatively assess

rigidity. Both these decisions have implications on how quickly the stereotatic frame is removed and the patient is attended which may compromise his health
- reliability of communication protocol (radio-frequency, Bluetooth)
- device overheating

7.4.1.3 Additional Requirements

The developer may identify additional requirements related to the user scenarios considered that must be met, to be included in the previously prepared list. Overall the requirements may be related to:

- functional performance
- interface
- regulatory
- manufacturing
- training
- installation
- non-functional (environmental, usability, ergonomics, labeling, storage and cleaning and disinfection)

These requirements are related to the user needs and are applied to each of the components of the system: hardware and software.

Also, a development plan should be created and activities hierarchized. Furthermore, several products design should be done. Then, these are reviewed, by checking whether they meet the requirements. Finally, one design should be chosen and frozen, to produce a prototype and to proceed with its validation.

7.4.1.4 Clinical Evaluation

A manufacturer when performing clinical evaluation verifies whether the characteristics and performance of the device under normal conditions of use are compliant with the customer/market requirements (in respect to the intended use and instructions of use, exemplified in Figure 7.6), relying on clinical data (be it relevant scientific literature, be it result of clinical investigations made).

As stated in the article 15 of the Council Directive concerning medical devices (Official Journal of the European Communities), the occurrence of these clinical investigations should be communicated to the competent authorities of the Member States in which the investigations are to be conducted and authorization should be given.

This communication should be accompanied by:
- data allowing identification of the device in question
- an investigation plan (purpose, scientific, technical or medical grounds, scope and number of devices concerned)

Statements

Intended Use "The iHandU sensor is a wireless inertial measurement unit intended to be used by neurologists during Deep Brain Stimulation surgeries to act as a second opinion for the evaluation and assessment of the muscular rigidity under different stimulation parameters. It is intended to be held by a textile band and located on the palm of the hand, while measuring kinematic data and transferring it to a mobile application for processing and displaying of relevant clinical data. The classification functions are expected to be improved over time, as long as surgeries are being done, thus improving the adaptability and customization of the system to the end-user."

Indications for use "It is indicated for use on Deep Brain Stimulation surgeries, in which the neurologist think that it may be appropriate to perform the passive flexion movement of the hand for rigidity evaluation."

Figure 7.6: Proposal of statements for Intended Use and Indications for use

- opinion of the ethics committee
- place, starting date and scheduled duration for the investigations
- statement that the device in question confirms to the essential requirements apart from the aspects covered by the investigations and that, with regard to these aspects, every precaution has been taken to protect health and safety of the patient

Over the course of the clinical investigation, documentation about the device should be available for the competent national authorities with (1) a general description of the product, (2) design drawings, methods of manufacture envisaged, diagrams of components, sub-assemblies, circuits, etc, (3) respective descriptions and explanations, (4) results of the risk analysis and list of standards to be met applied in full or in part, and descriptions of the solutions adopted to meet the requirements and (5) results of the design calculations, and of the inspections and technical tests carried out, etc.

The methodology of a clinical investigation must:

- be performed reflecting the latest scientific and technical knowledge
- be defined in such a way to refute the manufacturer's claim
- include an adequate number of observations to guarantee scientific validity
- be performed in similar conditions to the normal use of the device
- be performed under the responsibility of a medical practitioner or another authorized qualified person in an appropriate environment
- include all adverse incidents record and notification

This should be accompanied by a written report with a discussion of all the data collected over the course of the clinical evaluation.

Documentation for CE mark

System Technical File to enable affixing CE Mark to the system, which shall include:

- Supplier qualification records and quality agreements
- Manufacturing qualifications, verifications, process validations plans and reports
- Final manufacturing plan
- Final system validation test plan and results
- First article reports
- Device Master Records (released at production, includes work instructions and production methods)
- Design Verification and Validation plans and reports
- Hazard and security analysis and risk management report
- Labeling
- Design reviews

Compliance with all the regulatory and global requirements including testing and certification to IEC 60601, 3^{rd} and 4^{th} editions as applicable

Completed Declaration of Conformity and Essential Requirements Matrix

Figure 7.7: Documents for application for CE marking.

7.4.2 Application for CE mark

To affix the CE marking necessary to market a medical device of this category (IIa), more than confirming the compliance of the device with its requirements is necessary. The manufacturer should perform an EC declaration of conformity, where it ensures and declares that the products concerned meet the provisions of this Directive which apply to them. This would be coupled with either a production quality assurance, a product quality assurance or EC verification (Annexes V, VI and IV of the Directive 93/42/EEC, respectively) [73]. All the requisites are summarized in Figure 7.7.

7.5 Intellectual Property

7.5.1 Protection Methods

Patent When in a very competitive market, the replication/copying of new-solutions may occur. Thus, before any publication, the original developers (João Paulo Cunha and Pedro Ferro Costa)

recurred to the intellectual property (IP) system by applying for a patent, to protect this rigidity evaluation method:

1. having a sensor (either gyroscope or accelerometer) placed in the anterior or posterior face of the hand (in a skin-contacting patch, coupled with an elastic band or fingerless glove) to which flexion/extension was imposed (in the context of deep brain stimulation surgery of a patient), which allowed extracting the angular velocity around the axis of joint rotation

2. the angular velocity signal enables distinguishing joint's rigid and non-rigid state and was used in a processing unit to compute a non-rigidity index.

3. the latter index is then displayed by a wireless connected device (the method encompasses having the data processor either electrically connected to the sensor or wirelessly)

4. the angular velocity signal may also be used to determine cogwheel rigidity, by the procedure in Chapter 3.

As in "Guidelines for Examination in the European Patent Office (EPO)", a process, machine, manufacture or composition of matter is patentable when:

1. there is an "**invention**", belonging to any field of technology
2. the invention is **susceptible of industrial application**
3. the invention is **new**
4. the invention involves an "**inventive step**"

and this acknowledgment gives exclusive right to the inventor(s) to earn from a product or process, thus enabling them with bargaining power in negotiations with business partners to launch the proposed solution. This protection lasts generally for 20 years from the application date.

The several stages of the patenting process are in Figure 7.8. Initially, a provisional patent application had been submitted to secure priority of this request and ensures privacy up to 12 months. Presently, a definite submission has been done and a filing date (Stage 2) has been given (which indicates that documentation apparently is correct). This is be followed by a formalities examination to ensure whether documentation is correct and complete. Up to 12 months after the filing date assignment, the inventors may decide how many countries he wishes to include to be covered by this patent protection (with the same filing date). Next, a search report will be sent to the inventors (Stage 3), which includes a list of other prior art documents found by the examiner that may be of interest for the invention and, possibly, an initial opinion on the patentability of the proposed system. 18 months after the filing date, the application is published in databases available around the world (Stage 4). At his point a final decision will be made about both proceeding with the patent application (by requesting a substantive examination - Stage 5) and which countries to include in the patent protection. Finally, after deep analysis of the application, a decision is reported to the inventor (Stage 6) and then it must be validated in each of the countries/states where the inventor has applied. In Europe, a patent may only be opposed up to 9 months after granting the patent (Stage 8) and appeal the decision (Stage 9).

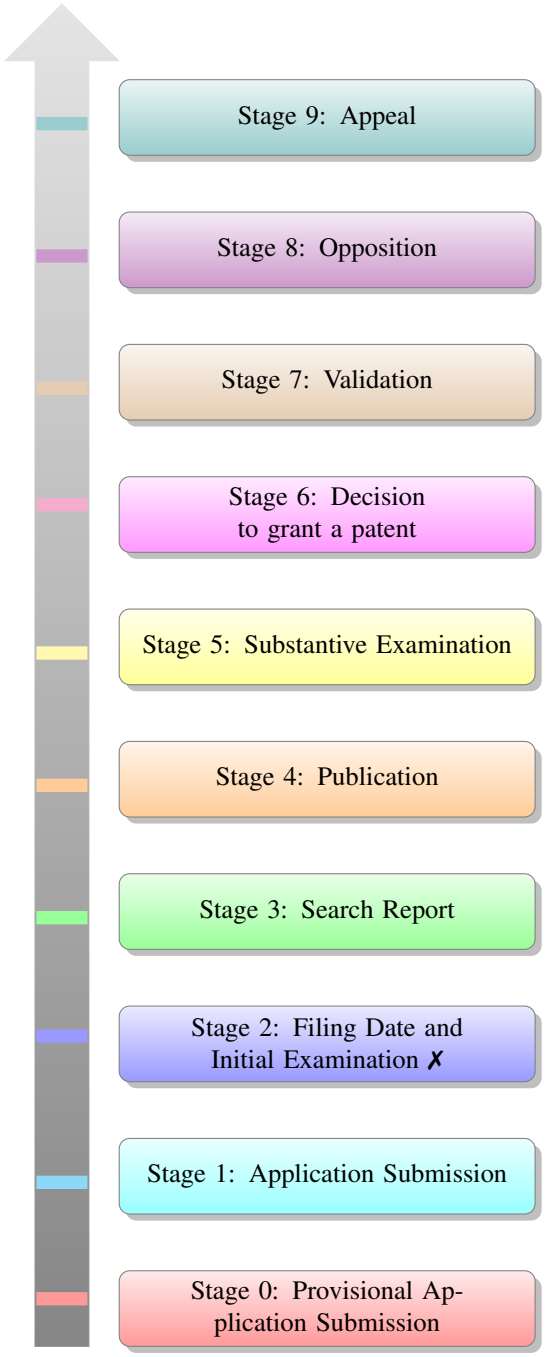

Figure 7.8: Stages of the patenting process. Adapted from European Patent Office. ✗ indicates current stage.

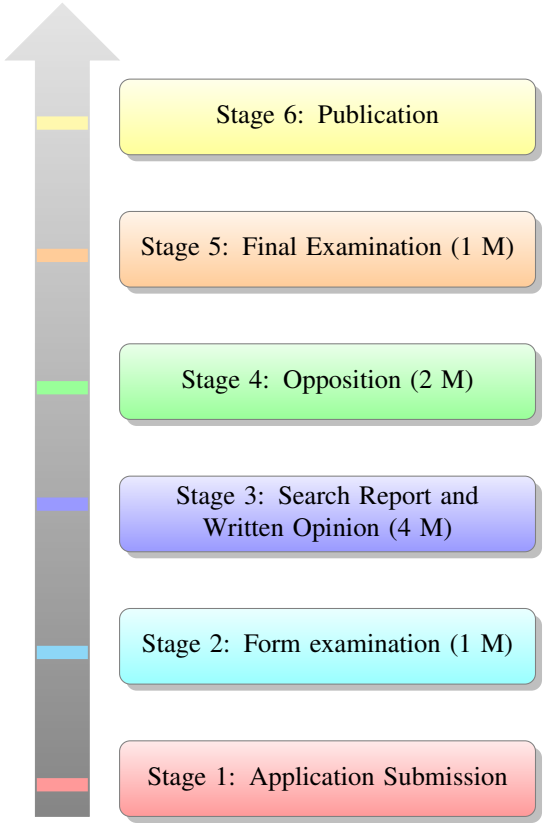

Figure 7.9: Stages and respective duration for Utility Model grant (*M* stands for month).

Utility Model In case this system is not deemed inventive, then an adequate solution to pursue is applying for utility model (UM). This is very similar to patenting but differs in the following [74]:

- even thought novelty is still a mandatory requirement, the significance of the "inventive step" or "non-obviousness" may be much lower or even absent
- may grant IP protection after 3-6 months after applying whereas when patenting it takes on average 43.1 months ($\approx$ 3.5 years)
- last from 7 to 10 years without possibility of renewal
- much cheaper to obtain and to maintain
- the search process is often significantly simpler and faster, taking, on average, six months
- a small number of countries and regions (however significant because must European countries are included) provide the option of UM protection (in Appendix H)
- does not include inventions which cover biological matter or substances or pharmaceutical and chemical processes

The steps for getting UM protection are in Figure 7.9.

7.5.2 Related Prior Art

To verify the illegibility of this method for rigidity assessment for IP protection, a search was performed regarding hand or arm sensorized systems to evaluate movement. The following patents and UM have been granted in this context (Figure 7.10):

- US 7892189 B2 (2006): system comprising of a movement sensor for sensing an acquiring movement data of a subject with a brain disorder (including PD), which is coupled to a analyzing unit and a display unit to show the analysis results related to the severity of the disorder and based on the movement's energy, as in Figure 7.10a; it focus on a magnetic sensor used in the fingers

- CN 104522949 B (2015): a wristband comprising of a motion sensor module (3 axial accelerometer, gyroscope and magnetometer) to detect different motion states of a Parkinson's patient and sending to a central processing module, which analyzes and processes the motion state signals to extract parameters and/or disease-relate information. The latter are then communicated to the upper computer (smart phones, tablet, or computer) wirelessly; the valid actions for evaluation include unilateral action palming, bilateral palming action, unilateral arm action, bilateral arm action; additionally, the target symptom described is tremor

- US 7862522 B1 (2006): multi-sensorized glove (Force-Resistor Sensor, potentiometer, bend sensors and accelerometer) for control of motion, sound and light comprising hand and fingers (Figure 7.10b);

- US 8581856 B2 (2009): system comprising of a receiver component that receives body gesture data from a sensor (measuring myogenic activity through a wristband, a band on the forearm, device coupled to the human shoulder or necklace), which controls a display component;

- US 8981765 B2 (2011): the invention is a device with simplified calibration for finger-tapping evaluation by using magnetic sensors (Figure 7.10c);

- US 6589190 B1 (2001): the patent comprises the device in Figure 7.10d, which imposes non-sinusoidal and non-ramp trajectories to a joint and the method to evaluate muscle stiffness, by extraction of stiffness, inertial and viscosity parameters;

- CN 203733070 U (2014): glove comprising of finger stalls, palm part and a hand back part, with a pressure sensing assembly and a photoelectric sensor, connected to a processing unit which wirelessly transmits function as to replace an ordinary mouse or simple keyboard adjustment operations for an improved user experience;

- US 5050618 A (1990, prescribed): apparatus to measure elastic component of resistance of angular displacement of a body joint, using a motor to impose movement and measuring the strain (Figure 7.10e)

Furthermore, several applications for patents were found which use sensorized systems to evaluate upper limb movement (displayed in Figures 7.11 and 7.12):

- US 20120127070 (2012, rejected): wearable device which combines data from wrist, arm and fingers, each with inertial sensors as gyroscopes and accelerometers; different movements generate different signals which allow controlling an external device (Figure 7.11a)
- EP 2733578 (2013, examination requested): wearable device with one or more sensor for gesture recognition which estimated the position of arm and hand from the sensor measurements (Figure 7.11b)
- US 20120025945 (2011, rejected): hand wearable glove with one or more sensors coupled to it and positioned to measure hand movement; there is, at least, temporary data storage from the sensors, which may be wirelessly synchronized with an external device in real-time (Figure 7.11c)
- US 20120319940 (2012, rejected): wearable device to control electronic devices, as an alternative to other input devices (mouse, keyboard, or game controller). Such device is able to recognize complex gestures, such as a person signing American Sign Language and may include a plurality of motion sensors affixed to a user's fingers and a plurality of motion sensors affixed to a user's wrists, a processing component and a communication component designed to communicate with a second electronic device (Figure 7.11d)
- JP 2010193936 A (2010, request for patent): system which evaluates muscle rigidity, in particular, cogwheel rigidity, by measuring myogenic activity and resistive torque when a step-motor imposes bending to the upper limb of a subject (Figure 7.11e)
- US 20140276242 (2014, revised claims under-examination): wearable body sensor system to monitor body posture with or without an assistive walking device (considering the center of gravity and base of support); system comprising of a sensor placed at the center of gravity of the body, a network of sensors placed in pre-determined positions; each sensor composed of 3D accelerometer, gyroscope and magnetometer (Figure 7.11f)
- CN 104127187 (2014, under examination): system for cardinal symptom quantitative detection of Parkinson Patients, comprising of a glove and a computer (connected through wires or wirelessly); the glove comprises of a wrist module (3-axis accelerometer and gyroscope, two pressure sensors for data acquisition related to muscle stiffness, and a microcontroller) and a fingertip module (3-axis accelerometer and gyroscope, for data collection related to tremor and bradykinesia); through a microcontrollers, the data is sent to a computer for processing a display (Figure 7.12a)
- WO 2014108883 (2014, examination requested): wearable device with tri-axial inertial sensors to monitor "on-the-fly" human limbs biomechanics; sensors placed in the distal phalanxes of the fingers (Figure 7.12b), with the possibility of communicating wirelessly or not to an external device

- EP 2714188 A4 (2012, to be refused): mentioned in Chapter 2, method for adjusting DBS parameters after surgery based on quantitative motor assessment, using an accelerometer/-gyroscope placed in a finger connected to a processing module which communicates with a external device for display. The quantified parameters are related to clinician score to the motor disorder (UPDRS in the case of PD) (Figure 7.12c)

Among the granted protection, the herein proposed invention is novel because there has not been anyone tackling rigidity evaluation using only kinematic information and to correlate it to resistive force (rather than coupling the system with strain or pressure gauges) and requiring only the placement of a sensor in the anterior face of the hand (rather than using fingers). Still, other patents may deem this proposal "obvious". For example, in the apparatus of US 5050618 A, a controlled angular velocity is imposed to any joint and the resistive force is measured , which translates its rigidity. The solution proposed reverses the mindset: because the technique to evaluate rigidity clinically is standardized, possibly one may consider that about the same force is applied by the movement-imposing subject to the joint (*i. e.*, clinician), hence differences in angular velocity will translate differences in resistive force of the patient's joint and, consequently, in rigidity. Also, in 2014 a patent application was filed, which also comprised of a system to evaluate biomechanics which uses inertial sensors and also real-time feedback of extracted parameters; still, as many others, they focus on the fingers and having a processing unit in the wrist. The wireless connection to provide data from a sensor and/or processing unit to an external device to provide feedback has been issued both in the latter as in the patent CN 104522949 B, deeming "obvious" this feature. The aforementioned patent applications which were rejected had most of its claims considered as obvious namely by prior art Barclay (US 7862522 B1). Among those systems found, we may emphasize JP 2010193936 A for rigidity evaluation, in particular, cogwheel rigidity, still the setup is quite different recurring to a motor to impose movement and also capturing the myogenic signal.

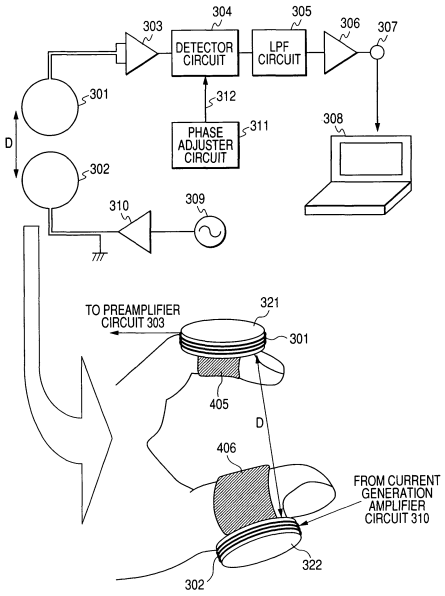

(a) Movement analysis display apparatus and movement analyzing method (US 7892189 B2) by Akihiko Kandori, Tsuyoshi Miyashita and Kuniomi Ogata.

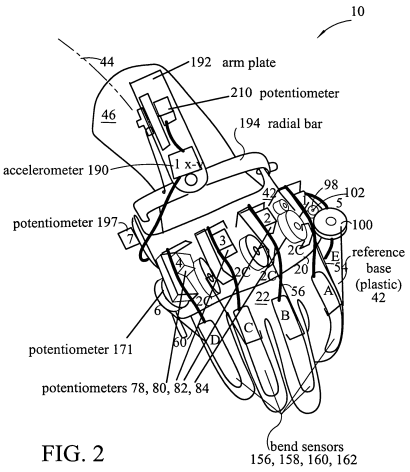

FIG. 2

(b) Sensor Glove (US 7862522 B1) by David Barclay, Glenn Silver, Johan Versteegh and Bruce Lanoil.

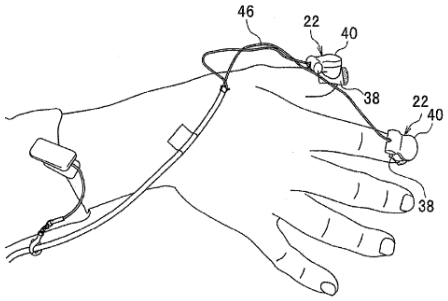

(c) Motor Function Analyzing Apparatus (US 8981765 B2) by Yuko Sano, Akihiko Kandori, Tsuyoshi Miyashita, Katsuya Morohoshi and Kouichi Ishizuka.

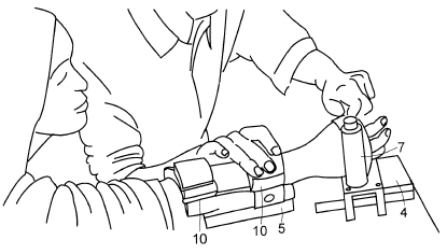

(d) Quantification of Muscle Tone (US 6589190 B1) by Sami Kanderian, Randal Goldberg, Katrina Obell, Barbara de Lateur, Louis Whitcomb and Fred Lenz.

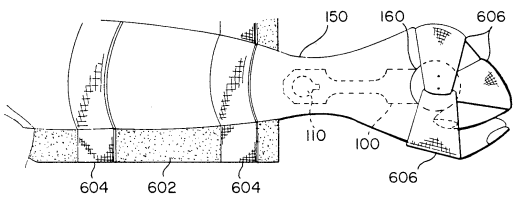

(e) Method and apparatus for measurement of joint stiffness (US 5050618-3 A) by Lawrence E. Larsen.

Figure 7.10: Granted Patent Figures.

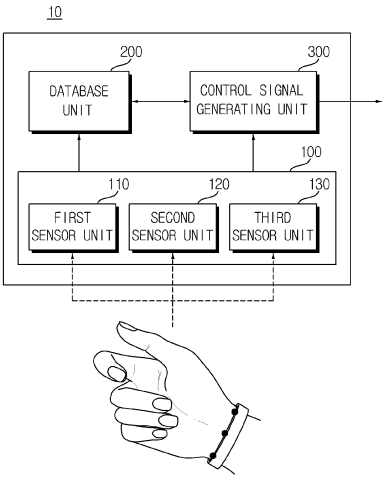

(a) Control signal input device and method using posture recognition (US 20120127070) by Don Wan Ryuoo and Jun Seok Park.

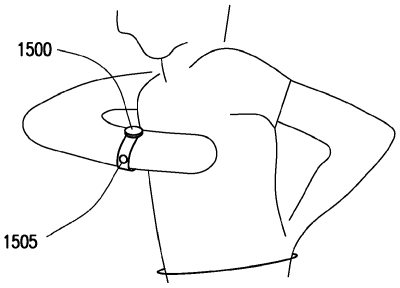

(b) User gesture input to wearable electronic device involving movement of device (EP 2733578) by Pranav Mistry, Sajid Sadi, Lining Yao, John Snavely.

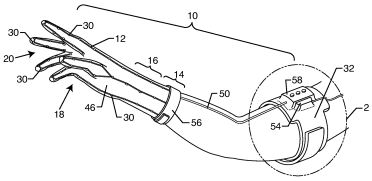

(c) Motion capture data glove (US 20120025945) by Faisal M. Yazadi, Mark Schelbert and Lawrence Miller.

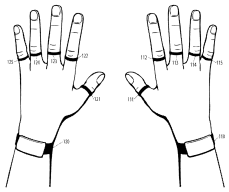

(d) Wearable Digital Input Device for Multipoint Free Space Data Collection and Analysis (US 20120319940) by Daniel Bress, Mark Bernard Jacobs, James Edward Dunstan and Steven Bress.

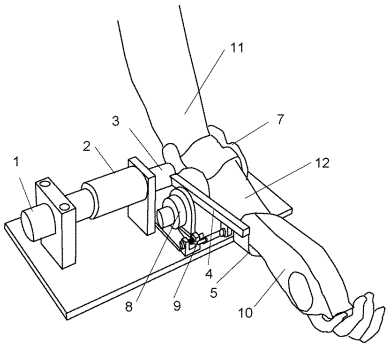

(e) Muscle Rigidity Degree Quantitative Evaluation (JP 2010193936) by Tetsuya Maeda and Nakamura Kazuhiro.

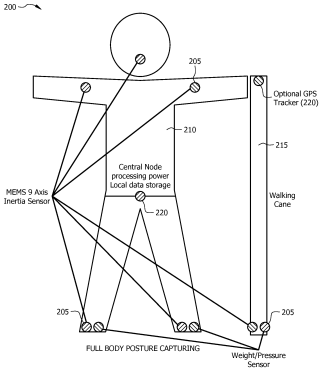

(f) Wearable body 3d sensor network system and method (US 20140276242) by Shyh-Min Chen, Manli Yang and Arthur Tu.

Figure 7.11: Patent Applications Figures (Part 1).

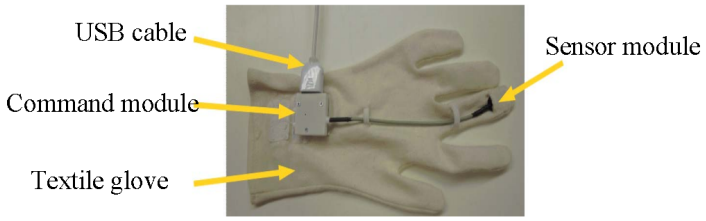

(a) Wearable system and method for cardinal symptom quantitative detection of Parkinson patients (CN 104127187) by Houde Dai.

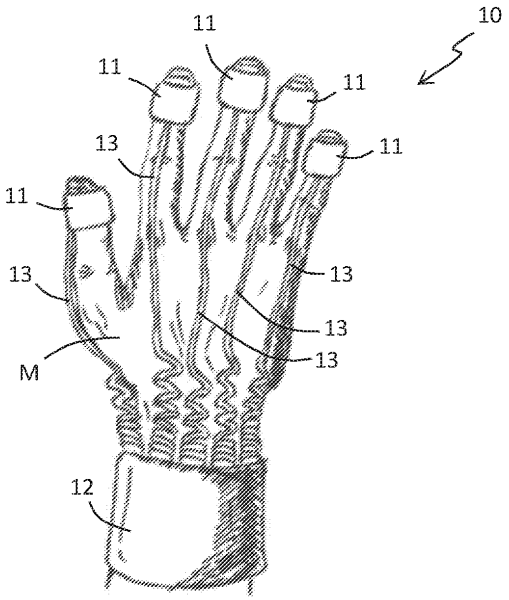

(b) Method and related apparatus for monitoring biomechanical performances of human limbs (WO 2014108883 A1) by Filippo Cavallo, Carlo Maremmani, Dario Esposito, Erika Rovini, Michela Aquilano, Paolo Dario and Maria Chiara Carrozza.

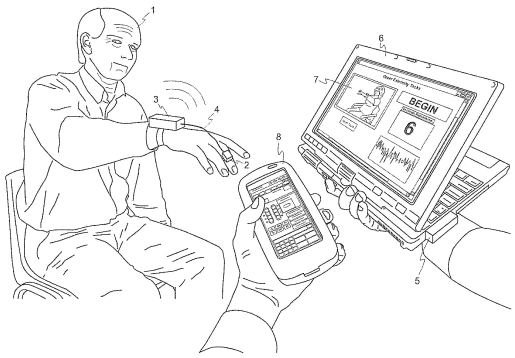

(c) Method and system for tuning of movement disorder therapy devices (EP 2714188 A4) by Joseph P. Giuffrida, Dustin A. Heldman and Thomas O. Meraa.

Figure 7.12: Patent Applications Figures (Part 2).

7.6 Final Remarks

In this chapter, the intricacies of the DBS-related market were explored as well as the pathway from investigation-to-market and IP protection.

It is widely agreed the growth of the DBS devices market, in particular, for movement disorders as in the case of PD. This is related not only to the aging population (thus, an expected increase in incidence of PD) but also to the effectiveness of the surgery. To supply and support DBS specialized centers for these disorders, there are few suppliers (Medtronic Inc., St. Jude Medical Inc. and Boston Scientific Corp.) and there is possibility of growth by establishment of symbiotic relationships with them as has already occurred (by complementing their systems). Easy access to centers performing DBS surgeries and expertise on medical devices regulation (as introduced, extremely tortuous) would be great add-ons for the introduction of a new product originating from an institution focused on research. A tool for bargaining is the application for patent of the existing device which protects the developers and institution of having the concept stolen from these established companies. The patent and UM search revealed mostly systems for control of external devices but as well as for assessment of motor symptoms. Still, the patent should be granted considering the unique design (finger-less glove or elastic band) and kinematic-only information acquired which is used for rigidity evaluation; other existent systems (waiting examination, rejected and patent/UM granted) (1) rely mostly on sensors positioned in the fingers, (2) target controlling external devices or (3) tremor or bradykinesia quantification or (4), when focused on rigidity, they encompass motors and pressure gauges. Even if the proposed system is deemed obvious, applying for UM (which may provide protection over the same product simultaneously to a patent [75]), could secure IP protection, which is not as strict with the aforementioned feature as in patents examination.

Anyhow, granting a patent may still take over 2 years and in the meantime, other procedures should be undertaken to take the system to market. Feedback of the research device should be gathered from a significant number of medical doctors, nurses and patients and even with possible partners (to design it to best complement current procedures and their devices), comply with the ISO and IEC standards, as well as the essential requirements demanded, propose several candidates for final design and review them in regards to the aforementioned requirements. Finally, a design is chosen which leads to the prototype production and clinical evaluation. Only then, accompanied by the adequate documentation and manufacturing planning, this system may be proposed for CE mark, which enables marketing.

In summary, from this point onwards, the research work should be pitched to current players in this market. If successful, this will provide help in having this technology tested cross-center and thus a rich and diversified feedback from the stakeholders. Otherwise, several clinical collaborations should be established to fulfill that purpose. Such information is pivotal namely in the sense of enabling us to best overcome the reluctance to change of the involved parties Moreover, innovation competitions (*e. g.* Web Summit, Health Acceleration Challenge, Imagine Cup) should be targeted to get funding for to take the steps towards CE marking and even advisors in legislation

related to medical devices. To assure protection in case patent is rejected an application for UM is advisable: in case of rejection of the application, other medical device companies may overthrow the efforts in the current system and produce similar solutions, to distinguish their own already established products in this highly competitive market.

Chapter 8

Other Applications of the System

This system for rigidity assessment during DBS can be applied to other scenarios, namely other motor symptoms evaluation or even to control on-demand the stimulation, according to the severity of rigidity. This will be further explored next.

8.1 Tremor

Tremor is a motor symptom related to Parkinson's Disease, which is more noticeable in rest position with a prevalence over 70% in the patients with Parkinson's Disease. Postural and rest tremor are more strongly associated to Essential tremor [6, 7]. As introduced in Chapter 2, several parameters in time- and frequency-domain have been used to study tremor. Herein, we will be comparing the impact of tremor on some of these parameters, using the MoMo to acquire signal and validating its use for motor symptoms assessment, other than rigidity. Time- and frequency-domain parameters will be experimented and validated which could be later to further enlarge the scope of the system to other neurological diseases, where Deep Brain Stimulation (DBS) surgery may be applied.

8.1.1 Methodology

8.1.1.1 Acquisition Protocol

The data acquisition protocol encompasses two distinct settings:

- simulation, with healthy subjects who had tremor elicited
- real-life, as in acquiring data from patients who were subjected to DBS surgery, before and after the surgery

Using MoMo in the subject hand (introduced previously in Chapter 3) broadcasting acceleration, angular velocity and quaternion data via Bluetooth to a computer or smartphone, signal acquisitions were performed.

To simulate a tremoric conditions, a shaker was used, comprising of a rotating plate parallel to the ground, where a subject rested his arm (as in Figure 8.1). The range of rotations allowed

were from 160 to 640 rotations *per* minute. This setup was chosen instead of asking for a subject to simulate tremor because more data variability could be acquired under controlled conditions.

So, when dealing with healthy subjects, we proceeded as follows:

- Extend both arms forward, to get the baseline status relative to an healthy subject
- Rest the arm whose hand has the sensor over the shaker, holding up hand as in Figure 8.1
- Perform measurements for each of the following rotation frequencies of the shaker: 160 rpm, 320 rpm, 480 rpm and 640 rpm. This range encompasses the neurological tremor frequency range from 3 - 12 Hz [7]
- Repeat in the opposite arm

The patients subjected to DBS surgery would perform the usual tasks to assess postural tremor and dynamic tremor as introduced in Chapter 2, *i. e.*:

- postural tremor by extending arms forward
- dynamic tremor by successively extending and bending an arm to tap the nose (as in Figure 8.2)

8.1.1.2 Signal Processing

For data processing, the focus was on the Euler angles computed from the quaternion data, given by the MoMo:

$$\mathbf{o} = [\theta \quad \psi \quad \phi] \tag{8.1}$$

where θ, ψ and ϕ stand for yaw, pitch and roll, respectively.

Focus was given to the Euler angles since both angular velocity and acceleration are derived from the positioning of the hand, being redundant data. Furthermore, acceleration translated linear movement and not rotational, which is the type that occurs in human tremor (as a rotation of a joint).

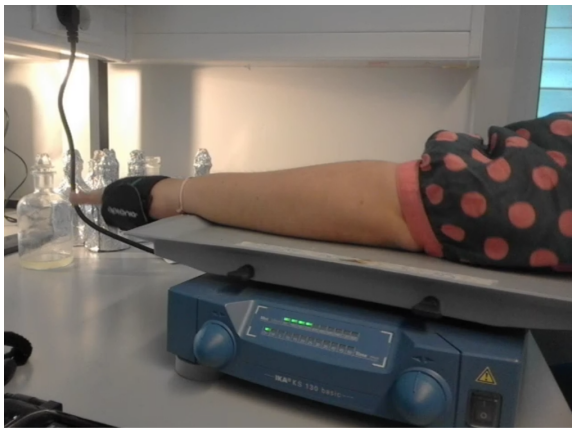

Figure 8.1: Positioning of arm over the shaker's plate.

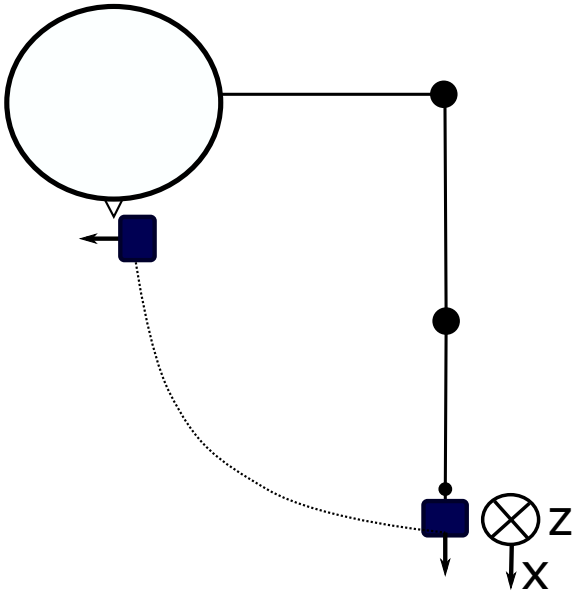

Figure 8.2: Representation of dynamic tremor assessment task. The orientation of the z- and x-axis of the sensor are shown.

In the time domain, the *RMS* was computed (equivalent to the standard deviation of the original signal when average of the signal is removed). Also, other parameters were computed such as skewness, which is a measure of the asymmetry of the signal given by:

$$S = \frac{\sqrt{n(n-1)}}{(n-2)} \quad \frac{\frac{1}{n}\sum_{i=1}^{n}(x_i-\mu)^3}{\sigma^3} \tag{8.2}$$

and, aiming for low computational cost, a local deviation measure (*LD*), where for every sample of the signal, the absolute deviation towards the mean value μ_{local} of the window with width of 17 samples was computed and then summed and normalized by dividing by the length of the signal:

$$LD = \frac{\sum_{i}^{n}|x_i-\mu_{local}|}{n} \tag{8.3}$$

The size of this window was selected considering the lower bound of the tremor frequency range of interest, 3 Hz. Because the sample frequency is about 50 Hz, hence a full oscillation is represented by $50/3 \approx 17$ samples and, by performing a local averaging within this window, we have the angular deviation from an approximate "tremorless-state".

For a frequency analysis, the fast Fourier transformation was applied and the *PF* in 1-15 Hz band and *C-factor*, computed as follows:

$$C-factor = \frac{Power_{PF}}{Power_{total}} \tag{8.4}$$

translating the ratio between the power of the detected frequency and the total power of the signal. To compute these frequency parameters, the signal was detreended by removing to its average.

By simulating tremor, we envisioned to identify a relationship between the peak frequency

found and other measures of the tremor angular magnitude (*RMS*, *S* and *LD*) and also *C-fator*, which has been correlated with the tremor severity. In previous work [30, 76, 77], such endeavor has been made but towards comparing frequency, f to a linear displacement measurement, d, as $log(f) = f(log(d))$.

Therefore, for each of the features, the best fitting linear function was found in a least-squares sense as follows:

$$\mathrm{p} = f(log(PF)) \tag{8.5}$$

$$log(\mathrm{p}) = f(log(PF)) \tag{8.6}$$

where log is the natural logarithm and p the parameter used.

8.1.2 Experiments

8.1.2.1 Simulation Setting

A total of 181 signals, 300 samples long, were acquired from healthy subjects, either related to their baseline state and to the simulated tremor with different rotations by the shaker. In Figure 8.3a, the differences found in the orientation of the hand overtime and in the frequency domain are presented. As expected, we find a sinusoidal wave for simulation settings translating the evoked tremor, a frequency behavior with a peak frequency of 7.81 Hz and a *C-Factor* of 0.45.

As expected, with the simulation setup, we were able to simulate various tremors (different frequency and amplitudes) due to different RPM tested in the shaker device and also inherent difference in the subject anatomy (hand's length and weight). This is proven by Figure 8.4, where Figure 8.4a translates the variability of the main frequency of simulated tremor elicited by a same rotation speed. Likewise, some amplitude of rotation of the wrist joint due to induced-tremor was achieved.

A statistically significant difference was found between the healthy baseline state and tremor-induced for *RMS*, *LD*, and *C-factor*, with the exception of *S* (Figure 8.5). Furthermore, it was inspected whether the peak frequency was related to these features as shown in Figure 8.6. No correlation whatsoever or extremely reduced was found regarding *S* and *RMS*, either considering them as function of *PF* and $log(PF)$, whereas related to *C-factor* and *LD*, some interdependence between them and peak frequency was found (approximately 20% of the variation of either features may be explained by changes of frequency).

8.1.2.2 Clinical Setting: Postural Tremor

From the total of patients, only the data of those diagnosed with tremor was considered (3 patients, 5 limbs). The variation of *RMS*, *LD*, *S* and *C-factor* caused by implantation of stimulation electrodes may be found in Figure 8.7 and the tremor frequency in Table 8.1. The latter presents as well the *C-factor* and *LD* for each limb analyzed and the computed frequency relying on the functions found relating these and the tremor frequency (presented in Figure 8.6).

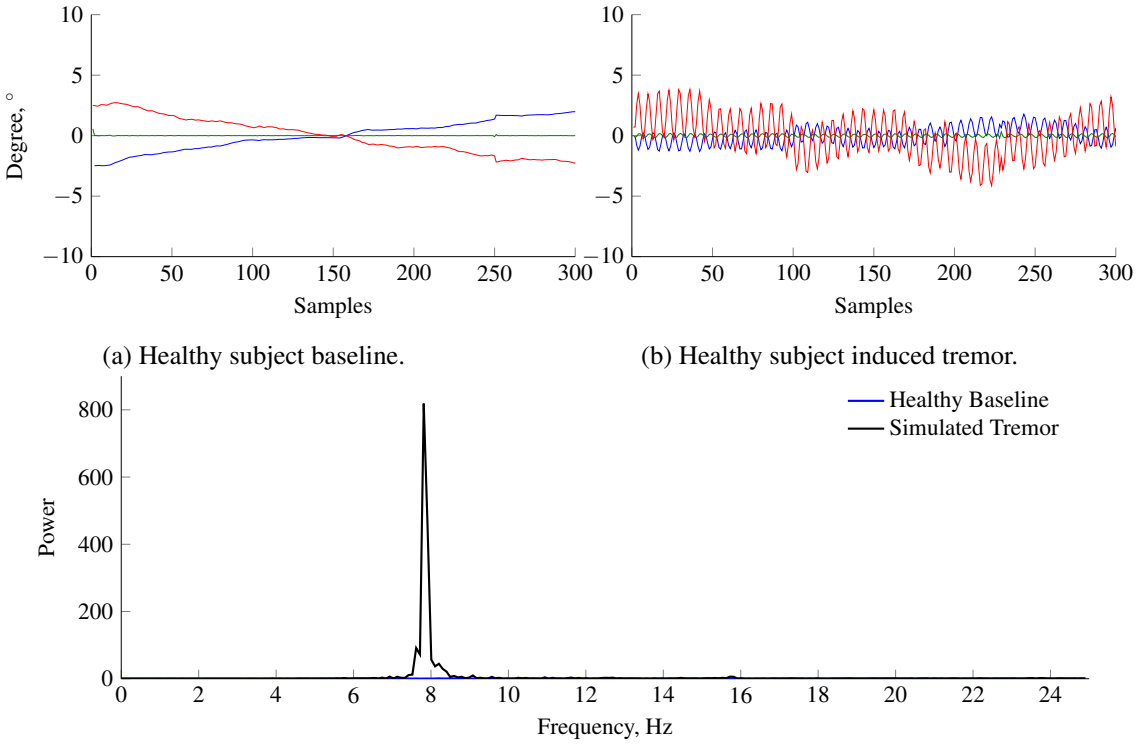

(a) Healthy subject baseline.

(b) Healthy subject induced tremor.

(c) Power Spectrum of healthy subject baseline and induced tremor of ψ.

Figure 8.3: Comparison between baseline and induced tremor of healthy subject in the time and frequency domain.

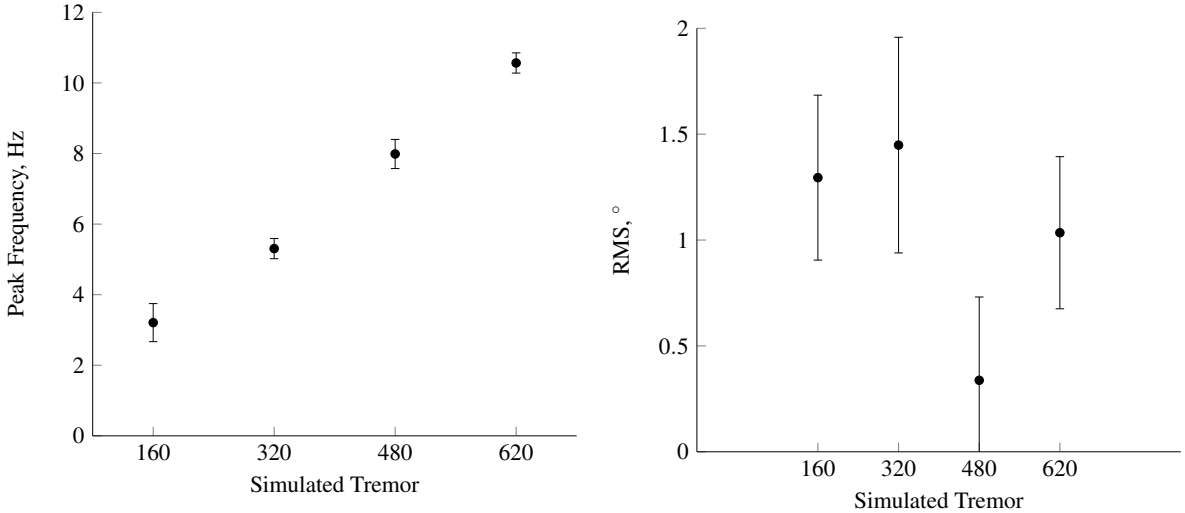

(a) Peak Frequency vs RPM. Mean ± standard deviation of peak frequency.

(b) RMS vs RPM.

Figure 8.4: Achieved tremor behavior with simulation method. RPM stands for rotation *per* minute. Mean ± standard deviation of RMS.

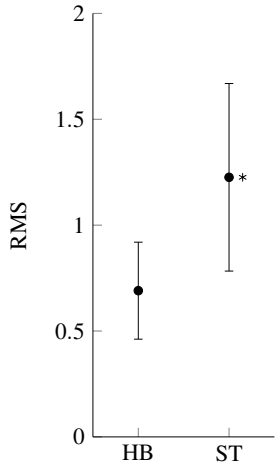

(a) Root-mean Square (RMS). $p < 0.001$.

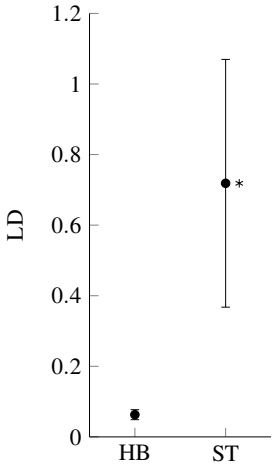

(b) Local Deviation (LD). $p < 0.001$.

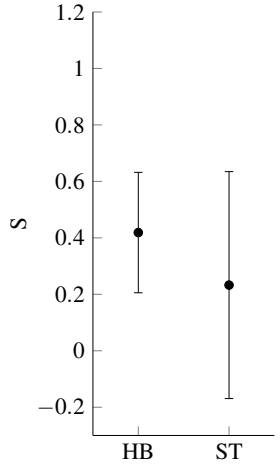

(c) Skewness (S). $p = 0.09$.

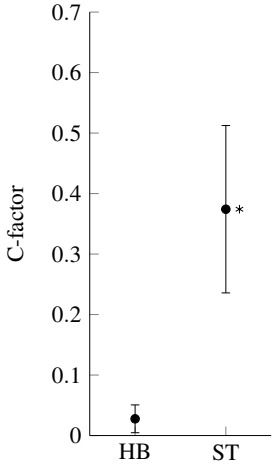

(d) Crest factor (C-factor). $p < 0.001$.

Figure 8.5: Distinguishing healthy baseline (HB) from simulated tremor (ST). The mean $\pm$ standard deviation of each feature is represented for both HB and ST. * indicates a significant difference was found between HB and ST ($p < 0.01$).

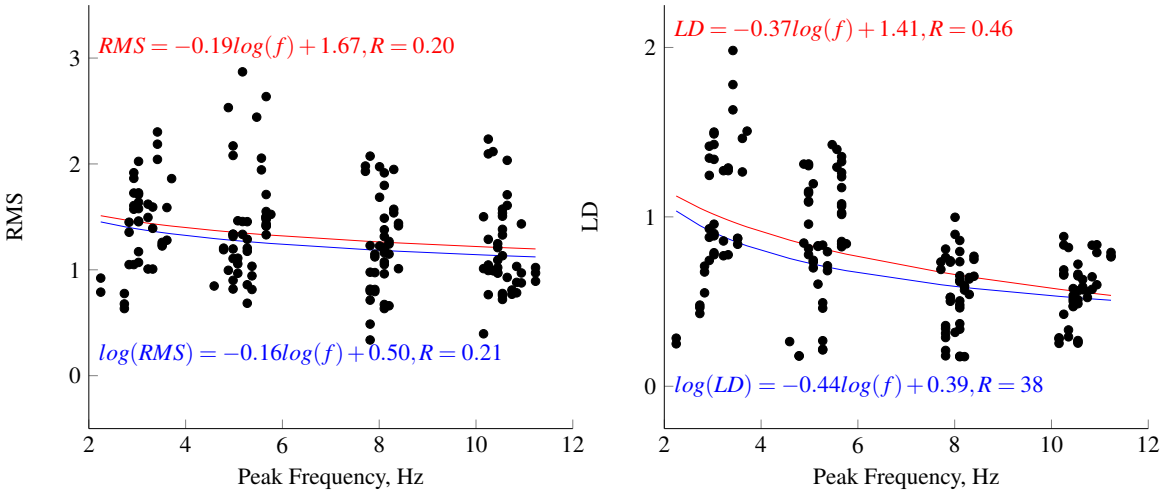

(a) RMS vs peak frequency.

(b) LD vs peak Frequency.

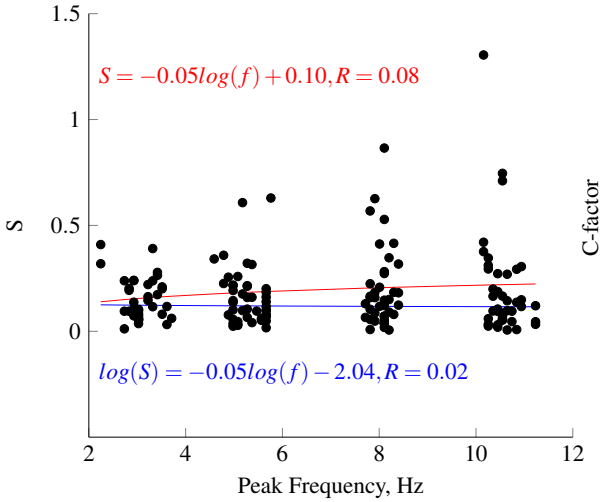

(c) Skewness vs peak frequency.

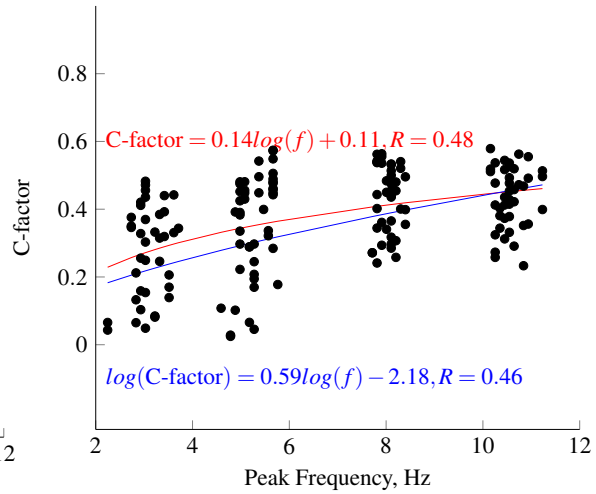

(d) C-Factor vs peak Frequency.

Figure 8.6: Relationship found between several parameters and simulated-tremor frequency. R stands for correlation coefficient.

Overall, the DBS surgery lead to a decrease in both *LD* and *RMS*, which can distinguish these two states as in simulation settings (healthy baseline versus induced-tremor). Still, an annotation should be done to the range of these parameters in both settings:

- the most severe tremor situation had a *RMS* before surgery of 14.62 ° and a *LD* of 7.18 °
- the most subtle fits into the simulated tremor range, with a $RMS = 0.84$ and $LD = 0.29$

whereas, the mean± standard deviation of *RMS* and *LD* values of simulated tremor were, respectively, 1.22±0.44 and 0.71±0.35. On a different note, a tendency of increase in *S* was found, whilst the *C-factor* decreased.

To test the validity of the functions relating the most correlated features with the peak frequency in simulation settings:

$$C\text{-}factor = 0.14log(PF) + 0.11 \tag{8.7}$$

$$log(C\text{-}factor) = -0.59log(PF) - 2.18 \tag{8.8}$$

$$LD = -0.37log(PF) + 1.41 \tag{8.9}$$

$$log(LD) = -0.44log(PF) + 0.39 \tag{8.10}$$

The consequent PF was compared to the directly computed from the signal. The results are in Table 8.1. A mean absolute deviation from the true frequency of:

- 3.39 Hz for *F=f(log(C-factor))*
- 3.02 Hz for *F=f(C-factor)*
- 9.85 Hz for *F=f(log(LD))*
- 6.14 Hz for *F=f(LD)*

Considering that the tremor frequency range is between 3 and 12 Hz, these deviations are extremely high, covering the frequency band of interest from 38% to over 100%.

8.1.2.3 Clinical Setting: Dynamic Tremor

For analysis of dynamic tremor, there is only a single patient study to present (correspondent to limbs 1 and 2 referenced in Table 8.1). In Figure 8.8, a limb's data is represented from before and after DBS surgery. The wider and higher arcades correspond to the movement of flexion/extension of elbow joint (Figure 8.8a and 8.8b), whereas the lower amplitude oscillation (of higher frequency) is the pathological tremor (Figure 8.8b). These correspond in the frequency domain, respectively, to the peaks in a lower frequency range and higher frequency (~5Hz in Figure 8.8c).

Table 8.1: Peak Frequency (PF) measured in each of the examined limbs. *C-factor* stands for crest factor, *ID* for identification assigned for different limbs, *LD* for local deviation and F as frequency computed from a function f determined previously.

ID	PF	C-factor	LD	F=f(log(C-factor))	F=f(C-factor)	F=f(log(LD))	F=f(LD)
1	3.71 Hz	0.367	3.80	7.36 Hz	6.27 Hz	0.12 Hz	<0.01 Hz
2	3.41 Hz	0.148	3.66	1.58 Hz	1.31 Hz	0.13 Hz	<0.01 Hz
3	6.15 Hz	0.463	0.29	10.91 Hz	12.45 Hz	40.44 Hz	20.64 Hz
4	3.03 Hz	0.351	0.57	6.82 Hz	5.59 Hz	8.71 Hz	9.68 Hz
5	2.44 Hz	0.305	7,18	5.38 Hz	4.03 Hz	0.03 Hz	<0.01 Hz

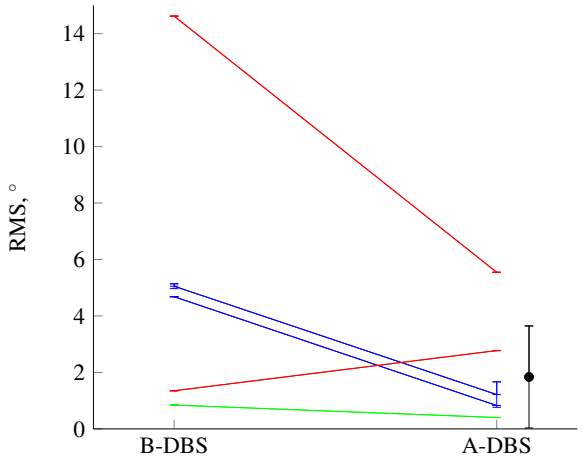

(a) Root-mean square (RMS).

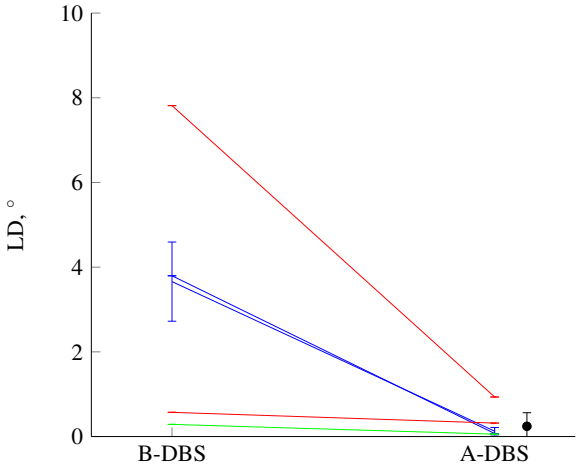

(b) Local Deviation (LD).

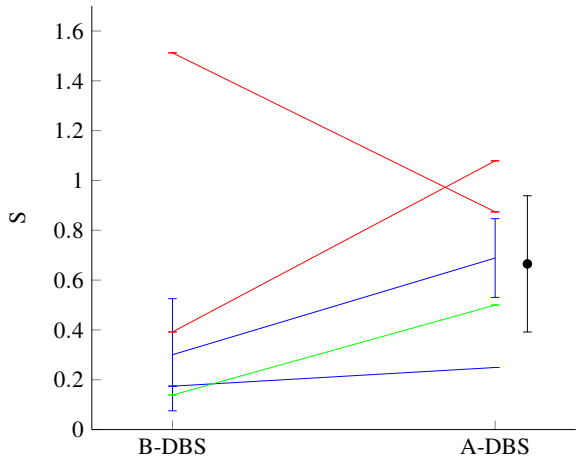

(c) Skewness (S).

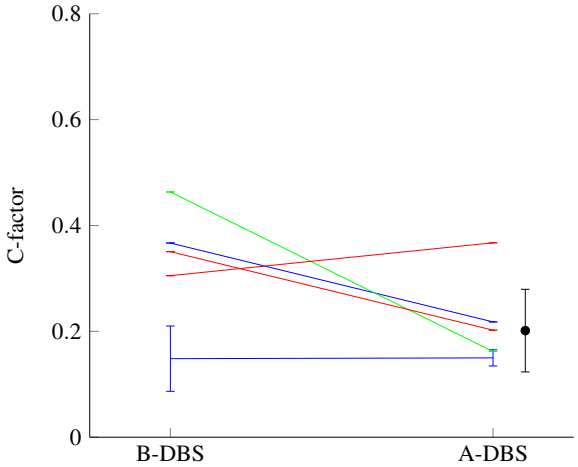

(d) Crest factor (C-Factor).

Figure 8.7: Influence of surgery on motor performance given by *RMS*, *LD*, *S* and *C-factor* (mean + standard deviation, if applicable). Each color represents a patient. Blue, green and red correspond respectively to limbs 1 and 2 (mean $\pm$ standard deviation), 3 and 4 and 5. Black dot indicates mean value $\pm$ standard deviation of parameters across all patients after surgery. B-DBS and A-DBS stand for before and after DBS surgery.

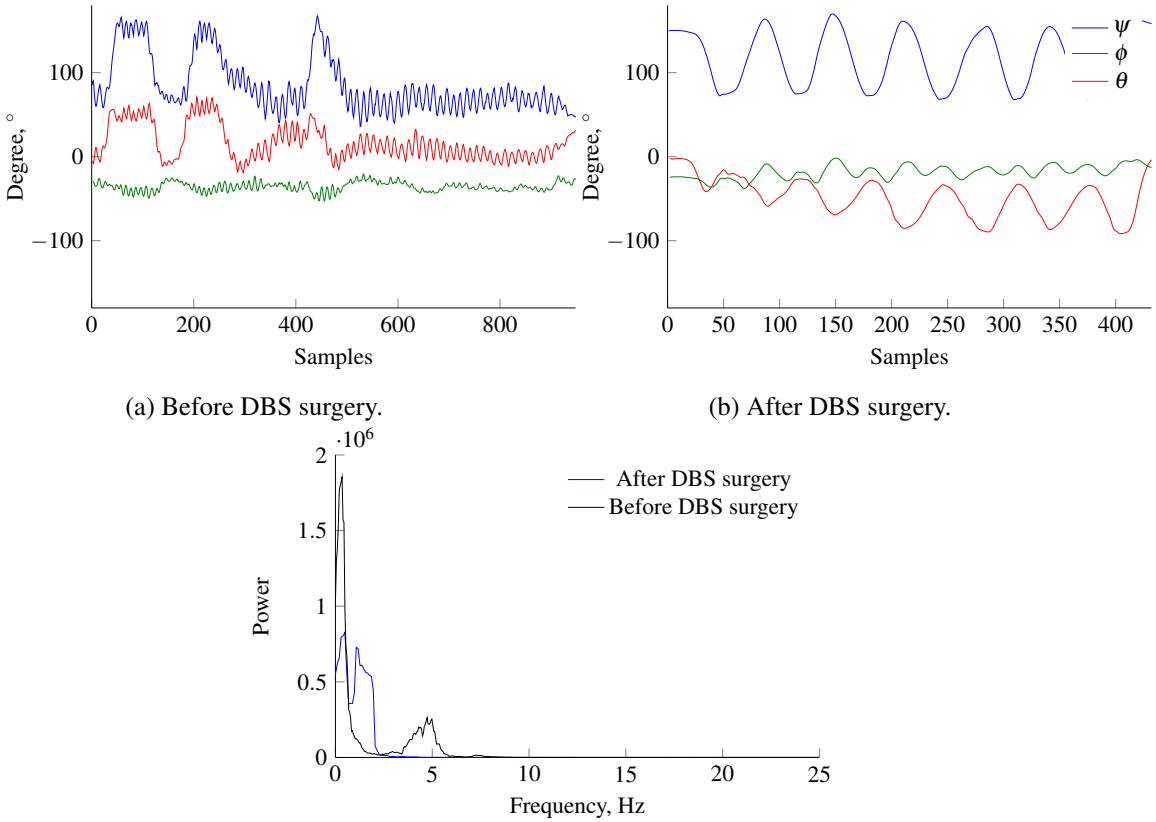

(a) Before DBS surgery.

(b) After DBS surgery.

(c) Power Spectrum of a limb's dynamic tremor assessment, before and after surgery.

Figure 8.8: Comparison of dynamic tremor before and after DBS surgery, in the time and frequency domain.

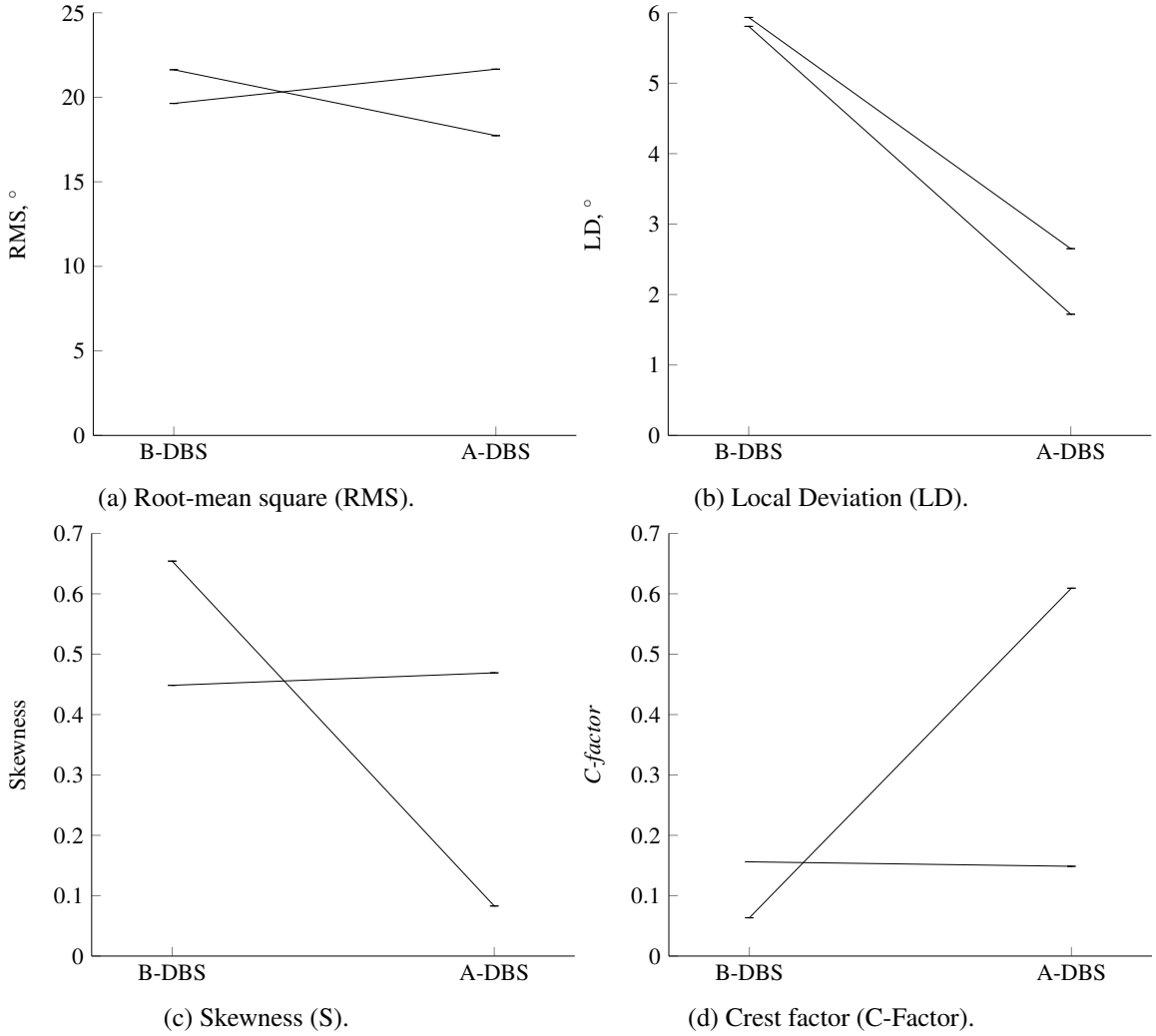

(a) Root-mean square (RMS).

(b) Local Deviation (LD).

(c) Skewness (S).

(d) Crest factor (C-Factor).

Figure 8.9: Influence of surgery on motor performance given by *RMS*, *LD*, *S* and *C-factor*.

The movement may be perceived as much smoother after DBS surgery by the disappearance of high frequency "noise" related to tremor, which shows the efficacy of stimulation in nullifying the abnormal firing pattern which triggers tremor.

Relatively to the parameters *RMS*, *LD*, *S* and *C-factor*, the only coherent variation due to the effect of electrical stimulation is in *LD*; all others have opposite trends comparing both patient's limbs.

8.1.3 Discussion

8.1.3.1 Postural Tremor

Regarding postural tremor, to a certain extent, recreating tremor allowed the identification of parameters which allowed discerning an healthy and tremoric state of the hand, where *RMS*, *LD*, related to the variation of hand orientation overtime, and *C-factor*, related to the relative strength

of the peak frequency found in the signal. These had higher values in tremor was induced as expected. Although not statistically significant, a growth-tendency was found in *S*.

Such results are in agreement with the comparison made between before and after DBS surgery, proving the efficacy of reducing this motor symptom by having a less defined peak frequency and having variations in orientation that may be associated to muscle noise-like activity causing an increase of *S*. Because the existence of tremor may be modeled after a sinusoidal wave (as seen in Figure 8.3b), then this may be perceived as a more symmetric signal, in comparison to random variation of the orientation of the outstretched arms occurring with less significant tremor or in its absence.

Also, by mechanically inducing tremor in healthy subjects, we were aiming for a relationship between some parameters and the peak frequency of the signal correspondent to the assessment of postural tremor. This had been previously done, correlating the logarithm of the peak frequency and the logarithm of linear displacement [30, 76], having a range of correlation coefficient from -0.50 to -0.70. The parameters which revealed higher correlation with peak frequency were *LD* and *C-factor* (-0.46 and 0.48, respectively), showing some degree of interdependence, still not as significant as in the literature. Another point is the difference between ranges of hand oscillation which, in a real clinical setting, is much broader than the one achieved in the simulation-setup. This is related to the design of both acquisition protocols: when inducing-tremor, the hand was free to move and its oscillation were dependent on the weight and length of the hand (as well as in the shaker), *i. e.*, we only regarded hand tremor. When dealing with tremoric patients, the measurements encompass oscillation of the three joints: wrist, elbow and shoulder. This higher number of degrees of freedom allow a much wider range of variation in hand orientation occurring during the outstretched-arms position. Consequently, the poor results achieved when applying the amplitude-based models to get the frequency of tremor were expectable. Such could only be improved by gathering clinical data, representative of the reality we want to tackle.

8.1.3.2 Dynamic Tremor

We may hypothesize greater adequacy of *LD* to distinguish tremor states, even though there is not significant evidence. Still, its better performance was expected in comparison to *RMS* and *C-factor* due to the interference in amplitude and frequency of the movement for nose-tap: *RMS* considers the deviation of every sample to the mean of the signal which is high by nature because of the rotation in ψ, relatively to the amplitude caused by tremor. Also, for an analysis in frequency domain, it is highly susceptible to how fast the patient performs the movement, leading to associating a maximum frequency found within the range of interest to tremor. That may be seen in Figure 8.8: with loss of tremor after surgery, the patient is faster to execute the task, hence the movement frequency comes inside the focused range, "contaminating" *C-factor*. Consequently, local-analysis within a smaller window of samples is favored, as is in the computation of *LD*. Additionally by comparing the peak frequencies of postural (<4 Hz) and dynamic tremor (~5Hz) in the same patient, an increase is noticed which is agreement with the literature [78].

8.2 Bradykinesia

One other symptom that may be found in patients with PD is bradykinesia, also referred to as akinesia and hypokinesia, related to the slowness in performing movement. This may manifest itself as decreased arm swing and leg stride when walking and decreased amplitude of voice, for example [9]. As others symptoms, this is related to a dopamine-deficiency in both striatum and *substantia nigra*, which may be compensated by a levodopa-based drug therapy or by DBS surgery to the subthalamic nucleus (STN). Hence, we propose the usage of this same sensor to identify improvements related to this motor symptom.

8.2.1 Methodology

8.2.1.1 Acquisition Protocol

Two approaches were considered to identify slowness in movement:

- analyze time in-between nose taps during the dynamic tremor assessment task
- analyze time and amplitude of each hand pronation/supination cycle

As in tremor, a simulation trial was performed on healthy subjects, consisting of:

1. having subject perform the hand pronation/supination, taking about 2 seconds *per* cycle
2. repeating, but reproducing a 1-second long cycle

Additionally, true patients would perform as well this task, but without the time-instruction given to the healthy subjects, before and after their DBS surgery. Instead, they were instructed to do it as fast as they could, without stopping until told otherwise and to do hand rotation as complete as possible.

8.2.1.2 Signal Processing

The first exercise performed is represented in Figure 8.2. The flexion performed can be perceived as a rotation of the sensor in the plane xy of the sensor and around the axis z of the sensor. Thus, the sensor yaw rotation, ϕ, was considered to identify the duration of each flexion towards the nose (NT).

ϕ, as in tremor analysis, was detrended, by removing the signal average value. Then, a mean filter was applied using a 10-sample window, centered in the sample under analysis (to reduce interference of existing tremor artifacts). Then, the signals' local maxima were detected considering a threshold of 60°. Having found these moments, the number of samples in-between consecutive peaks were extracted, representing the time of the finger-to-nose task.

On regards to the hand pronation/supination task, the rotation around the x-axis was considered, *i. e.*, θ from the Euler angles vector. Its mean value was removed. The rotation time (RT) was considered as the distance between consecutive peaks (local maxima) and its average

was considered. For a clinical analysis, additionally, the peak-to-peak distance (distance between consecutive minima and maxima) in the signal was considered (PP) to verify whether there was increased range of motion in the wrist joint. The threshold for peak detection considered was 90 $^{\circ}$.

8.2.2 Experiments

8.2.2.1 Nose Tapping Task

The possibility of using the finger-to-nose exercise (the task performed to assess dynamic tremor) to extract some information on changes on its execution-time was explored. Signals were acquired from 5 patients (9 limbs) who were subjected to DBS surgery. The obtained mean and standard deviation of NT is represented in Figure 8.10.

Slowness of movement or bradykinesia is a common symptom in several neurological disease hence it was expected to have an higher NT before surgery rather than after. The majority of this cohort confirms our expectations however, with some exceptions.

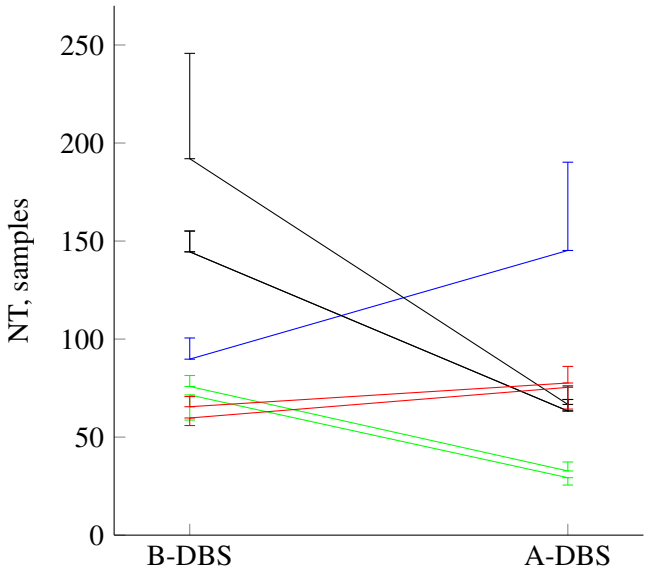

Figure 8.10: Nose-tapping Time (NT) for each patient (represented by different colors) before and after DBS surgery (B-DBS and A-DBS, respectively). Mean + or − standard deviation of NT are represented.

8.2.2.2 Hand Pronation/Supination Task: Simulation Setting

69 400-samples long signals were acquired from 7 subjects. An example of signal is shown in Figure 8.11a, where the peaks and every RT is shown. As expected, clear distinction between the two task-rates were found, using the period of a cycle of hand pronation/supination.

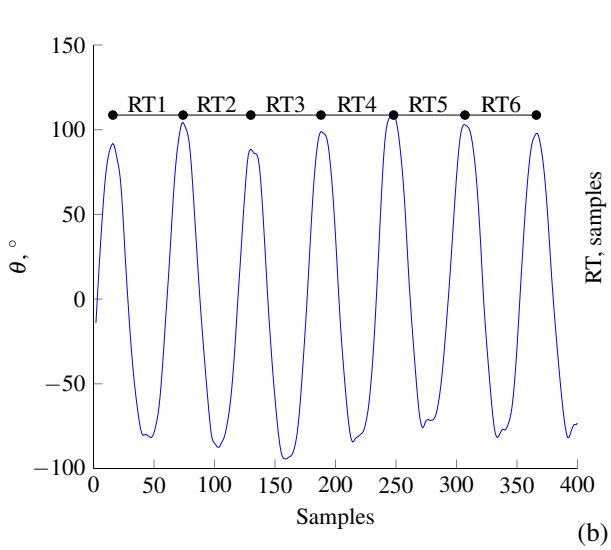

(a) Representation of rotation time between cycles of hand pronation/supination, RT_i.

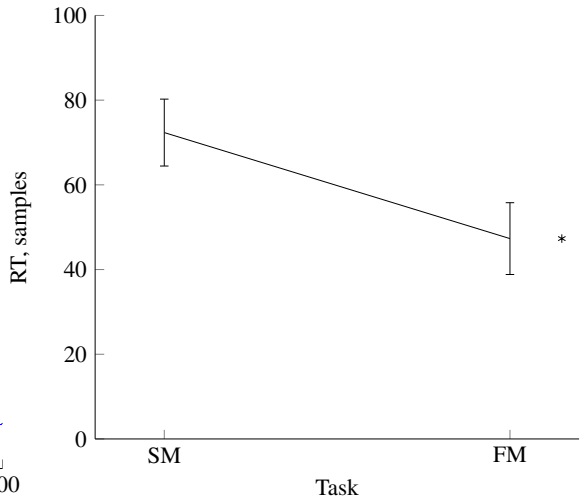

(b) Mean ± standard deviation of rotation time (RT) is represented. Comparison of slow and fast pronation/supination (SM and FM, respectively).

Figure 8.11: Rotation time computation over a signal and differences found in simulation settings. * statistically significant difference was found ($p < 0.001$).

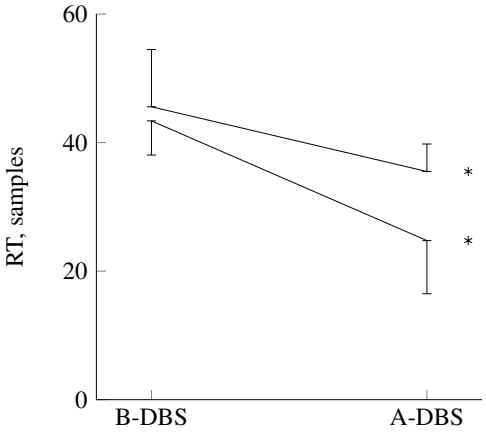

(a) Rotation time (RT), $p < 0.05$.

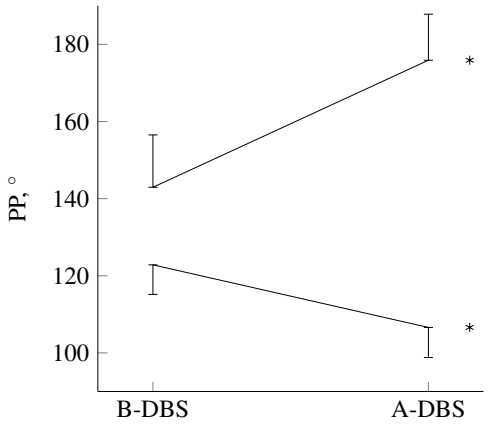

(b) Peak-to-Peak distance (PP), $p < 0.005$.

Figure 8.12: Change of parameters with DBS surgery (mean + or − standard deviation of RT and PP). B-DBS and A-DBS stand for before and after DBS surgery, respectively.* stands for statistically significant difference.

8.2.2.3 Hand Pronation/Supination Task: Clinical Setting

Data from only data one patient (2 limbs) was acquired from analysis of the influence of surgery on the motor performance in regards to range-of-motion (*PP*) and time of task (*RT*). On the latter, a significant decrease was found which is in agreement with report of efficacy of DBS surgery on bradykinesia [13], as in Figure 8.12a. However, one of those had a reduction on the range of motion with surgery, hence, the difference found in time-domain may be associated with the more incomplete rotation of the wrist.

8.2.3 Discussion

By having patients perform the nose-tapping task, which is done for dynamic tremor assessment, we could find in most of our group of patients a reduction on the task's time. This supports the possibility of dual evaluation, having synchronous quantitative assessment of bradykinesia and dynamic tremor using this sensor and motor task.

Regarding the standard-task used for bradykinesia assessment, the simple determination of the local minima and maxima enabled distinguishing two simulated rates of task performance with healthy subjects. However, in a clinical sense, the expected improvements were only conclusively identified in one of the two limbs analyzed both in range-of-motion and slowness of movement.

8.3 Closed-Loop DBS

It has been been proposed [80], the control of stimulation settings of DBS relying on the assessment of the neurochemical environment in the brain and adapting the parameters as necessary (Figure 8.13), instead of scheduling several appointments to reprogram the stimulator, as before-therapeutic parameters may lose its efficacy due to disease progression, change in interactions of electrode-environment or lead displacement. There have been some studies on animal-models of this approach which supported improved motor-performance than in standard DBS [78]. Another

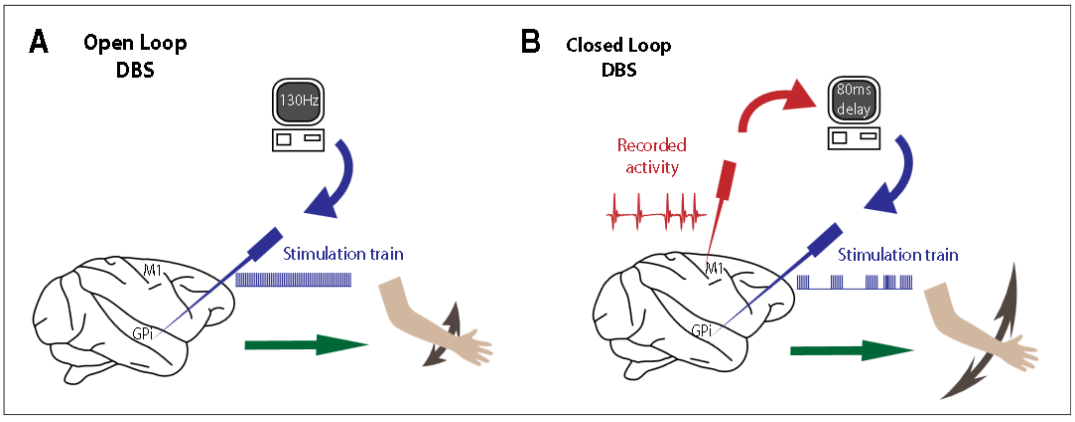

Figure 8.13: Illustration of an Open-Loop and an Adaptive Closed-Loop Deep Brain Stimulation. From [79].

proof-of-concept relied on surface-electroencephalography where the stimulation was controlled by sensing movement intentions [81]. Also it has been proposed to use a quantitative method of assessment of tremor to further support this type of system to only turn-on stimulation when needed. This closed-loop approach could reduce side-effects of DBS to only when it is required and prolong stimulator batteries lifetime. Within this context, this could be another route to be explored, but by combining with rigidity assessment.

8.4 Final Remarks

This system's application is not restricted to rigidity evaluation: in this chapter we have proved the ability to identify improvements due to DBS surgery, both in tremor (postural and action) and bradykinesia using Euler angles and the system in question. Thus, its target evaluation could become broader, supporting quantitatively in the assessment of other motor symptoms in this intra-operatory setting. Furthermore, the data suggested that, using the standard exercise to assess dynamic tremor, we could identify some improvement in time-of-task. Still, these possibilities must be supported with a larger dataset. We attempted to verify a relationship between angular amplitude-related parameters and frequency of tremor, in order to verify if a relationship was found as in previous work (between displacement and frequency). However, related to unrealistic data, such models were not achieved.

The fact of having the MoMo broadcasting Euler angles makes easy the task of identifying on-demand which clinical assessment is being performed among those experimented: postural, dynamic tremor and bradykinesia through hand supination/pronation, and also because these are highly standardized.

On one hand, there is a broader range of motor symptoms that may be analyzed with this type of system. On another, this could be used to support others, as in the case of closed-loop DBS, as an additional informant tool to decide when to stimulate or not to better use the battery of the stimulator and maximize the patient's quality of life by reducing side-effects.

Chapter 9

Conclusions and Future Work

The project was born out of a need in the clinic, in particular, in the Movement Disorders Unit of Centro Hospitalar de S. João, where the surgery of deep brain stimulation for treatment of the Parkinson's Disease (PD) was introduced 14 years ago. In this context, the patient's wrist rigidity is assessed to decide the parameters for stimulation, to identify when the motor improvement is maximal. With that purpose, in the aforementioned unit, this is decided by the agreement of two physicians. However, a quantitative element was missing, which motivated the collaboration with the Biomedical Research and Innovation group in INESC TEC to tackle that absence. An initial proposal was done relying on kinematic measurements and a polynomial model, which unregarded the initial severity of rigidity and cogwheel occurrence.

One of the goals stated for this dissertation in Chapter 1 was to improve the modeling of rigidity reduction relying on velocity of the wrist flexion, imposed by a physician. Previously, other methods were attempted rather than polynomial modeling, yet the only which revealed equivalent performance was the use of random forest (Appendix C). This prompt to further explore the potentialities of the initial proposal by both following a multiple model approach (baseline-dependent) and to incorporate the cogwheel effect. It was expected that the performance would benefit from this input enrichment, namely for reducing the impact of the variability of force applied by physicians in different assessment trials. However, such hope was unfunded because the best performances had similar results to the initial approach. This further supports the limitation of kinematic information. Also, the measurements are performed during the rigidity assessment of two experienced physician. Over the past validations (as in Chapter 4) of polynomial-base models, consistently a performance over 75% and mean errors under 5% are achieved, which supports the system's usability in this single context. However, over-fitting to the two experienced physicians is expected and the lack of variability of the dataset may partially justify the plateau in performance. It is a mandatory step to increase the clinical partners, to perform cross-center validation of this system. For this purpose, the cooperation with existing companies in the field of DBS may be advantageous. Additionally, it would be interesting performing a cross-observer study about the difference in the assessment of rigidity, namely to identify the importance of experience by comparing interns with experienced physicians and also validate its use in DBS programming

appointments.

Even though cogwheel detection in the signal did not improve the model itself, it was considered as an important supporting information to be provided, translating the smoothness of the movement. Thus, it was incorporated into the user-interface of the mobile application to provide smoothness related categorization (severe, moderate and low cogwheel severity), as a function of the signal acquired before any stimulation (which translates the baseline rigidity state of a patient). This required further changes to the mobile application (recording a significant baseline signal) which still did not compromised its usability. Additionally, the blending in of the system into the operating room was further enhanced by introducing the smartwatch to be worn by the assessing physician, to serve as display as well. This was experimented in a surgery and proved to be comfortable and handy. However it must be emphasized that the physician is responsible for first performing his own evaluation and only then consult the computed rigidity reduction because the system developed is intended to support and not to replace the doctor.

The last goal was to ascertain about the ability of this system to be used to assess other motor symptoms: tremor and bradykinesia. For that purpose, two approaches were followed through: simulating those in healthy subjects and perform measurements in patients before and after DBS surgery. The measures of the quadratic mean (root mean square), local deviation, crest factor and skewness were considered for tremor evaluation (both postural and dynamic) and, as for bradykinesia, time and amplitude of movement were considered, all extracted from the Euler angle domain. For tremor, in both conditions, the difference was perceived by the parameters still few patients were considered. Regarding slowness of movement during the task specific for its assessment, a single patient (2 limbs) was considered, hence no conclusive results may be extracted. Yet, by considering the dynamic tremor task performed by 4 patients (7 limbs), most often the execution time decreased with DBS surgery. This opens up the possibility of even extracting from a single task type measurements related to different motor symptoms. Furthermore, there is also the possibility of incorporating the sensor and processing into a closed-loop DBS, to enrich the input signals which control stimulation (combining brain-sensing with motor sensing). In short, a similar setup for other symptoms analysis was confirmed. This work could be followed-up by:

- further proceed with acquisitions in patients (irrespective to their neurological disorder) before and after DBS surgery
- acquire data from routine consults of the latter to distinguish “on” and “off” states (under the effect of medication or not, respectively)

Finally, as to investigate the potential of the proposed system for rigidity assessment into the market, this context was explored, as well as the stages for getting CE mark (compliance label in Europe) and the options of intellectual property protection and prior art that may hinder the assignment of patent to this method. Briefly, forecasts for 2020 expect a significant growth of the market segment of DBS, in particular, for PD patients and currently in Europe and USA it has an estimated size of €808.1 million, 51% of the global market. This has some main players as Medtronic, St. Jude Medical Inc. and others which could hinder a newcomer entry. However,

by cooperating with these, complementing their systems and helping them in differentiating and potentiating their established products one can smoothly enter this field, as other start-ups have done (and some were even later acquired by them). This cooperative mindset, for INESC TEC, would be greatly advantageous because, on one hand, these companies have access to a large number of centers performing DBS surgery and, on the other, their own expertise in placing a medical device in the market, which in itself is a major struggle to a newcomer to the area, could be helpful. As probed in Chapter 7, that is a very intricate process especially considering the diagnostic-nature of the afore proposed system, in which we still are in the early stages. As it has been already done, feedback from the different stakeholders has to be gathered but should be more diverse than just Centro Hospitalar de S. João; essential requirements, IEC and ISO standards to be met have to be identified, there should proposals of product design and examine their compliance with the requirements, create and validate a prototype and finally apply for CE-marking.

An important decision was applying for patent with this method for rigidity evaluation which may prove to become a bargaining tool when negotiating with prospective partners. The latter without a doubt is novel; still it may be deemed as obvious in regard to the patent and utility models search. In such case, applying for utility model (protection regime not worldwide available with exception of most European countries) would be an interesting alternative because it is far less rigorous in terms of obviousness than patents and a much faster and cheaper procedure (yet, enables shorter protection time).

In short, even though several efforts have been made, the performance of the model for rigidity reduction seems to have reached a plateau, which allows consistently an accuracy of over 75% and mean error of 5%. It seems important to widen the variability of specialists in the growing dataset so other centers are necessary to collaborate. The output of the model is now supported by a smoothness related indicator which relies on the cogwheel artifacts detection. These may be displayed in a smartphone to the support technician of the DBS surgery's operational team and in a smartwatch worn by the physician during the rigidity assessment step. Both these "use cases" have been already validated. Additionally, the broadening the range of applications to tremor and bradykinesia has been proved possible but requires a larger cohort of patients. Even though the uniqueness of the device is related to rigidity, extending its application may turn it more interesting for a buyer. In fact, the commercial potential is already large because a significant growth is expected in the segment of market of DBS devices for PD. In that view, there should be an endeavor to find an industrial partner to assist in its introduction or even take over it, with whom the application for patent will grant the researchers with bargaining power. In case the patent is not granted, applying for a utility model should be done meanwhile because it provides as well intellectual property protection with a less strict non-obviousness requirement.

Bibliography

[1] J. Parkinson, "An essay on the shaking palsy. 1817." *J Neuropsychiatry Clin Neurosci.*, vol. 14, no. 2, pp. 223–36, 2002.

[2] T. Pringsheim, N. Jette, A. Frolkis, and T. D. Steeves, "The prevalence of Parkinson's disease: A systematic review and meta-analysis," *Movement Disorders*, vol. 29, pp. 1583–1590, 2014.

[3] L. J. Findley, "The economic impact of Parkinson's disease," *Parkinsonism & Related Disorders*, vol. 13, pp. S8–S12, 2007.

[4] A. C. Guyton and J. E. Hall, *Tratado em Fisiologia Médica*, 11th ed. Elsevier, 2006.

[5] G. Rao, L. Fisch, and S. Srinivasan, "Does This Patient Have Parkinson Disease?" *Jama*, vol. 289, no. 3, p. 347, 2003.

[6] J. M. Beitz, "Parkinson's Disease: a review," *Frontiers in Bioscience*, vol. 6, pp. 65–74, 2014.

[7] C. R. Baumann, "Epidemiology, diagnosis and differential diagnosis in Parkinson's disease tremor," *Parkinsonism & Related Disorders*, vol. 18, pp. S90–S92, 2012.

[8] J. Jankovic, "Parkinson's disease: clinical features and diagnosis," *Journal of Neurology, Neurosurgery & Psychiatry*, vol. 79, pp. 368–376, 2008.

[9] S. Fahn, "Description of Parkinson's disease as a clinical syndrome." *Annals of the New York Academy of Sciences*, vol. 991, pp. 1–14, 2003.

[10] J. W. Lance, R. S. Schwab, and E. A. Peterson, "Action tremor and the cogwheel phenomenon in parkinson's disease," *Brain*, vol. 86, no. 1, pp. 95–110, 1963.

[11] I. Teva Neuroscience, "A well-established measure : The Unified Parkinson ' s Disease Rating Scale (UPDRS)," Tech. Rep., 2006.

[12] A. L. Benabid, S. Chabardes, J. Mitrofanis, and P. Pollak, "Deep brain stimulation of the subthalamic nucleus for the treatment of Parkinson's disease," *The Lancet Neurology*, vol. 8, pp. 67–81, 2009.

[13] A. M. Lozano and N. Mahant, "Deep brain stimulation surgery for Parkinson's disease: mechanisms and consequences." *Parkinsonism & related disorders*, vol. 10 Suppl 1, pp. S49–57, 2004. [Online]. Available: http://www.ncbi.nlm.nih.gov/pubmed/15109587

[14] P. Costa, M. J. Rosas, R. Vaz, and J. P. Cunha, "Wrist Rigidity Assessment During Deep Brain Stimulation Surgery," in *Proceedings of the IEEE Internacional Conference of the Engineering in Medicine and Biology Society (EMBS)*, 2015.

[15] S. Assis, P. Costa, M. J. Rosas, R. Vaz, and J. P. S. Cunha, "An Adaptive Model Approach for Quantitative Wrist Rigidity Evaluation during Deep Brain Stimulation Surgery," in *Proceedings of the IEEE Internacional Conference of the Engineering in Medicine and Biology Society (EMBS)*, 2016.

[16] R. J. Elble, S. L. Pullman, J. Y. Matsumoto, J. Raethjen, G. Deuschl, and R. Tintner, "Tremor amplitude is logarithmically related to 4- and 5-point tremor rating scales," *Brain*, vol. 129, no. 10, pp. 2660–2666, 2006.

[17] H. Dai, P. Zhang, and T. Lueth, "Quantitative Assessment of Parkinsonian Tremor Based on an Inertial Measurement Unit," *Sensors*, vol. 15, no. 10, pp. 25 055–25 071, 2015.

[18] M. B. Shapiro, D. E. Vaillancourt, M. M. Sturman, L. V. Metman, R. A. E. Bakay, and D. M. Corcos, "Effect of STN DBS on Rigidity in Parkinson's Disease," *IEEE Transactions on Neural Systems and Rehabilitation Engineering*, vol. 15, pp. 173–181, 2007.

[19] S. K. Patrick, A. a. Denington, M. J. a. Gauthier, D. M. Gillard, and A. Prochazka, "Quantification of the UPDRS rigidity scale," *IEEE Transactions on Neural Systems and Rehabilitation Engineering*, vol. 9, no. 1, pp. 31–41, 2001.

[20] T. Endo, R. Okuno, M. Yokoe, K. Akazawa, and S. Sakoda, "A novel method for systematic analysis of rigidity in Parkinson's disease," *Movement Disorders*, vol. 24, no. 15, pp. 2218–2224, 2009.

[21] J. Levin, S. Krafczyk, P. Valkovicč, T. Eggert, J. Claassen, and K. Bötzel, "Objective measurement of muscle rigidity in parkinsonian patients treated with subthalamic stimulation," *Movement Disorders*, vol. 24, no. 1, pp. 57–63, 2009.

[22] B. K. Park, Y. Kwon, J. W. Kim, J. H. Lee, G. M. Eom, S. B. Koh, J. H. Jun, and J. Hong, "Analysis of viscoelastic properties of wrist joint for quantification of parkinsonian rigidity," *IEEE Transactions on Neural Systems and Rehabilitation Engineering*, vol. 19, no. 2, pp. 167–176, 2011.

[23] Y. Kwon, S.-H. Park, J.-W. Kim, Y. Ho, H.-M. Jeon, M.-J. Bang, S.-B. Koh, J.-H. Kim, and G.-M. Eom, "Quantitative evaluation of parkinsonian rigidity during intra-operative deep brain stimulation." *Biomedical materials and engineering*, vol. 24, no. 6, pp. 2273–81, 2014.

[24] J. Van Den Noort, K. Van Dijk, H. Kortier, N. Van Beek, R. Verhagen, L. Bour, and P. Veltink, "Applications of the PowerGlove for Measurement of Finger Kinematics," *Wearable and Implantable Body Sensor Networks Workshops (BSN Workshops), 2014 11th International Conference on*, pp. 6–10, 2014.

[25] M. K. Y. Mak, E. C. Y. Wong, and C. W. Y. Hui-Chan, "Quantitative measurement of trunk rigidity in parkinsonian patients." *Journal of neurology*, vol. 254, no. 2, pp. 202–9, 2007.

[26] B. Sepehri, A. Esteki, E. Ebrahimi-Takamjani, G. A. Shahidi, F. Khamseh, and M. Moinodin, "Quantification of rigidity in Parkinson's disease," *Annals of Biomedical Engineering*, vol. 35, no. 12, pp. 2196–2203, 2007.

[27] R. Xia, J. Sun, and a. J. Threlkeld, "Analysis of interactive effect of stretch reflex and shortening reaction on rigidity in Parkinson's disease." *Clinical neurophysiology : official journal of the International Federation of Clinical Neurophysiology*, vol. 120, no. 7, pp. 1400–7, 2009.

[28] A. Salarian, H. Russmann, C. Wider, P. R. Burkhard, F. J. G. Vingerhoets, and K. Aminian, "Quantification of Tremor and Bradykinesia in Parkinson's Disease Using a Novel Ambulatory Monitoring System," *IEEE Transactions on Biomedical Engineering*, vol. 54, no. 2, pp. 313–322, 2007.

[29] S. Patel, K. Lorincz, R. Hughes, N. Huggins, J. Growdon, D. Standaert, M. Akay, J. Dy, M. Welsh, and P. Bonato, "Monitoring Motor Fluctuations in Patients With Parkinson's Disease Using Wearable Sensors," *IEEE Transactions on Information Technology in Biomedicine*, vol. 13, no. 6, pp. 864–873, 2009.

[30] Z. Farkas, A. Csillik, I. Szirmai, and A. Kamondi, "Asymmetry of tremor intensity and frequency in Parkinson's disease and essential tremor," *Parkinsonism and Related Disorders*, vol. 12, pp. 49–55, 2006.

[31] R. Edwards and A. Beuter, "Indexes for identification of abnormal tremor using computer tremor evaluation systems," *IEEE Transactions on Biomedical Engineering*, vol. 46, no. 7, pp. 895–898, 1999.

[32] G. Grimaldi and M. Manto, "Neurological tremor: Sensors, signal processing and emerging applications," *Sensors*, vol. 10, no. 2, pp. 1399–1422, 2010.

[33] "Motus Bioengineering." [Online]. Available: http://motusbioengineering.com/index.htm

[34] K. Lorincz, B.-r. Chen, G. Challen, A. Chowdhury, S. Patel, P. Bonato, and M. Welsh, "Mercury: A Wearable Sensor Network Platform for High-Fidelity Motion Analysis," *SenSys '09: Proceedings of the 7th ACM Conference on Embedded Networked Sensor Systems*, pp. 1–14, 2009.

[35] D. D. a. Heldman, J. Jankovic, D. E. Vaillancourt, J. Prodoehl, R. J. Elble, J. P. Giuffrida, J. Prodehl, R. J. Elble, J. P. Giuffrida, P. Prodehl, R. J. Elble, and J. P. Giuffrida, "Essential tremor quantification during activities of daily living," *Parkinsonism & related . . .*, vol. 17, no. 7, pp. 537–542, 2011.

[36] D. Heldman, P. LeWitt, and J. Giuffrida. (2016). [Online]. Available: https://glneurotech.com/docrepo/posters/Automated%20Parkinson's%20Disease%20Motor%20Assessment%20for%20Clinical%20and%20Ambulatory%20Monitoring.pdf

[37] J. Giuffrida, D. Heldman, and T. Mera, "Method and system for tuning of movement disorder therapy devices," May 16 2013, uS Patent App. 13/153,063. [Online]. Available: https://www.google.com/patents/US20130123684

[38] T. Mera, J. L. Vitek, J. L. Alberts, and J. P. Giuffrida, "Kinematic optimization of deep brain stimulation across multiple motor symptoms in Parkinson's disease." *Journal of neuroscience methods*, vol. 198, no. 2, pp. 280–6, 2011.

[39] H. Dai, "Wearable system and method for cardinal symptom quantitative detection of Parkinson patients," 2014. [Online]. Available: http://worldwide.espacenet.com/publicationDetails/biblio?FT=D{&}date=20141105{&}DB={&}locale=en{_}EP{&}CC=CN{&}NR=104127187A{&}KC=A{&}ND=2

[40] H. Dai and L. D'Angelo, "Quantitative assessment of tremor during deep brain stimulation using a wearable glove system," *IEEE International Workshop of Internet-of-Things Networking and Control (IoT-NC)*, vol. 13, pp. 53–57, 2013.

[41] W. Hall, "Hand-held gyroscopic device," Oct. 22 1991, uS Patent 5,058,571. [Online]. Available: http://www.google.co.uk/patents/US5058571

[42] G. Gear. (2016). [Online]. Available: http://gyrogear.co/

[43] R. a. Joundi, J. S. Brittain, N. Jenkinson, A. L. Green, and T. Aziz, "Rapid tremor frequency assessment with the iPhone accelerometer," *Parkinsonism and Related Disorders*, vol. 17, no. 4, pp. 288–290, 2011.

[44] J. Synnott, L. Chen, C. D. Nugent, and G. Moore, "WiiPD–objective home assessment of Parkinson's disease using the Nintendo Wii remote." *IEEE transactions on information technology in biomedicine : a publication of the IEEE Engineering in Medicine and Biology Society*, vol. 16, no. 6, pp. 1304–12, 2012.

[45] J. Spyers-Ashby, M. Stokes, P. Bain, and S. Roberts, "Classification of normal and pathological tremors using a multidimensional electromagnetic system," *Medical Engineering & Physics*, vol. 21, no. 10, pp. 713–23, 1999.

[46] P. E. O'Suilleabhain and R. B. Dewey, "Validation for tremor quantification of an electromagnetic tracking device," *Movement Disorders*, vol. 16, no. 2, pp. 265–271, 2001.

[47] P. Sá, "NeuroGait: Mobile Recording of Gait in Patients with Neurological Diseases," Ph.D. dissertation, Faculdade de Engenharia da Universidade do Porto, 2014.

[48] A. K. Bera, C. M. Jarque, and A. K. Bera, "Efficient tests for normality, homoscedasticity and serial independence of regression residuals," *Economics Letters*, vol. 6, no. 3, pp. 255–259, 1980.

[49] A. S. Assis, R. Vaz, M. J. Rosas, P. Costa, and J. P. S. Cunha, "A real-time intra-operatory system for rigidity evaluation during deep brain stimulation surgery," in *Neurocirugia.*, vol. 27, 2016, p. 28.

[50] S. Assis, "Kinematic evaluation of parkinson's disease patients during deep brain stimulation surgery and preoperative procedures," Feb. 16 2016, monograph.

[51] N. a. Obuchowski, "Computing sample size for receiver operating characteristic studies." *Investigative radiology*, vol. 29, no. 2, pp. 238–243, 1994.

[52] a.P. Bradley and I. Longstaff, "Sample size estimation using the receiver operating characteristic curve," *Proceedings of the 17th International Conference on Pattern Recognition, 2004. ICPR 2004.*, vol. 00, no. C, pp. 428–431 Vol.4, 2004. [Online]. Available: http://ieeexplore.ieee.org/lpdocs/epic03/wrapper.htm?arnumber=1333794

[53] T. Fawcett, "An introduction to ROC analysis," *Pattern Recognition Letters*, vol. 27, no. 8, pp. 861–874, 2006.

[54] M. Wiklund, *Medical Device and Equipment Design: Usability Engineering and Ergonomics*. Taylor & Francis, 1995. [Online]. Available: https://books.google.pt/books?id=fLybkzNdQSIC

[55] Markets and Markets. (2015) Neuromodulation market by technology (deep brain stimulation, spinal cord stimulation, transcranial magnetic stimulation) & by application (depression, parkinson's, tinnitus, alzheimer's, epilepsy, ischemia, obesity) - trends & global forecast to 2020. [Online]. Available: http://www.marketsandmarkets.com/Market-Reports/neurostimulation-devices-market-921.html

[56] T. M. Research. (2015) Deep brain stimulation devices market for parkinson's disease expected to reach usd 3.21 billion globally in 2020. [Online]. Available: http://www.medgadget.com/2015/05/deep-brain-stimulation-devices-market-parkinsons-disease-expected-reach-usd-3-21-billion-globally-2020.html

[57] M. LLC. (2015) Deep brain stimulation devices market trends. [Online]. Available: http://www.strategyr.com/MarketResearch/Deep_Brain_Stimulation_Devices_Market_Trends.asp

[58] S. von Campenhausen, B. Bornschein, R. Wick, K. Bötzel, C. Sampaio, W. Poewe, W. Oertel, U. Siebert, K. Berger, and R. Dodel, "Prevalence and incidence of parkinson's disease in europe," *European Neuropsychopharmacology*, vol. 15, no. 4, pp. 473 – 490, 2005. [Online]. Available: http://www.sciencedirect.com/science/article/pii/S0924977X05000702

[59] W. H. Organization, "Parkinson's Disease," in *Neurological disorders : public health challenges.*, 2006, pp. 140–150.

[60] B. M. Stuart, "Deep Brain Provides Stimulating Market," no. March, pp. 14–21, 2012.

[61] Medtronic. (2009) Medtronic announces fda approval of two deep brain stimulation devices that offer programming advances and new tools for patients with movement disorders. [Online]. Available: http://newsroom.medtronic.com/phoenix.zhtml?c=251324&p=irol-newsArticle&ID=1773114

[62] J. Enriquez. (2015) Fda clears st. jude's brain implant for parkinson's disease. [Online]. Available: http://www.meddeviceonline.com/doc/fda-clears-st-jude-s-brain-implant-for-parkinson-s-disease-0001

[63] B. S. Corporation. (2012) Boston scientific launches vercise^{TM} deep brain stimulation system in europe. [Online]. Available: http://news.bostonscientific.com/2012-09-28-Boston-Scientific-Launches-Vercise-Deep-Brain-Stimulation-System-in-Europe

[64] F. N. Inc. (2015) About us: Our partners & investors. [Online]. Available: http://www.functionalneuromodulation.com/about/partners.php

[65] P. Maresova and K. Kuca, "Porter's Five Forces on Medical Device Industry in Europe," *Military Medical Science Letter*, vol. 83, no. 4, pp. 134–144, 2014.

[66] T. M. Ellis, K. D. Foote, H. H. Fernandez, A. Sudhyadhom, R. L. Rodriguez, P. Zeilman, C. E. Jacobson IV, and M. S. Okun, "Reoperation for suboptimal outcomes after deep brain stimulation surgery," *Neurosurgery*, vol. 63, no. 4, pp. 754–760, 2008.

[67] Público. (2002) Hospital de S. João realiza primeiro tratamento cirúrgico da doença de Parkinson em Portugal. [Online]. Available: https://www.publico.pt/ciencia/noticia/hospital-de-s-joao-realiza-primeiro-tratamento-cirurgico-da-doenca-de-parkinson-em-portugal-191843

[68] E. C. D. Health, C. D. B. U. B. Cosmetics, and medical devices., "European Medical Devices Directive - 93/42/EEC with 2007/47/EC," pp. 52–56, 2007.

[69] E. C. D. Health, C. Consumer Directorate B Unit B2, and medical devices., "MEDICAL DEVICES: Guidance document-Classification of medical devices," 2010.

[70] Food and D. A. (FDA). (1997) Design Control Guidance For Medical Device Manufacturers. [Online]. Available: http://www.fda.gov/MedicalDevices/DeviceRegulationandGuidance/GuidanceDocuments/ucm070627.htm

[71] O. J. of the European Union., "Commission communication in the framework of the implementation of the Council Directive 93/ 42/EEC of 14 June 1993 concerning medical devices," pp. 52–56, 2015.

[72] T. Deer, M. Ranson, and J. Pope, *Reducing Risks and Complications of Interventional Pain Procedures*, ser. ClinicalKey 2012. Elsevier/Saunders, 2012. [Online]. Available: https://books.google.pt/books?id=woSvKw4fxHgC

[73] E. Commission and D. G. Enterprise, "Guidelines relating to the application of: The Council Directive 90/385/EEC on Active Implantable Medical Devices and the Council Directive 93/42/EEC on Medical Devices," 1998.

[74] W. I. P. Organization. Protecting innovations by utility models: What is a utility model? [Online]. Available: http://www.wipo.int/sme/en/ip_business/utility_models/utility_models.htm

[75] L. Ramsay, "How to get a patent quicker - Europe," 2010. [Online]. Available: http://www.dehns.com/cms/document/how_to_get_a_patent_quicker_europe.pdf

[76] S. Calzetti, M. Baratti, M. Gresty, and L. Findley, "Frequency/amplitude characteristics of postural tremor of the hands in a population of patients with bilateral essential tremor: implications for the classification and mechanism of essential tremor." *Journal of neurology, neurosurgery, and psychiatry*, vol. 50, no. 5, pp. 561–7, 1987. [Online]. Available: http://www.pubmedcentral.nih.gov/articlerender.fcgi?artid=1031967{&}tool=pmcentrez{&}rendertype=abstract

[77] R. J. Elble, C. Higgins, K. Leffler, and L. Hughes, "Factors influencing the amplitude and frequency of essential tremor." *Movement disorders : official journal of the Movement Disorder Society*, vol. 9, no. 6, pp. 589–596, 1994.

[78] R. C. Helmich, I. Toni, G. Deuschl, and B. R. Bloem, "The pathophysiology of essential tremor and parkinson's tremor," *Current Neurology and Neuroscience Reports*, vol. 13, no. 9, pp. 1–10, 2013. [Online]. Available: http://dx.doi.org/10.1007/s11910-013-0378-8

[79] F. J. Santos, R. M. Costa, and F. Tecuapetla, "Stimulation on demand: Closing the loop on deep brain stimulation," *Neuron*, vol. 72, no. 2, pp. 197–198, 2011. [Online]. Available: http://dx.doi.org/10.1016/j.neuron.2011.10.004

[80] P. J. Grahn, G. W. Mallory, O. U. Khurram, B. M. Berry, J. T. Hachmann, A. J. Bieber, K. E. Bennet, H. K. Min, S. Y. Chang, K. H. Lee, and J. L. Lujan, "A neurochemical closed-loop controller for deep brain stimulation: Toward individualized smart neuromodulation therapies," *Frontiers in Neuroscience*, vol. 8, no. 8 JUN, pp. 1–11, 2014.

[81] J. Herron, T. Denison, and H. J. Chizeck, "Closed-loop DBS with movement intention," *2015 7th International IEEE/EMBS Conference on Neural Engineering (NER)*, pp. 844–847, 2015. [Online]. Available: http://ieeexplore.ieee.org/lpdocs/epic03/wrapper.htm?arnumber=7146755

[82] W. Y. Wong, M. S. Wong, and K. H. Lo, "Clinical applications of sensors for human posture and movement analysis: a review." *Prosthetics and Orthotics International*, vol. 31, pp. 62–75, 2007.

[83] V. Kecman, *Learning and soft computing: support vector machines, neural networks, and fuzzy logic models*. MIT Press, 2001.

[84] R. O. Duda, P. E. Hart, and D. G. Stork, *Pattern Classification*, 2nd ed. Wiley, 2000.

[85] S. Theodoridis and K. K., *Pattern Recognition*. Elsevier, 2009.

[86] V. Franc and V. Hlaváč, "Statistical pattern recognition toolbox for Matlab," Center for Machine Perception, K13133 FEE Czech Technical University, Prague, Czech Republic, Research Report CTU–CMP–2004–08, June 2004.

[87] B. Schölkopf, K. K. Sung, C. J. C. Burges, F. Girosi, P. Niyogi, T. Poggio, and V. Vapnik, "Comparing support vector machines with gaussian kernels to radial basis function classifiers," *IEEE Transactions on Signal Processing*, vol. 45, no. 11, pp. 2758–2765, 1997.

[88] Mathworks, "Support Vector Machines (SVM)." [Online]. Available: http://www.mathworks.com/help/stats/support-vector-machines-svm.html

[89] T. Al-ani and D. Trad, "Signal processing and classification approaches for brain-computer interface," in *Intelligent and Biosensors*, V. S. Somerset, Ed. InTech, 2010, no. January, pp. 25–65. [Online]. Available: http://www.intechopen.com/source/pdfs/6798/InTech-Signal{_}processing{_}and...computer{_}interface.pdf

Appendix A

Hospital S. João Ethics Committee Authorization

18.1.2012

À Direcção Clínica
24/1 2012

Centro Hospitalar São João
Centro de Investigação
Prof. Dra. Ana Azevedo
Coordenadora CIC

À Direcção Clínica
24/1 2012

CONSELHO DE ADMINISTRAÇÃO
24/1 2012

SÃO JOÃO

AUTORIZADO

CONSELHO DE ADMINISTRAÇÃO REUNIÃO DE 10 FEV. 2012
(Presidente do Conselho de Administração)
Prof. Doutor António Ferrer
Directora Clínica | Enfermeira Directora | Administrador Executivo
Dr. João Oliveira

Exma. Sra.
Dra. Margarida Tavares
Directora Clínica do Centro Hospitalar de São João

Assunto: Parecer da Comissão de Ética para a Saúde do Centro Hospitalar de São João

Projecto de Investigação: "*Weakpark – um dispositivo móvel incorporado em vestuário para telemetria do movimento e optimização dos parâmetros de estimulação cerebral profunda na Doença de Parkinson*"
Investigadores Principais: Eng.º João Paulo Cunha e Prof. Doutor Rui Vaz

Junto envio a V. Exa. para obtenção de decisão final do Conselho de Administração o parecer elaborado pela Comissão de Ética para a Saúde relativo ao projecto em epígrafe.

Com os melhores cumprimentos.

Porto, 13 de Dezembro de 2011

Dr. Pedro Brito
Secretário da Comissão de Ética para a Saúde

Appendix B

EMBS 2016 Conference Paper

An Adaptive Model Approach for Quantitative Wrist Rigidity Evaluation during Deep Brain Stimulation Surgery

Sofia Assis[1], Pedro Costa[1], Maria José Rosas[2], Rui Vaz[2,3,4] and João Paulo Silva Cunha[1], Senior Member, *IEEE*

***Abstract*— Intraoperative evaluation of the efficacy of Deep Brain Stimulation includes evaluation of the effect on rigidity. A subjective semi-quantitative scale is used, dependent on the examiner perception and experience. A system was proposed previously, aiming to tackle this subjectivity, using quantitative data and providing real-time feedback of the computed rigidity reduction, hence supporting the physician decision. This system comprised of a gyroscope-based motion sensor in a textile band, placed in the patients hand, which communicated its measurements to a laptop. The latter computed a signal descriptor from the angular velocity of the hand during wrist flexion in DBS surgery. The first approach relied on using a general rigidity reduction model, regardless of the initial severity of the symptom. Thus, to enhance the performance of the previously presented system, we aimed to develop models for high and low baseline rigidity, according to the examiner assessment before any stimulation. This would allow a more patient-oriented approach. Additionally, usability was improved by having *in situ* processing in a smartphone, instead of a computer. Such system has shown to be reliable, presenting an accuracy of 82.0% and a mean error of 3.4%. Relatively to previous results, the performance was similar, further supporting the importance of considering the cogwheel rigidity to better infer about the reduction in rigidity. Overall, we present a simple, wearable, mobile system, suitable for intra-operatory conditions during DBS, supporting a physician in decision-making when setting stimulation parameters.**

I. Introduction

The Parkinson's Disease (PD) is a neurodegenerative disorder, characterized by the loss of dopaminergic cells in the substantia nigra. Usually, signals are propagated from substantia nigra to the striatum and, from here, to the motor cortex. With a decrease of dopamine release, the ability to effectively control movement is lost and abnormal neurofiring patterns occur. This leads to the cardinal motor symptoms of PD: tremor at rest, rigidity and bradykinesia [1]. To evaluate the severity of the aforementioned symptoms and others (psychological and speech, for example), the most used scale is the Unified Parkison Disease Rating Scale (UPDRS) [2], which was first introduced in 1987. In particular, for the case of wrist rigidity, present in almost all PD patients [3], an examiner imposes its flexion and extension and subjectively grades it from absent (0) to severe rigidity (4). The wrist joint, relatively to the elbow, is easy to manoeuvre and to assess its motor performance and, therefore, to evaluate its rigidity. One considers a joint more rigid when more force than expected is needed to move it over. During examination of the wrist, cogwheel rigidity in the movement may be identified, which is similar to the ratchet pattern of a gear [3].

So far, there are no methods to cure the PD, only to control its symptoms. The gold-standard is levodopa (L-dopa)[4], which is believed to convert to dopamine in the brain [5]. When the efficacy L-dopa decreases and incidence and severity of side-effects increase, a different approach is needed. That is deep brain stimulation (DBS), which relies on the electrical stimulation with a tretapolar electrode at high frequencies (130 Hz) with pulse length at 60 μs in the basal ganglia structures (subthalamic nucleus (STN) or internal *globlus pallidus* (GPi)). To evaluate the improvement, or not, of the patient with electrical stimulation, the severity of rigidity is evaluated in a semi-quantitative manner for different settings [6]. The scale used for rigidity reduction is based on the subjective assessment of the examiner involved in this process, therefore, influenced by his experience and perception. In some cases, a second examiner performs blind testing for confirmation of the best improvement achieved, however the subjectivity prevails. Thus, a quantitative method for the assessment of this rigidity reduction is lacking.

The effectiveness of STN-DBS has been assessed by Shapiro and colleagues using the elbow joint, where they compared the rigidity UPDRS scores from when patients had the stimulation activated and deactivated [7]. Also, they built a setup comprised by a motor which imposed movement of the elbow joint and measured the resistive torque over the movement. This allowed the computation of the mechanical work, a measure that was able to distinguish parkinsonian patients from the healthy control group and also to identify the improvement of rigidity. Other biomechanical variables have been related to rigidity: mechanical impedance [8], peak torque [9], impulse [8], [10],difference of bias [11], elastic stiffness [8], [10] and damping constant [8], [10]. Surface electromyography (EMG) of *biceps* and *triceps brachii* has been proposed to quantify rigidity [11]. With this, strong correlation was found between the clinical rigidity score and EMG-derived variable [11].

Even though work has been done towards the quantification of rigidity both in the elbow and wrist joints, to the authors knowledge, only Kwon et al. [8] have performed measurements in intra-operative conditions during DBS, using the wrist joint. Still, no real-time feedback related to the patients rigidity was provided to the examiner. Also,

[1]INESC TEC and Faculdade de Engenharia, Universidade do Porto.
[2]Unidade de Doenças do Movimento e Cirurgia Funcional do Hospital de São João; Porto, Portugal.
[3]Departamento de Neurociências Clínicas da Faculdade Medicina da Universidade do Porto; Porto, Portugal.
[4]Unidade de Neurociências do Hospital CUF Porto; Porto, Portugal.

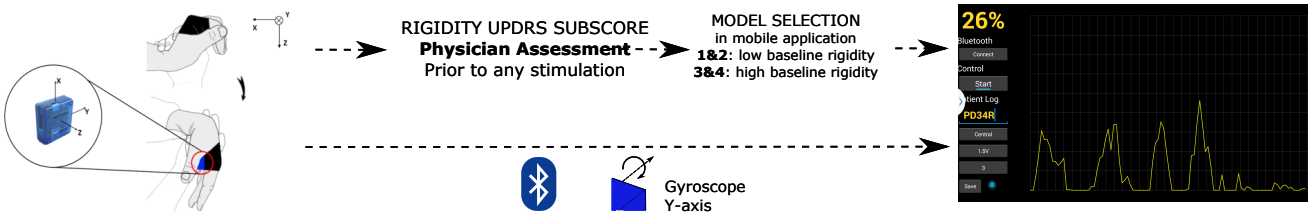

Fig. 1: System architecture. The sensor communicates via Bluetooth with a smartphone. In the mobile application, the user selects the UPDRS subscore related to rigidity assigned by the physician prior to any stimulation. The correspondent model is then used to compute the reduction in rigidity.

most setups designed for quantification of rigidity are bulky and complex, hence inappropriate to take into the operating room; during DBS surgery it is easier to assess wrist rigidity and some setups that have been proposed target the elbow joint. With this is mind, a novel, comfortable, wearable and wireless sensor has been validated [12], to measure angular velocity during passive wrist flexion in DBS surgery. The sensor was communicating with a computer, which derived a signal descriptor from peak and mean values of angular velocity and then applied a general model to compute a percentage of improvement in rigidity. Such system could have its usability improved for intra-operatory usage. Additionally, the model obtained was indifferent to the baseline rigidity, which can be expressed as an UPDRS subscore. The output of this model translated into a reduction relative to an average baseline rigidity. Yet significant differences may be found in the population in terms of the symptom severity. Thus, we propose the usage of this sensor during DBS surgery to provide real-time feedback by performing *in situ* processing in a smartphone, where a multi-model system, specific for each baseline rigidity and estimated based on the *in situ* measures and previous UPDRS scores, will be explored. By considering the data for different levels of rigidity, prior to any stimulation and building the respective models, the most appropriate model could be selected at start-off of the surgery, according to the physician initial assessment. We hypothesize that such approach, with its increased personalization, would allow an improved performance of the system. For the models definition, alternative signal descriptors were experimented, relating peak and mean angular velocity and those which enable lowest training error would be used for validation in DBS surgery.

II. Methodology

a) ***System architecture****:* The sensor was introduced in previous work [12]. The overall system, in Fig. 1, differs from before because we have Bluetooth communication with a smartphone a smartphone (Samsung Galaxy Note II, Quad Core 1.6 GHz), which received the raw data relative to angular velocity and performed local processing. Such system aimed to improve usability in DBS surgery. The data was transmitted at 50 Hz, instead of 42 Hz, as in [12]. The smartphone has stored the models specific for each of the two levels of baseline rigidity considered.

b) ***Subjects and Experiments****:* The system was used during the bilateral DBS surgery (both to the STN and GPi) of parkinsonian patients, while an examiner was assessing the improvement in rigidity for different stimulation settings. The subjects had their medication withdrawn 12h prior to the procedure and were under local anaesthesia during the surgical intervention. A stereotactic target for stimulation and a trajectory for the electrode were defined beforehand based on medical imagery; electrophysiological exploration was done during surgery in order to define the best electrode placement. The stimulation frequency was set at 130 Hz; voltage and placement were varied while rigidity was assessed, by imposition of passive wrist flexion. Definite conditions of stimulation were agreed by two experienced physicians. To train the classification models, data was acquired from a total of 17 patients, correspondent to a total of 237 signals; to test them, 2 patients were considered and 38 evaluations were performed. Before any stimulation, the physician assessed the patient rigidity, using the UPDRS scale. That subscore was used to select in the mobile application the appropriate model for such rigidity severity, which would be used to compute the rigidity reduction. The signal classifications presented by the mobile application were compared to the assessment of the two physicians and were accepted if they were within a range of 5% away from their classification. Patient monitoring was authorized by the Hospitals Ethic Committee and all patients signed an Informed Consent form.

c) ***Signal Processing****:* The processing was done as described in [12], for the exception that no filtering was used. The signal correspondent to the rotation over the y-axis of the sensor (Fig. 1) was acquired and processed by a smartphone. First the raw data was converted to angular velocity; then only its negative values were considered (restricting the analysis to the flexion wrist movement). Two features were considered: average angular velocity (μ_ω) and average peak value (μ_p). A signal descriptor, by combination of both features, was used to describe the decrease in rigidity. This can be perceived as a kernel function, whose purpose is to reduce the model susceptibility to signal plateaus and low occurrence of peaks. Other kernel functions are proposed in the next section to build the rigidity reduction models.

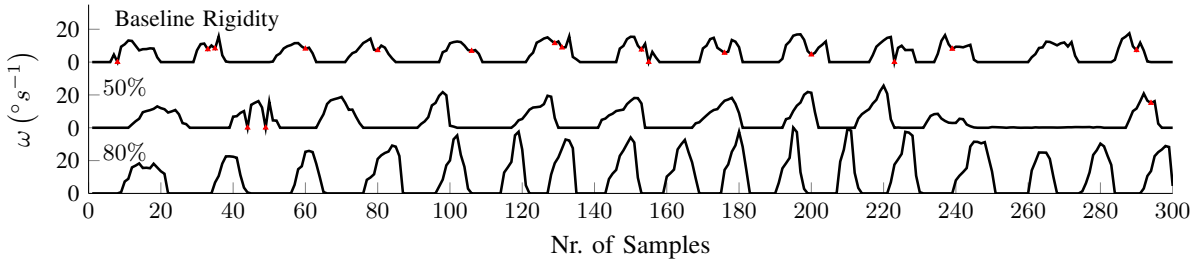

Fig. 2: Example of angular velocity signals corresponding to when baseline rigidity was being assessed (UPDRS score of 3), to 50% and 80% improvement in rigidity. Each arcade corresponds to a wrist flexion. With reduction of rigidity, the signal becomes smoother and higher peak values are achieved (events of cogwheel rigidity are evidenced with red triangles). ω stands for angular velocity.

TABLE I: Number of signals *per* initial UPDRS score.

	Baseline Rigidity (UPDRS)	**# Signals**
Low baseline	1	24
rigidity patients	2	74
High baseline	3	139
rigidity patients	4	0

TABLE II: List of kernels for regression.

Kernel	$k(x,y)$
Hellinger's	$\sqrt{xy}$
Intersection	$\min(x,y)$
χ^2	$2\frac{xy}{x+y}$
JS	$\frac{x}{2}log_2\left(\frac{x+y}{x}\right)+\frac{y}{2}log_2\left(\frac{x+y}{y}\right)$
Gaussian Homogeneous	$\sqrt{xy}\cdot exp\left(-\frac{log\left(\frac{y}{x}\right)^2}{2\sigma^2}\right)$

*d) **Classification Model**:* In previous work [12], a single signal descriptor was used to build the general models. Herein, an alternative approach will be presented, relying on other kernel functions, experimented to develop specific model for high and low rigidity severity. By combining in different ways the aforementioned features, we can identify which one allows better data separation for each initial severity of the symptom. The training set was separated in two different clusters, where those signals associated to an UPDRS scores of 1 or 2 were apart from the remainder (number of signals *per* rigidity level in Table I). Each of these subsets was used to obtain a second degree polynomial mathematical model that would better relate the perceived improvement in rigidity with the mean value of signal descriptor. A higher-degree could lead to over-fitting to the training data. Polynomial models were built, considering as signal descriptor each of the kernel functions in Table II. For each baseline rigidity, the kernel which allowed lowest training error was used for validation in intra-operatory conditions, as afore described.

III. Results

Fig. 2 shows the signals for three levels of rigidity (baseline rigidity, 50% and 80% improvements). Higher reduction in rigidity leads to a smoother waveform and overall higher amplitude signal in each wrist flexion. In addition, the artifacts in the signals, abundant in the initial rigidity state, are evidence of cogwheel rigidity.

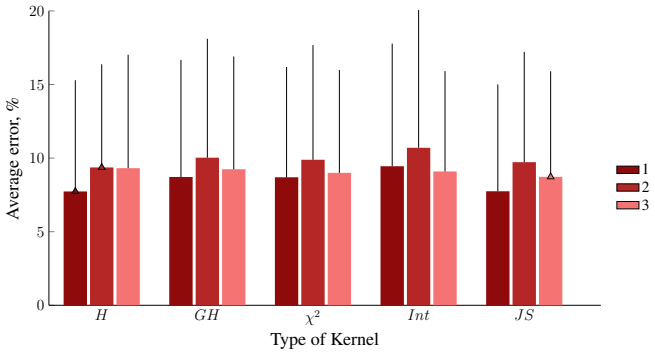

Fig. 3: Mean training error $\pm$ standard deviation for each kernel function as signal descriptor. H stands for Hellingers, GH for Gaussian homogeneous, Int for intersection and JS for Jensen-Shannon divergence. The colors correspond to UPDRS rigidity subscores 1, 2 and 3, from darker to lighter, respectively.

In Fig. 3, the training error of the polynomials models defined by different signal descriptors are presented. For both UPDRS rigidity subscores, 1 and 2, the Hellingers function allowed lowest error of classification ($7.7\pm7.55\%$ and $9.4\pm7.0\%$). For a baseline rigidity of 3, it was the Jensen-Shannon the optimal signal descriptor ($8.7\pm7.1\%$). The respective polynomial models may be found in Fig. 4.

This multi-model system, during DBS surgery, allowed an accuracy of 82.0% and a mean error of 3.4%.

IV. Discussion

The polynomial models which allowed the least training error (Hellinger's and Jensen-Shannon kernel functions) were used to test a multi-model system during DBS surgery. If we consider Figure 4, a high fitting of the mean values of the signal descriptor for high initial rigidity states for each step of improvement over the whole range of improvement may be found. For reduced rigidity decreases in patients initially less rigid, we can identify worst fitting, which could

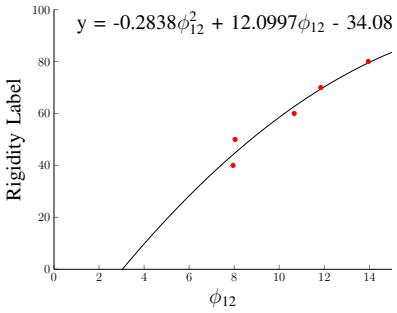

(a) For patients with low rigidity severity.

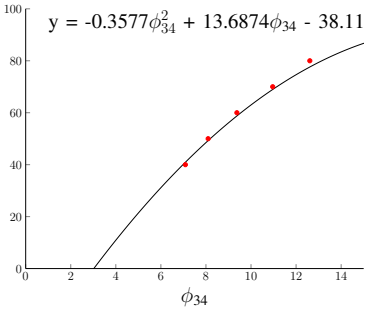

(b) For patients with high rigidity severity.

Fig. 4: Polynomial functions which model the relationship between the signal descriptor and the percentage of rigidity improvement. Circles represent the mean value ofthe descriptors for each of the physician labels (40-80%). $\phi_{12} = \sqrt{\mu_\omega \mu_p}$ and $\phi_{34} = \frac{\mu_\omega}{2} log_2 \left(\frac{\mu_\omega + \mu_p}{\mu_\omega}\right) + \frac{\mu_p}{2} log_2 \left(\frac{\mu_\omega + \mu_p}{\mu_p}\right)$.

be related to a higher difficulty by the examiner to identify small differences when the baseline is, as well, small.

Approximately, the same accuracy was achieved as before (82.0%) [12], by using a larger training set and by defining a model for two levels of baseline rigidity. The error of classification of 3.4% supports that this model represent them quite well, even when we are comparing a continuous scale with a decimal one. Also, cogwheel rigidity may play a role for small improvements, where it may still be present: it causes a higher variability in the average angular velocity and average peak angular velocity, causing the model fitting to worsen. The achievement of similar results in both works supports the reliability of this approach to support an examiner assessment in intra-operatory conditions, by providing real-time feedback. However, it also proves the limitation of kinematic measures in further distinguishing different rigidity levels since both approaches lead to similar results, even though differences were expected. Hence, it is a pivotal step to include the cogwheel detection into the procedure and into the models. As evidenced in Fig. 2, one major feature in parkinsonian rigidity is the occurrence of cogwheel rigidity artifacts, correspondent to the disacceleration in wrist flexion, which highly distinguishes UPDRS subscores of 2 and 3. Hence, future work should encompass this cardinal feature of rigidity in PD patients.

Furthermore, this system is velocity-dependent, thus it requires the examiner to impose approximately the same force in every trial. Additionally, it is important to perform validation of this system across centers performing DBS surgery, to support the use of this system as a normal tool associated to the surgery.

V. Conclusions

This work supports the usability of a simple, wireless, comfortable and mobile system in intra-operatory. This is comprised of a small custom-made sensor placed in the patients hand, communicating with a smartphone, which provided real-time feedback to the examiners about the rigidity reduction under different stimulation settings. The improvement was computed using a set of polynomial mathematical models, specific for low and high initial rigidity states, which classified correctly 82.0% of the evaluated signals, with a mean error of 3.4%, which supports the reliability of this solution. Similar results as before were achieved but it is hypothesized that the detection of cogwheel rigidity artifacts and its inclusion into the models will enhance their performance. The inclusion of biomechanical measures could be beneficial to the system as well. The sensor could be also in the proximal end of the forearm, allowing measurements during the elbow joint rigidity assessment. In future work, the applications of this sensor for different symptoms analysis could be explored.

References

[1] T. Pringsheim, N. Jette, A. Frolkis, and T. D. Steeves, "The prevalence of Parkinson's disease: A systematic review and meta-analysis," *Movement Disorders*, vol. 29, no. 13, pp. 1583–1590, 2014.

[2] P. Trudelle, "Unified Parkinson Disease Rating Scale (UPDRS)," *Kinésithérapie, la Revue*, vol. 6, pp. 20–24, 2006.

[3] J. M. Beitz, "Parkinson's Disease: a review," *Frontiers in Bioscience*, vol. 6, pp. 65–74, 2014.

[4] S. Fahn, "Description of Parkinson's disease as a clinical syndrome." *Annals of the New York Academy of Sciences*, vol. 991, pp. 1–14, 2003.

[5] A. C. Guyton and J. E. Hall, *Tratado em Fisiologia Médica*, 11th ed. Elsevier, 2006.

[6] A. L. Benabid, S. Chabardes, J. Mitrofanis, and P. Pollak, "Deep brain stimulation of the subthalamic nucleus for the treatment of Parkinson's disease," *The Lancet Neurology*, vol. 8, no. 1, pp. 67–81, 2009.

[7] M. B. Shapiro, D. E. Vaillancourt, M. M. Sturman, L. V. Metman, R. a. E. Bakay, and D. M. Corcos, "Effects of STN DBS on rigidity in Parkinson's disease," *IEEE Transactions on Neural Systems and Rehabilitation Engineering*, vol. 15, no. 2, pp. 173–181, 2007.

[8] Y. Kwon, S.-H. Park, J.-W. Kim, Y. Ho, H.-M. Jeon, M.-J. Bang, S.-B. Koh, J.-H. Kim, and G.-M. Eom, "Quantitative evaluation of parkinsonian rigidity during intra-operative deep brain stimulation." *Biomedical materials and engineering*, vol. 24, no. 6, pp. 2273–81, 2014.

[9] M. K. Y. Mak, E. C. Y. Wong, and C. W. Y. Hui-Chan, "Quantitative measurement of trunk rigidity in parkinsonian patients." *Journal of neurology*, vol. 254, no. 2, pp. 202–9, 2007.

[10] B. K. Park, Y. Kwon, J. W. Kim, J. H. Lee, G. M. Eom, S. B. Koh, J. H. Jun, and J. Hong, "Analysis of viscoelastic properties of wrist joint for quantification of parkinsonian rigidity," *IEEE Transactions on Neural Systems and Rehabilitation Engineering*, vol. 19, no. 2, pp. 167–176, 2011.

[11] T. Endo, R. Okuno, M. Yokoe, K. Akazawa, and S. Sakoda, "A novel method for systematic analysis of rigidity in Parkinson's disease," *Movement Disorders*, vol. 24, no. 15, pp. 2218–2224, 2009.

[12] P. Costa, M. J. Rosas, R. Vaz, and J. P. Cunha, "Wrist Rigidity Assessment During Deep Brain Stimulation Surgery," in *Proceedings of the IEEE Internacional Conference of the Engineering in Medicine and Biology Society (EMBS)*, 2015.

Appendix C

Alternative approaches

C.1 Model of rigidity improvement

Both the assessment of training set size effect on the model performance and the exploration of different approaches to obtain the model (relying on the features μ_ω and μ_p). For modeling, classification and regression methods were experimented. Additionally, the possibility of using the current methodology for specific design for different levels of rigidity severity was explored.

C.1.1 Influence of training data size

For all modeling procedures, the amount of training data may be paramount so we aimed to ascertain its influence on the training error by the method leave-one-out.

With that purpose, the size of the training set was varied from 15 to 235 signals in steps of 10, which were randomly selected from a total of 237 and 4000 iterations were performed to determine the error's average and standard deviation.

The error of classification converges quite quickly with additional amount of data: from 85 signals onward, the error stabilize around 8.4% and the standard deviation does not vary significantly, as evidenced in Figure C.1. With a quite reduced amount of signals, a robust methodology is achieved, specially considering this 5-category problem, distancing itself 8.9% in average from the real classification, with 35 training samples. This supports that further acquiring data to improve this general polynomial model for rigidity reduction evaluation will not enhance the system performance. Also, another practical consequence is that, with a low number of surgeries attended for data acquisition, we can have an usable system specific for a new examiner (about 15-20 signals are acquired *per* surgery). This proves the versatility of the system, namely to adapt to new users.

C.1.2 Classification and Regression methods

After acquiring data, this can be used for machine learning, meaning, from a set of training examples to infer regularities/functional dependencies. In this particular context, we stand before a

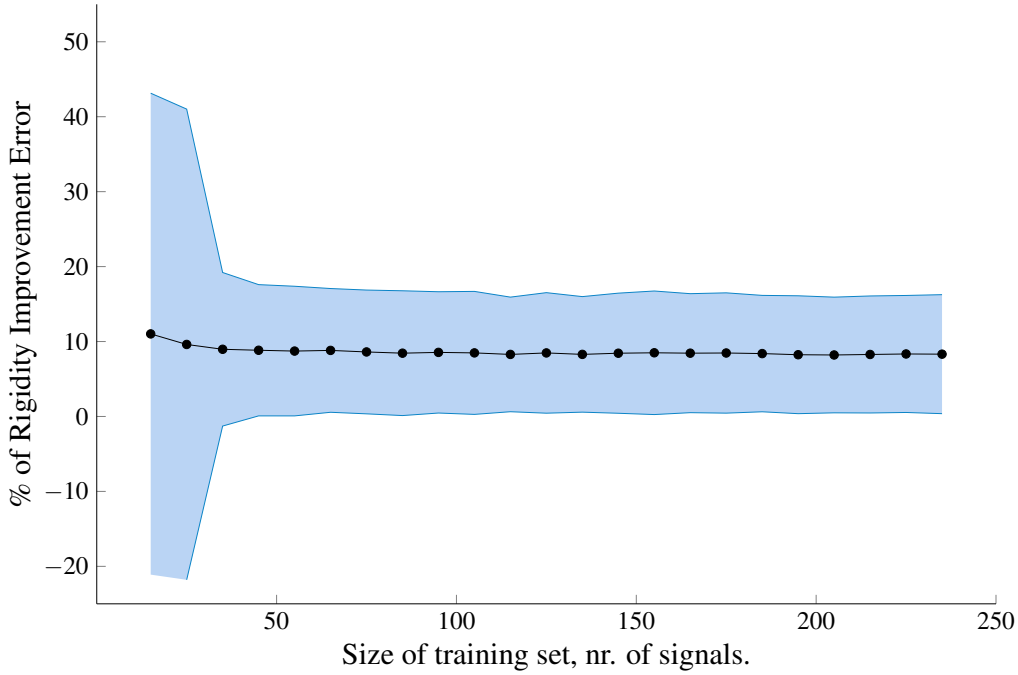

Figure C.1: Implications of the number of signals in the training set in the performance of the polynomial model. The average error ± standard deviation is represented.

case of supervised learning, where the training data is associated to a label, which is the examiner assessment of rigidity reduction in the wrist, from 0% to 80% in a decimal scale. Relying on this background information, we could predict based on regression methods, having a continuous variable as an output, or on classification methods, where this output is categorical [83].

The existent system relies on a regression method, by computing a polynomial model achieved by the least-mean square approach, considering the mean values in the training set for each level of rigidity reduction.

Various possibilities will be herein explored: k-nearest neighbors (kNN), k-means, decision trees (DT) and support vector machine (SVM). The performance analysis of each was performed using a training data set of 119 signals (number of signals available at the time of this analysis).

C.1.2.1 k-Nearest Neighbors

kNN is an algorithm for classification which relies on inspecting the label of the *k-nearest neighbors*, belonging to the training set, and upon that, classify according to their categories. In the simplest case ($k = 1$), to classify a new data point x, the nearest neighbor x' has to be identified and its label will be assigned to x. For larger values of k, the category assigned will be the one which occurs most often in the subset of k-nearest neighbors [84].

This approach requires defining the number of nearest neighbors to be inspected, k. Likewise, the type of distance to be used has also to be decided beforehand. Several possibilities are presented in Table C.1.

Table C.1: Type of distance metrics. x_s and y_t are two feature vector. The Euclidean and City Block distances are particular cases of the Minkowski metric ($p = 2$ and $p = 1$, respectively).

Distance	**Expression**
Minkowski	$\sqrt[p]{\sum_{j=1}^{n} \left\|x_{sj} - y_{tj}\right\|^p}$
Euclidean	$\sqrt{(x_s - y_t)(x_s - y_t)'}$
City Block	$\sum_{j=1}^{n} \left\|x_{sj} - y_{tj}\right\|$
Chebychev	$max_j \left(\left\|x_{sj} - y_{tj}\right\|\right)$
Correlation	$1 - \frac{(x_s - \bar{x}_s)(y_t - \bar{y}_t)'}{\sqrt{(x_s - \bar{x}_s)(x_s - \bar{x}_s)'}\sqrt{(y_t - \bar{y}_y)(y_t - \bar{y}_t)'}}$
Cosine	$1 - \frac{x_s y_t'}{\sqrt{(x_s x_s')(y_t y_t')}}$

This procedure is computationally heavy because, for every new data point x, a vector of distances to every point of the training set is computed to identify the nearest neighbors.

Nevertheless, its performance was assessed. Therefore, x_s and y_t were considered as vector comprising of μ_ω and μ_p. The accuracy and F1-score (as in Equation C.1) were determined.

$$F1 - score = 2\frac{P}{R} \tag{C.1}$$

where

$$R = \frac{TP}{TP + FP} \tag{C.2}$$

and

$$P = \frac{TP}{TP + FN}. \tag{C.3}$$

where TP stands for true positive, FP for false positive, FN for false negative, R for recall and P for precision. F1-score is a measure of accuracy which consists of the weighted average of P and R, and reaches its best value at 1 and worst at 0.

The error achieved using this approach for different k and distinct distance metrics is presented in Figure C.2. We find that, for every distance metric and number of neighbors considered, the performance of the classifier is quite weak: the maximum is 56% of accuracy. The overall behavior may be justified by the cross-category overlapping in the feature domain, as shown in later in Figure C.3. For a methodology that decides each label relying on its neighborhood labeling, this weakens its power before a problem of this nature. An increased number of neighbors benefits the classifier performance. However, at some point, the classifier will consistently assign the label of the most available category. The only distinguishable behavior regarding the distance metric is the clear worst performance of the correlation metric.

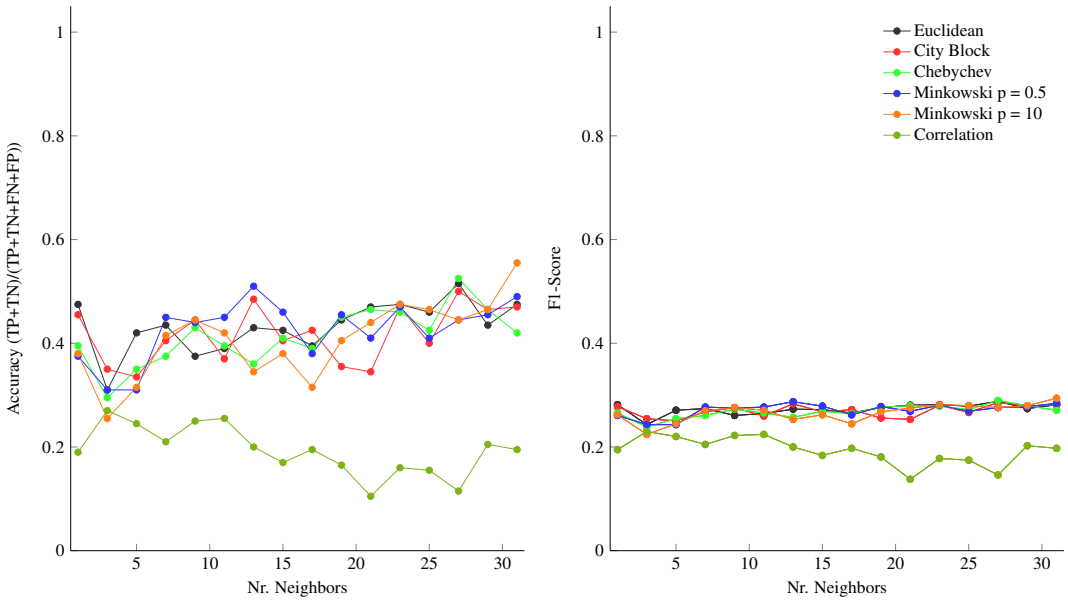

(a) Accuracy (b) F1-score

Figure C.2: Performance of the k-nearest neighbor classifier.

C.1.2.2 k-Means

Another approach for classification is relying on clustering, in this case, k-means clustering. This is an unsupervised method for learning which is initialized by defining the number of clusters, c, to be considered, equivalent to the number of categories in which the training data may be separated. Each of the cluster is associated to a seed point, μ_i , where its centre is located. All training data points is assigned to one of these clusters, by identifying which μ_i is closer to its coordinates. Afterward, a new cluster centre, μ_i', is computed by averaging the coordinates of every training point that had been assigned to the i^{th} cluster. After updating all cluster centres, this procedure of assignment and update is repeated until μ_i converges, for every $i = 1,...,c$ [84].

Contrary to the previous, this iterative method may be moderately time consuming but only when training; after attaining the final cluster centres, for every new data point, only c distances are computed to define its category. However, the main drawback is the need to set the seed coordinates when initializing which may greatly influence the final clusters positioning.

To evaluate the accuracy of k-means, a semi-supervised standpoint was used: after clustering, each cluster was associated to the category which had the closest mean feature value. The seed points were randomly selected and 1000 iterations were performed to determine the accuracy of such approach. A representation of the clustering is presented in Figure C.3. Different distance metrics, as before in the kNN approach analysis, were used, namely the Hamming distance, defined as:

As aforesaid, the high overlap of the categories in the feature domain is easily identifiable, which hinders categorization. This proves to have a clear influence on the final results, where an accuracy of under 20% was obtained, independently of the distance metric used. This supports the

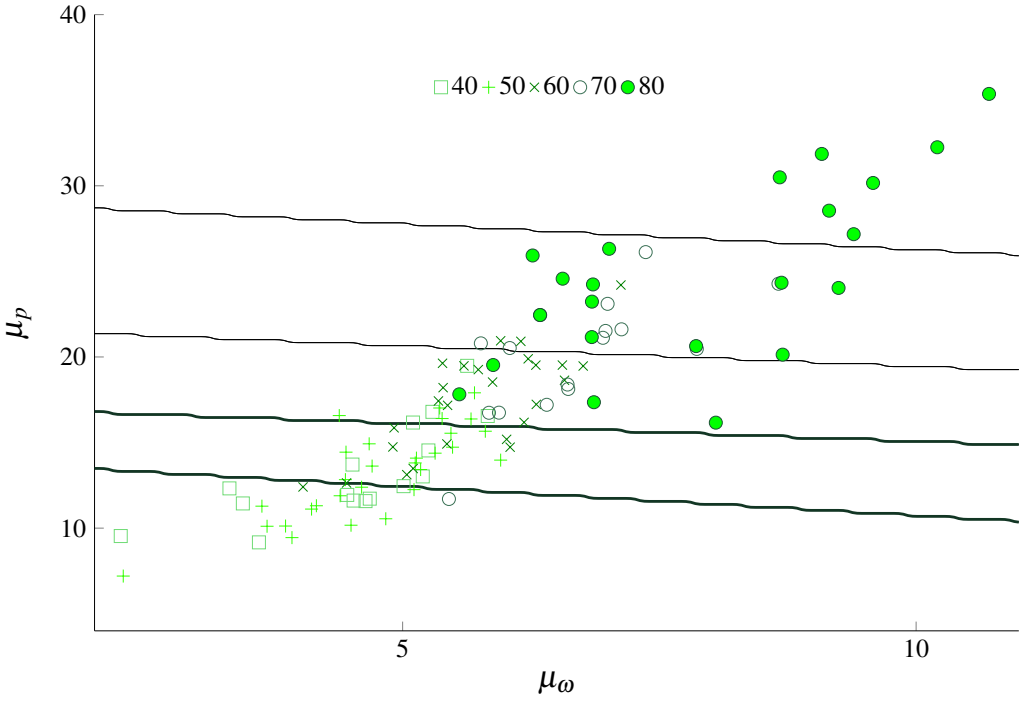

Figure C.3: Clustering achieved by the iterative process of k-Means.

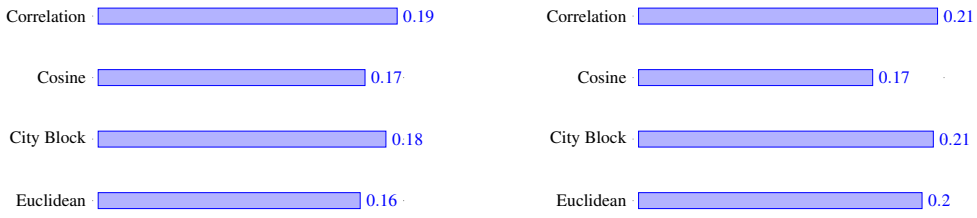

(a) Accuracy (b) F1-score

Figure C.4: Performance of the k-Means clustering approach for classification.

inability to tear the overlapping using non-linear metrics.

In addition to this, an increasing number of clusters was experimented (each assignment was performed as already described) , to evaluate whether it would have any effect. However, no improvements occur and we may incur in promoting over-fitting to the training data.

C.1.2.3 Decision trees

This approach to model a problem relies on classifying a pattern based on a chain of *"yes/no"* or *"value(property)* $\in$ *set of values"* questions.

When a DT is being built, as we go down, the training data is split in smaller and smaller subsets, at each node. To define which question/test should be performed at each node, a value for the property test T that maximizes the purity (or minimizes impurity) of the immediate descendent subsets is searched. Ideally, each subset would have the same category label, however they usually have a mixture. Thus, or (1) a stopping criteria is defined to stop tree branching, by defining how much imperfection we accept, or (2) a different feature is considered to further grow the tree.

When the stopping criteria has been reached, we are upon a terminal node, which need a label to be assigned. That labeling will correspond to the category that has most points represented (classification DT) or to the average value of the labeling in the terminal subset (regression DT) [84].

This procedure generates a tree as in Figure C.5: when considering a new input, it is subjected to a series of queries, which decide the links to be followed, until a terminal node is reached. Its label will be assigned to the new input.

A DT-base approach, other than being quite intuitive to understand, is enables quite rapid classification because it relies on simple and pre-defined queries [84].

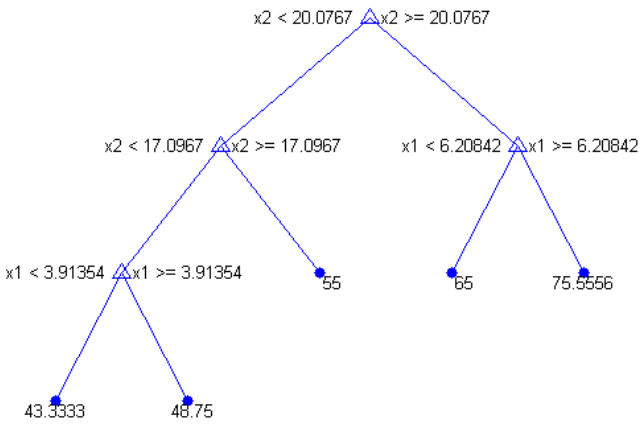

Figure C.5: Example of decision tree. Let x_1 be μ_ω and x_2 be μ_p. Only 30 signals were considered in order to have a short DT.

The use of a single tree may not guarantee by itself a good description of the patterns in the training data. Alternatively, we can rely on the creation of an ensemble of DT, a Random Forest, where each has its own splitting criteria and branches. By combining all DT classification, an improved ability to correctly model the problem may be expected. The different splitting needed is guaranteed by using for each node a randomly chosen feature to then minimize the impurity of the subsequent subsets [85].

To assess the performance of this approach, both classification and regression DT were experimented and the number of trees was varied from 1 to 300. 1000 iterations for each combination were performed and accuracy and training error were computed relying on the leave-one-out method, *i. e.*, one sample from the training set was randomly selected to test the model obtained from the remainder data-set.

Herein, the results of both classification and regression trees will be presented and discussed (Figure C.6).

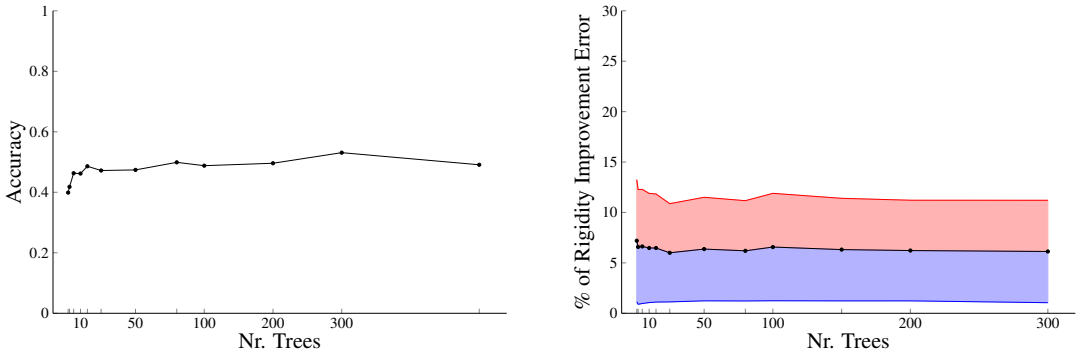

(a) Average accuracy of classification decision trees.

(b) Average ± standard deviation error of regression decision trees.

Figure C.6: Performance of the Random Forest approach.

By considering the different levels of rigidity as categories instead of its own numeric values (40%, 50%, 60%, 70% and 80%), a low accuracy (under 50%) is achieved, independently of the number of trees considered to support the final category assignment to the testing input. This may be related, as previously described, to the overlap of the different rigidity level domains, which turns inappropriate such an approach to evaluate new signals. Still, a subtle improvement is identified by considering additional trees for the final classification, from 40% with one DT to 53% of accuracy with 200 trees.

The use of regression DT, which consider the numerical value of the labeling of the subset at the terminal node encountered for the evaluation of a new signal, allows relatively low error (around 6.5%), which is quite small and offers results more comparable to the currently attained. The influence of the number of trees is noticeable in a small scale and lower range: by having the support of a second DT, is enough to have an error of $(6.6 \pm 5.7)\%$. With increased number of trees, the error diminishes until a minimum of $(6.0 \pm 4.9)\%$ for 25 trees. From them on, the number of trees did not improve any further the performance of the model computed.

This methodology could be adequate for local processing because it only relies on single feature inequalities. An disadvantage is the tiresome task to implement all nodes in the mobile application, especially by considering several DT. However, the queries and the classification criteria are easy to mimic, which would be rather fast to execute. A modeling solution relying on regression DT could be explored in the future.

C.1.2.4 Support Vector Machine

SVM is a machine learning approach to model binary problems. This relies on the definition of a hyperplane in the feature space, $\in \Re^d$ (where d is the number of features considered), which best separates the features of different classes, thus dividing the feature space into the two considered classes, according to the training data. The classification of the new input data is defined by its positioning in the feature space, in relation to the separation hyperplane, parametrized as follows:

$$w \cdot x + b = 0 \tag{C.4}$$

where, w is a vector orthogonal to the hyperplane and b a constant.

Considering the possible class labeling as $y = -1, 1$, the decision function can be obtained from the hyperplane expression, as:

$$f(x) = sgn\,(w \cdot x + b) \tag{C.5}$$

As aforementioned, the hyperplane is achieved by maximizing the distance between its closest data points, *i. e.*, by maximizing the margin as represented in Figure C.7. The performance of SVM relies on having perfectly separable training data. However, not always that is the case and the mapping into a higher dimensional space by the use of kernels is required (see Figure C.7b). In addition, when designing such model, one should consider the complexity in defining a separation hyperplane and the susceptibility to outliers by the SVM. So, when fitting of the model is being performed, one can tweak it is by tuning the cost C, which sets the acceptable number of wrongly classified observations during the fitting. This mindset leads to the definition of a soft margin model, which acceptably separates the training data but allows some misclassification.

Considering a given separation hyperplane, we can identify a set of vectors which represent the data points closest to the categories boundary, known as support vectors [86]. Equation C.5 can be further explicit as:

$$f(x) = sgn\left(\sum_{i=1}^{\ell} y_i \alpha_i \cdot K(x, x_i) + b\right) \tag{C.6}$$

where $y_i = -1, 1$ (indicates the category of the the ith support vector), α_i is the weight assigned to the ith support vector, $K(x, x_i)$ is the value of the kernel between a new feature vector x and the ith support vector and b is the bias, which is optimized during training of the SVM classifier [87].

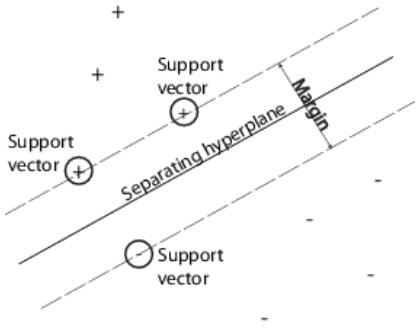

(a) Representation of a separation hyperplane and the margin. From [88].

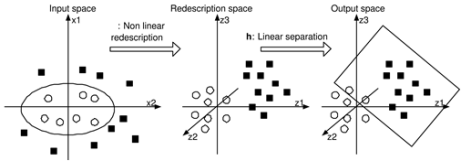

(b) Non-linear transformation for linear separation. From [89].

Figure C.7: Support Vector Machine.

A multi-class problem, as it is the case, may be solved by combining the solution obtained from several binary classifier (one for each category, against all others) [86].

To assess the power of SVM for this context and which are the best parameters, various kernels and respective *arg* (Table C.2) and C values (1, 10, 50, 100, 200), by cross validation [83]. The latter parameter is related to the constraints defined when determining the separation hyperplane: higher values of C lead to a stricter separation by increasing the cost associated to misclassification. Cross-validation, contrary to the leave-one-out method (as used before), consists on dividing data into two subsets: train and test sets. The number of folds is the number of data partitions into these pairs, randomly generated. Then, the performance of the classification approach is measured on the test data set.

The optimal C and *arg* were determined by making 20 iterations of 4-fold cross-validation and by finding the maximum accuracy. The kernel type was fixed (RBF). After first optimization, then, 20 other iterations were performed in order to reach to the most appropriate kernel, by having 3-fold cross-validation. The best trio was determined 13 times. These results are presented in Table C.3.

Table C.2: Kernels tested. x and y are both features vectors. For each new input, the value of the kernel is computed in relation to every support vector. RBF for radial basis function. [87]

Kernel	**Expression**	**arg values**
Linear	$x' \cdot y$	-
RBF	$exp\left(\frac{-0.5 \cdot \|\|x-y\|\|^2}{arg^2}\right)$	0.8 to 1.4, steps of 0.2
Sigmoid	$tanh\left(arg \cdot (x' \cdot y) + arg\right)$	0.8 to 1.4, steps of 0.2

Among the three kernel types tested, the radial basis function (RBF) consistently proved to be more effective in enhancing data separation by revealing higher accuracy values, yet, still low. For its particular case, when a new feature vector x arrives, the distance between this and the support vectors is computed and this is used for exponentiation. Consequently, when x is close to the

Table C.3: Results for the SVM classifier. For every iteration, the Radial Basis Function (RBF) revealed better performance than the remaining kernel functions. FP rate stands false positive rate.

# Iteration	**Kernel**	**C**	**arg**	**Acccuracy**	**FP rate**
1	RBF	50	1	42.8%	0.15
2	RBF	50	0.8	33.3%	0.17
3	RBF	100	1	28.7%	0.16
4	RBF	400	1	33.0%	0.20
5	RBF	100	1.4	30.3%	0.14
6	RBF	100	1.2	24.0%	0.14
7	RBF	200	0.8	30.0%	0.15
8	RBF	100	1	41.3%	0.10
9	RBF	200	1.4	34.7%	0.15
10	RBF	400	0.8	47.0%	0.13
11	RBF	10	1.4	20.0%	0.17
12	RBF	50	1	20.8%	0.19
13	RBF	100	1.2	37.3%	0.15

boundary (i.e., close to the some support vectors), the kernel value will be quite small; otherwise, faraway from the boundary, the exponential will tend to infinite. This mindset seems to improve class separation.

The utilization of a linear kernel is appropriate when linear separation may be achieved between classes. However, such is not the case (categories domain overlap in feature space), thus the algorithm is unable to define the separation hyperplanes required. The sigmoid kernel, as well, was ineffective.

One other reason for this disparity may be related to the order of optimization (first the kernel was fixed and varied C and arg). However, prior work (no results to be presented) comprised of ascertain workable range of arg, from 0.001 to 200, but the resultant performance did not improve.

Still, the achieved optimal combination of arg, C and kernel function lead to a minimum accuracy of 20.0% and a maximum of 47%. The SVM is known as a powerful machine learning approach which appear not to collaborate with the attained results. In addition, the false positive rate is not as bad, ranging from 0.10 to 0.19. This demeanor could be related to the inability by the SVM to the achieve data separability, even by considering these kernel functions.

C.2 Summary

An interesting finding was how early the polynomial modeling approach performance stabilized, in terms of data size required for training: with 85 signals, the error stabilize at around 8.4%. This fact leads to the conclusion that no further improvement in performance should be expected by simply increasing the data-set. New approaches may be explored, but there should be significant focus on exploring other applications of this system.

One other option to model this problem was by recurring to other methodologies, be it classification or regression ones. Still, in terms of accuracy for the classification approaches (kNN, kMeans and SVM), none achieved as high as the current system. This is related to considering categories instead of it numerical value, which hinders correct classification because each category domain significantly overlaps others. The regression methodology (DT) proved to have a relatively low error and improved performance was found by increasing the number of trees considered to support the final label assignment to a signal (Random Forest). This approach, contrary to the previous, is quite easy to implement and allows relatively fast processing because it relies on a series of pre-defined queries, given the non-excessive number of trees considered.

Appendix D

NeuroIberia 2016 Abstract

Neurocirugia. 2016;27(Espec Congr):28

Neurocirugía

http://www.revistaneurocirugia.com/

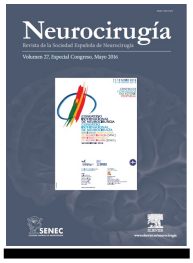

O-FUN-16 - A REAL-TIME INTRA-OPERATORY SYSTEM FOR RIGIDITY EVALUATION DURING DEEP BRAIN STIMULATION SURGERY

A.S. Assis[1], R. Vaz[2,3], M.J. Rosas[4], C. Chamadoira[2], P. Costa[1] and J.P. Silva Cunha[1]

[1]INESC TEC e Faculdade de Engenharia, Universidade do Porto, Porto. [2]Serviço de Neurocirurgia; [4]Serviço de Neurologia, Centro Hospitalar de São João, Porto. [3]Unidade de Neurociências, Hospital CUF, Porto.

Resumen

Objectives: Deep Brain Stimulation (DBS) has a proved value in the treatment of severe forms of Parkinson's Disease. Intraoperative evaluation of the efficacy of stimulation includes evaluation of the effect on rigidity. A subjective semi-quantitative scale is used, dependent on the examiner perception and experience. So, the system proposed herein aims to tackle this subjectivity, using quantitative data and providing real-time feedback of the computed rigidity reduction, hence supporting the physician decision.

Material and methods: This system comprises of a gyroscope-based motion sensor in a textile band, placed in the patient's hand, which communicates its measurements to a smartphone. The latter computes a signal descriptor from the angular velocity of the hand during wrist flexion in DBS surgery and applies a polynomial model to determine the rigidity reduction, which is communicated to the physician. This model was trained using signals from 8 patients (Mean Age: 61) and validated in 5 patients (Mean Age: 56) surgeries. These patients were subjected to bilateral DBS implantation and stimulation.

Results: The system presented 3.2% of error and 77.1% of accuracy (when compared to two specialists' agreement). The implemented descriptor proved to discriminate well high and low rigidity reduction ($p < 0.001$), but was unable to distinguish equal improvements from patients with different baseline rigidity. This will hinder the future design of different models for each baseline rigidity profile.

Conclusions: Overall, we present a simple, wearable, mobile system, suitable for intra-operatory conditions during DBS, providing a reliable second-opinion about the improvement in rigidity for different stimulation settings.

Appendix E

Classes Diagram for Smartphone-Smartwatch Communication

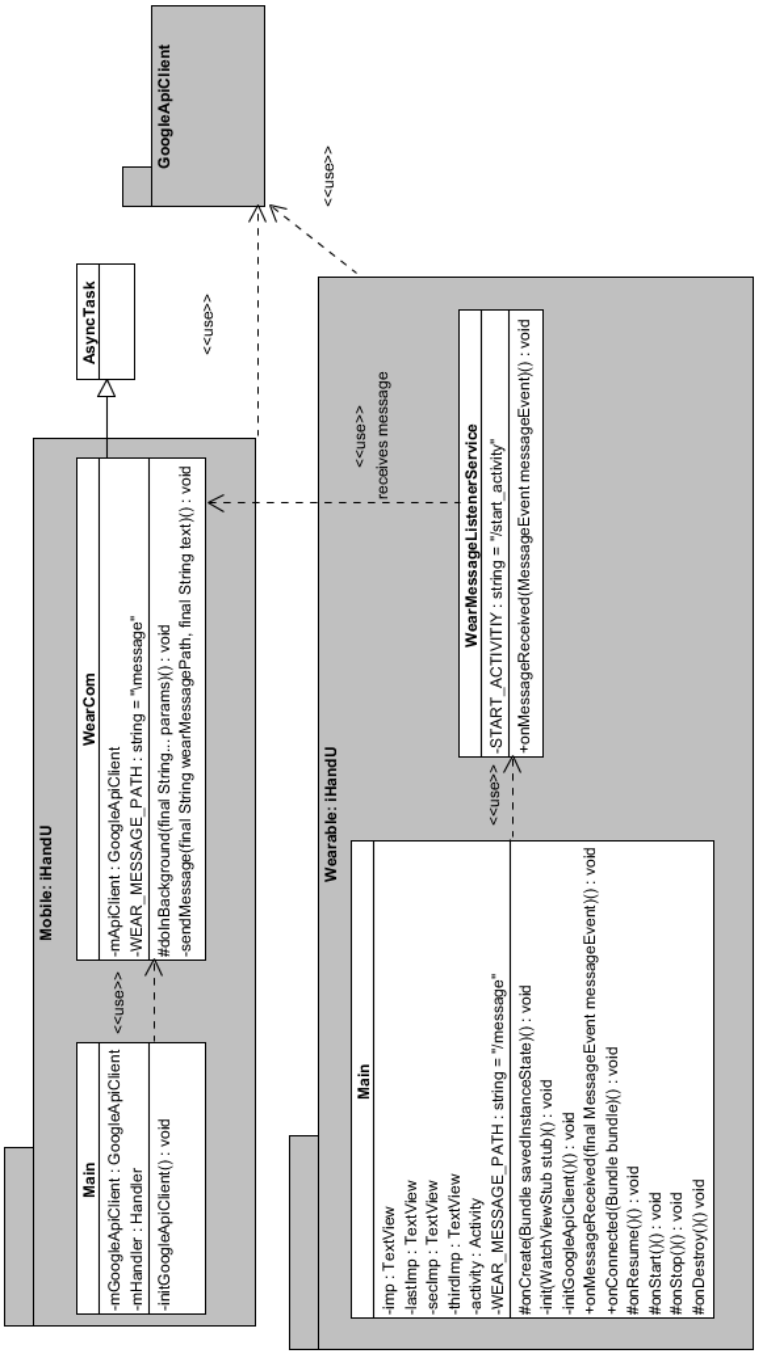

Figure E.1: Classes, methods and attributes involved in smartphone/handheld communication.

Appendix F

System introduced in DBS surgery

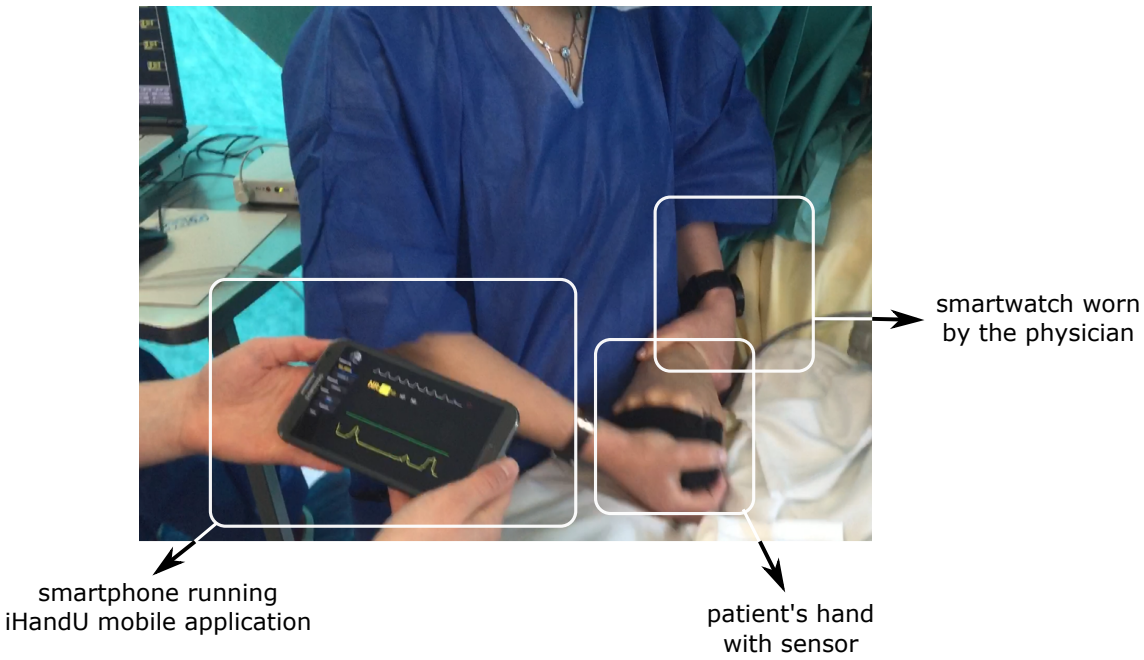

Figure F.1: Intra-operatory use of the system.

Appendix G

Usability Surveys

Inquérito sobre a Usabilidade do Sistema iHandU durante as cirurgias de Estimulação Cerebral Profunda

Data: [redacted]

Identificação: [redacted]

Função: Suporte

Enquadramento do sistema iHandU durante a cirurgia de estimulação cerebral profunda

De seguida são apresentados as várias etapas que constituem a utilização do sistema iHandU. Classifique numa escala de 1 a 5 a dificuldade de cada etapa em que 1 corresponde a muito difícil e 5 a muito simples.

	Muito Difícil	Difícil	Indiferente	Simples	Muito Simples
	1	2	3	4	5
1. Colocação do sensor no paciente					X
2. Inicialização da aplicação móvel					X
3. Gravação do sinal de base					X
4. Observação aspecto do sinal de base					X
5. Observação do sinal em tempo real					X
6. Observação do feedback relativo à redução de rigidez					X
7. Observação feedback relativo à ocurrência de perturbações no movimento de flexão					X
8. Consulta do histórico de redução de rigidez					X
9. Comparação da amplitude do sinal em tempo real com o valor de referência de redução significativa de rigidez					X
10. Término da utilização do sistema				X	

Avaliação Geral: 5

Sugestões/Comentários:

Inquérito sobre a Usabilidade do Sistema iHandU durante as cirurgias de Estimulação Cerebral Profunda

Data: [redacted]

Identificação [redacted]

Função: Suporte

Enquadramento do sistema iHandU durante a cirurgia de estimulação cerebral profunda

De seguida são apresentados as várias etapas que constituem a utilização do sistema iHandU. Classifique numa escala de 1 a 5 a dificuldade de cada etapa em que 1 corresponde a muito difícil e 5 a muito simples.

	Muito Difícil	Difícil	Indiferente	Simples	Muito Simples
	1	2	3	4	5
1. Colocação do sensor no paciente					X
2. Inicialização da aplicação móvel					X
3. Gravação do sinal de base					X
4. Observação aspecto do sinal de base					X
5. Observação do sinal em tempo real					X
6. Observação do feedback relativo à redução de rigidez					X
7. Observação feedback relativo à ocurrência de perturbações no movimento de flexão					X
8. Consulta do histórico de redução de rigidez					X
9. Comparação da amplitude do sinal em tempo real com o valor de referência de redução significativa de rigidez					X
10. Término da utilização do sistema					X

Avaliação Geral: 5

Sugestões/Comentários:

Alterar /colocar TextView em fundo

Inquérito sobre a Usabilidade do Sistema iHandU durante as cirurgias de Estimulação Cerebral Profunda

Data: [redacted]

Identificação: [redacted]

Função: Suporte

Enquadramento do sistema iHandU durante a cirurgia de estimulação cerebral profunda

De seguida são apresentados as várias etapas que constituem a utilização do sistema iHandU. Classifique numa escala de 1 a 5 a dificuldade de cada etapa em que 1 corresponde a muito difícil e 5 a muito simples.

	Muito Difícil	Difícil	Indiferente	Simples	Muito Simples
	1	2	3	4	5
1. Colocação do sensor no paciente				X	
2. Inicialização da aplicação móvel					X
3. Gravação do sinal de base					X
4. Observação aspecto do sinal de base					X
5. Observação do sinal em tempo real					X
6. Observação do feedback relativo à redução de rigidez					X
7, Observação feedback relativo à ocurrência de perturbações no movimento de flexão					X
8. Consulta do histórico de redução de rigidez					X
9. Comparação da amplitude do sinal em tempo real com o valor de referência de redução significativa de rigidez					X
10. Término da utilização do sistema					X

Avaliação Geral: 5

Sugestões/Comentários:

Ao clicar no botão "Connect", surge uma lista com os dispositivos aos quais é possível conectar por bluetooth. Após selecionarmos o aparelho com o qual nos pretendemos emparelhar, seria interessante surgir uma mensagem ou uma indicação visual [redacted] de que foi realizada a seleção com sucesso. (ou sair da lista e voltar ao menu principal).

Inquérito sobre a Usabilidade do Sistema iHandU durante as cirurgias de Estimulação Cerebral Profunda

Data: [redacted]

Identificação [redacted]

Função: Suporte

Enquadramento do sistema iHandU durante a cirurgia de estimulação cerebral profunda

De seguida são apresentados as várias etapas que constituem a utilização do sistema iHandU. Classifique numa escala de 1 a 5 a dificuldade de cada etapa em que 1 corresponde a muito difícil e 5 a muito simples.

	Muito Difícil	Difícil	Indiferente	Simples	Muito Simples
	1	2	3	4	5
1. Colocação do sensor no paciente					X
2. Inicialização da aplicação móvel					X
3. Gravação do sinal de base					X
4. Observação aspecto do sinal de base					X
5. Observação do sinal em tempo real					X
6. Observação do feedback relativo à redução de rigidez					X
7. Observação feedback relativo à ocurrência de perturbações no movimento de flexão					X
8. Consulta do histórico de redução de rigidez					X
9. Comparação da amplitude do sinal em tempo real com o valor de referência de redução significativa de rigidez					X
10. Término da utilização do sistema					X

Avaliação Geral: 5

Sugestões/Comentários:

Inquérito sobre a Usabilidade do Sistema iHandU durante as cirurgias de Estimulação Cerebral Profunda

Data: [redacted]

Identificação

Função: Enfermeira

Enquadramento do sistema iHandU durante a cirurgia de estimulação cerebral profunda

De seguida são apresentados as várias etapas que constituem a utilização do sistema iHandU. Classifique numa escala de 1 a 5 a dificuldade de cada etapa em que 1 corresponde a muito difícil e 5 a muito simples.

	Muito Difícil	Difícil	Indiferente	Simples	Muito Simples
	1	2	3	4	5
1. Colocação do sensor no paciente					X
2. Inicialização da aplicação móvel					X
3. Gravação do sinal de base				X	
4. Observação aspecto do sinal de base				X	
5. Observação do sinal em tempo real					X
6. Observação do feedback relativo à redução de rigidez				X	
7. Observação feedback relativo à ocurrência de perturbações no movimento de flexão				X	
8. Consulta do histórico de redução de rigidez				X	
9. Comparação da amplitude do sinal em tempo real com o valor de referência de redução significativa de rigidez				X	
10. Término da utilização do sistema					X

Avaliação Geral: 4.5

Sugestões/Comentários:

- ESCONDER BOTÃO BASELINE ATÉ INICIAR AQUISIÇÃO;
- BOTÃO PARA INICIAR E TERMINAR A AQUISIÇÃO DO SINAL DA BASELINE;
- HISTÓRICO DA RIGIDEZ EM FUNÇÃO DA POSIÇÃO DOS ELÉCTRODOS
- TEXTO INDICATIVO DOS DIFERENTES PASSOS (EX: QUANDO A BASELINE NASCE NO TOPO DO ECRÃ, DIZER QUE AQUILO É A BASELINE)

Appendix H

List of countries where Utility Model Protection is applied

- Albania
- Angola
- Argentina
- African Regional Intellectual Property Organization
- Armenia
- Aruba
- Australia
- Austria
- Azerbaijan
- Belarus
- Belize
- Brazil
- Bolivia
- Bulgaria
- Chile
- China (including Hong Kong and Macau)
- Colombia
- Costa Rica
- Czech Republic
- Denmark
- Ecuador
- Egypt
- Estonia
- Ethiopia
- Finland
- France
- Georgia
- Germany
- Greece
- Guatemala
- Honduras
- Hungary
- Indonesia
- Ireland
- Italy
- Japan
- Kazakhstan
- Kuwait
- Kyrgyzstan
- Laos
- Malaysia
- Mexico
- Organisation Africaine de la Propriété Intellectuelle
- Peru
- Philippines
- Poland
- Portugal
- Republic of Korea
- Republic of Moldova
- Russian Federation
- Slovakia
- Spain
- Taiwan
- Tajikistan
- Trinidad & Tobago
- Turkey
- Ukraine
- Uruguay
- Uzbekistan